

การเพิ่มความไม่ชอบน้ำของอิเล็กโทรสปีนพอลิไวนิลแอลกอฮอล์ไฟเบอร์

โดยปฏิกิริยาเคมีของหมู่ไฮดรอกซิล



นางสาวณรรักษ์ เจียมเงิน

วิทยานิพนธ์นี้เป็นส่วนหนึ่งของการศึกษาตามหลักสูตรปริญญาวิทยาศาสตรมหาบัณฑิต

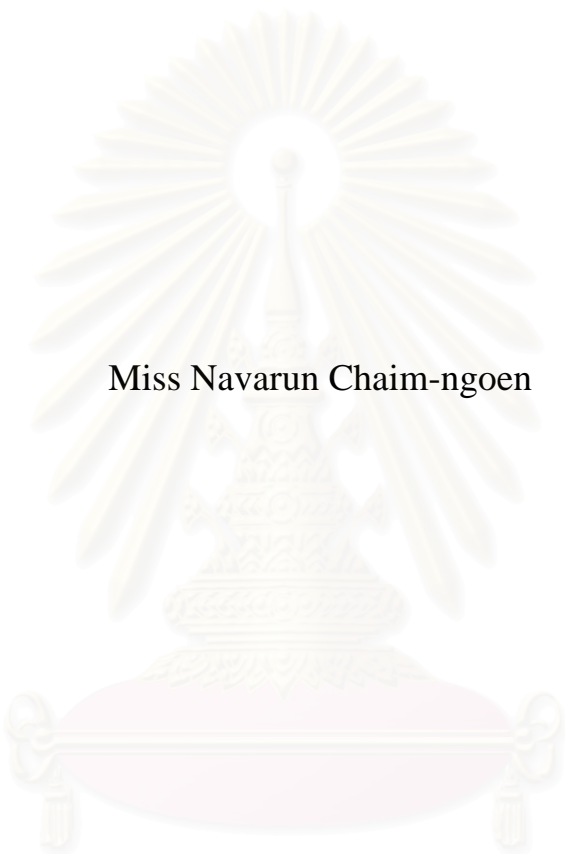
สาขาวิชาปิโตรเคมีและวิทยาศาสตร์พอลิเมอร์

คณะวิทยาศาสตร์ จุฬาลงกรณ์มหาวิทยาลัย

ปีการศึกษา 2550

ลิขสิทธิ์ของจุฬาลงกรณ์มหาวิทยาลัย

ENHANCING HYDROPHOBICITY OF ELECTROSPUN
POLY(VINYL ALCOHOL) FIBERS BY CHEMICAL
REACTION OF HYDROXYL GROUPS



Miss Navarun Chaim-ngoen

สถาบันวิทยบริการ
จุฬาลงกรณ์มหาวิทยาลัย

A Thesis Submitted in Partial Fulfillment of the Requirements
for the Degree of Master of Science Program in Petrochemistry and

Polymer Science

Faculty of Science

Chulalongkorn University

Academic Year 2007

Copyright of Chulalongkorn University

Thesis Title ENHANCING HYDROPHOBICITY OF ELECTROSPUN
POLY(VINYL ALCOHOL) FIBERS BY CHEMICAL REACTION
OF HYDROXYL GROUPS

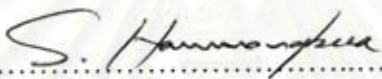
By Miss Navarun Chaim-ngoen

Field of Study Petrochemistry and Polymer Science

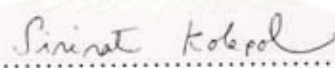
Thesis Advisor Assistant Professor Voravee P. Hoven, Ph.D.

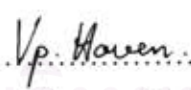
Thesis Co-Advisor Associate Professor Pitt Supaphol, Ph.D.

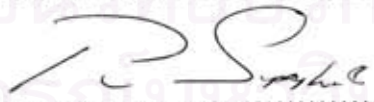
Accepted by the Faculty of Science, Chulalongkorn University in Partial
Fulfillment of the Requirements for the Master's Degree

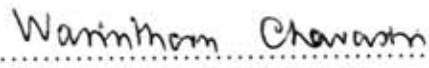

.....Dean of the Faculty of Science
(Professor Supot Hannongbua, Dr.rer.nat.)

THESIS COMMITTEE


.....Chairman
(Associate Professor Sirirat Kokpol, Ph.D.)


.....Thesis Advisor
(Assistant Professor Voravee P. Hoven, Ph.D.)


.....Thesis Co-Advisor
(Associate Professor Pitt Supaphol, Ph.D.)


.....Member
(Assistant Professor Warinthorn Chavasiri, Ph.D.)


.....Member
(Assistant Professor Varawut Tangpasuthadol, Ph.D.)

ณวัฒน์ เจียมเงิน: การเพิ่มความไม่ชอบน้ำของอิเล็กโทรสปินพอลิไวนิลแอลกอฮอล์ไฟเบอร์โดยปฏิกิริยาเคมีของหมู่ไฮดรอกซิล (ENHANCING HYDROPHOBICITY OF ELECTROSPUN POLY(VINYL ALCOHOL) FIBERS BY CHEMICAL REACTION OF HYDROXYL GROUPS) อาจารย์ที่ปรึกษา: ผศ.ดร.วรวิทย์ โฮვნัน, อาจารย์ที่ปรึกษาร่วม: รศ.ดร.พิชญ์ ศุภผล, จำนวนหน้า 87 หน้า

ในขั้นแรกเตรียมแผ่นเส้นใยพอลิไวนิลแอลกอฮอล์ (พีวีเอ) ที่มีขนาดเส้นใยในระดับต่ำกว่าไมโครเมตรด้วยกระบวนการอิเล็กโทรสปินนิง ปฏิบัติการตัดแปรรูปทางเคมีส่วนใหญ่ใช้แผ่นเส้นใยที่เตรียมจากสารละลายพีวีเอ 10 เปอร์เซ็นต์ (น้ำหนัก/ปริมาตร) เส้นใยมีเส้นผ่าศูนย์กลางเท่ากับ 297.05 ± 33.59 นาโนเมตร และค่ามุมสัมผัสของน้ำบนพื้นผิวเท่ากับ $52.31^\circ \pm 1.22^\circ$ ปฏิบัติการเอสเทอร์ฟิเคชันระหว่างหมู่ไฮดรอกซิลของพีวีเอกับเอซิลคลอไรด์เป็นวิธีที่ไม่เหมาะสมในการทำให้แผ่นเส้นใยพีวีเอมีความไม่ชอบน้ำ เนื่องจากทำให้เส้นใยเกิดการเสีรูปร่าง ดังนั้นจึงสร้างชั้นอนินทรีย์เหมือนซิลิกาของ SiO_2/SiOH ด้วยการทำปฏิกิริยากับซิลิกอนเตตระคลอไรด์สลับกับน้ำในอากาศ 3 รอบเพื่อเพิ่มความแข็งแรงและความคงตัวให้แผ่นเส้นใยพีวีเอ จากนั้นจึงเพิ่มความไม่ชอบน้ำให้แก่แผ่นเส้นใยพีวีเอ-โซลานอลด้วยการทำปฏิกิริยาโซลานในเซชันกับอัลคิลคลอไรโซเลน ทั้งในภาวะไอและสารละลาย วิเคราะห์พื้นผิวของแผ่นเส้นใยที่ถูกดัดแปลงด้วยการวัดมุมสัมผัสของน้ำและกล้องจุลทรรศน์อิเล็กตรอนแบบส่องกราด ผลการทดลองแสดงว่าการเกิดชั้นเหมือนซิลิกาทำให้แผ่นเส้นใยพีวีเอมีความชอบน้ำอย่างมาก โดยมีมุมสัมผัสของน้ำเท่ากับ 0 หลังจากการทำปฏิกิริยาโซลานในเซชันกับอัลคิลคลอไรโซเลนแต่มุมสัมผัสน้ำแบบแอดวานซ์มีค่าสูงถึง 150° มุมสัมผัสน้ำแบบรีซีดดิ้งยังคงมีค่าเท่ากับศูนย์ ส่งผลให้มีฮิสเทอรีซิสสูง นอกจากนี้ยังพบว่าหยดน้ำอยู่ค้ำบนแผ่นเส้นใยถึงแม้ว่าจะคว่ำแผ่นเส้นใยลงก็ตาม ลักษณะดังกล่าวแสดงให้เห็นว่าแผ่นเส้นใยพีวีเอที่ผ่านการทำปฏิกิริยาโซลานในเซชันแล้วยังไม่มีสมบัติไม่ชอบน้ำอย่างยั่งยืน

สาขาวิชา ปิโตรเคมีและวิทยาศาสตร์พอลิเมอร์ ลายมือชื่อนิสิต..... ณวัฒน์ เจียมเงิน

ปีการศึกษา..... 2550

ลายมือชื่ออาจารย์ที่ปรึกษา.....

ลายมือชื่ออาจารย์ที่ปรึกษาร่วม.....

4872279523: MAJOR PETROCHEMISTRY AND POLYMER SCIENCE

KEYWORD: SUPERHYDROPHOBIC / ELECTROSPINNING / POLY(VINYL ALCOHOL) / SILANIZATION / ESTERIFICATION

NAVARUN CHAIM-NGOEN: ENHANCING HYDROPHOBICITY OF ELECTROSPUN POLY(VINYL ALCOHOL) FIBERS BY CHEMICAL REACTION OF HYDROXYL GROUPS. THESIS ADVISOR: ASSISTANT PROFESSOR VORAVEE P. HOVEN, Ph.D., THESIS CO-ADVISOR: ASSOCIATE PROFESSOR PITT SUPAPHOL, Ph.D., PAGES 87 pp.

Poly(vinyl alcohol) (PVA) fiber mats having fiber diameters in a sub-micron range were first prepared by electrospinning. Most chemical modification reactions were conducted on PVA fiber mats electrospun from 10%(w/v) PVA solution, having a diameter of 297.05 ± 33.59 nm and an air-water contact angle of $52.31^\circ \pm 1.22^\circ$. Esterification of hydroxyl groups of PVA by acyl chlorides was not an effective route to hydrophobize the PVA fiber mats. The reactions led to the deformation of the fibers. Silica-like inorganic layer of SiO_2/SiOH was then introduced to the PVA fiber mats via 3 cycles of a reaction with SiCl_4 and H_2O in order to increase the strength and integrity of the PVA fiber mats. Hydrophobization of the PVA-silanol fiber mats were thus performed using silanization of alkylchlorosilanes both in vapor and solution phases. Surface modified PVA fiber mats were characterized by water contact angle (WCA) analysis and scanning electron microscopy (SEM). The PVA fiber mats became extremely hydrophilic with $\text{WCA} \sim 0^\circ$ after the SiO_2/SiOH layer was generated. Although the advancing WCA reached as high as 150° after silanization with alkylchlorosilanes, the receding WCA remained at 0° , leading to an extremely high contact angle hysteresis. The water drop remained intact with the silanized fiber mats and did not roll off although the fiber mats were flipped up-side down. These characteristics suggest that all silanized PVA fiber mats cannot be considered superhydrophobic.

Field of study Petrochemistry and Polymer Science Student's signature *Navarin Chaim-ngoen*
 Academic year 2007 Advisor's signature *V.P. Hoven*
 Co-advisor's signature *P. Supaphol*

ACKNOWLEDGEMENTS

First of all, I would like to express my heartfelt gratitude and appreciation to my advisor, Asst. Prof. Dr. Voravee P. Hoven, for her support both in science and in life, and encouragement throughout the course of my study. I would also like to thank my co-advisor, Assoc. Prof. Dr. Pitt Supaphol, for his valuable suggestion. Also, I am sincerely grateful to the members of the thesis committee, Assoc. Prof. Dr. Sirirat Kokpol, Asst. Prof. Dr. Warinthorn Chavasiri, and Asst. Prof. Dr. Varawut Tangpasuthadol for their suggestions, endless desire to share their comments on the subject and time to read the thesis.

Many thanks go to Assoc. Prof. Dr. Sanong Ekgasit for his support in ATR-FTIR analyses.

Many thanks go to all OSRU members for their assistance, suggestions concerning experimental techniques and their kind helps during my thesis work.

Finally, I would like to especially thank my family members: father, mother, grandmother, younger sisters and relatives for their love, kindness and support throughout my entire study.

สถาบันวิทยบริการ
จุฬาลงกรณ์มหาวิทยาลัย

CONTENTS

	Pages
ABSTRACT IN THAI.....	iv
ABSTRACT IN ENGLISH.....	v
ACKNOWLEDGEMENTS.....	vi
CONTENTS.....	vii
LIST OF TABLES.....	x
LIST OF FIGURES.....	xi
LIST OF ABBREVIATIONS	xv
CHAPTER I INTRODUCTION.....	1
1.1 Statement of Problem.....	1
1.2 Objectives.....	2
1.3 Scope of Investigation.....	2
CHAPTER II THEORY AND LITERATURE REVIEW.....	3
2.1 Surface Wetting.....	3
2.1.1 Wetting Theory.....	3
2.1.2 Definition of Commonly Used Terms in Hydrophobicity.....	5
2.1.3 Theory of Superhydrophobicity.....	6
2.1.4 Chemistry Driven Hydrophobicity.....	10
2.1.5 Literature Reviews.....	11
2.2 Electrospinning Process.....	23
2.3 Poly(vinyl alcohol).....	25
2.4 Electrospinning of PVA.....	27
2.5 Using Electrospining for Generating Superhydrophobic...	29
2.6 Esterification.....	34
2.7 Silanization.....	34
2.8 Characterization Techniques.....	38
2.8.1 Contact Angle Measurement.....	38

2.8.2	Scanning Electron Microscope (SEM).....	40
CHAPTER III EXPERIMENTAL.....		42
3.1	Materials.....	42
3.2	Equipment.....	42
3.2.1	Contact Angle Measurement.....	42
3.2.2	Scanning Electron Microscopy (SEM).....	43
3.3	Preparation of Electrospun Poly(vinyl alcohol) Fiber Mats.....	43
3.4	Chemical Modification of Poly(vinyl alcohol) Fiber Mats.....	45
3.4.1	Esterification with Acyl Chlorides.....	45
3.4.2	Preparation of PVA-silanol Fiber Mats.....	45
3.4.3	Vapor-phase Silanization of PVA-silanol Fiber Mats with Alkylchlorosilane.....	46
3.4.4	Solution-phase Silanization of PVA-silanol Fiber Mats with Alkylchlorosilane.....	47
CHAPTER IV RESULTS AND DISCUSSION.....		48
4.1	Preparation of Electrospun Poly(vinyl alcohol) Fiber Mats.....	48
4.1.1	Effect of Solution Concentration of Poly(vinyl alcohol) (PVA) on Morphology of Fiber Mats.....	48
4.1.2	Effect of Solution Concentration on Wettability of Fiber Mats.....	51
4.2	Chemical Modification of Poly(vinyl alcohol) Fiber Mats.....	52
4.2.1	Esterification with Acyl Chlorides.....	52
4.2.2	Confirmation of Esterification Formation.....	57
4.2.3	Preparation of PVA-silanol Fiber Mats.....	57
4.2.4	Silanization of PVA-silanol Fiber Mats.....	60

4.2.5 Confirmation of Silanization Formation	63
4.2.6 Morphology of PVA-silanol Fiber Mats after Silanization.....	63
CHAPTER V CONCLUSIONS	73
REFERENCES.....	76
APPENDICES.....	83
VITAE.....	87



สถาบันวิทยบริการ
จุฬาลงกรณ์มหาวิทยาลัย

LIST OF TABLES

Tables	Pages
2.1 Water contact angle and surface energies of common plastics.....	10
2.2 General chemical identity and physical properties of Poly(vinyl alcohol).....	25
4.1 Conditions used for the esterification in vapor phase and water contact angle data of PVA fiber mats.....	55
4.2 Water contact angle data of PVA-silanol fiber mats after silanization with alkylchlorosilanes.....	62
4.3 Water contact angle data of PVA-silanol beaded fiber mats after silanization with alkylchlorosilanes.....	71
A-1 Viscosity at 27°C of water and as-prepared PVA solutions at various solution concentrations.....	84
A-2 Some properties of as-prepared PVA solutions.....	84
A-3 Water contact angle data (θ_A) for surface prepared by reaction in vapor phase of Acyl chloride.....	84
A-4 Water contact angle (θ_A) and EDX for PVA-silanol fiber mats.....	85
A-5 Water contact angle data (θ_A) of PVA-silanol fiber mats after silanization with Alkylchlorosilane in vapor phase.....	85
A-6 Water contact angle data (θ_A) of PVA-silanol fiber mats after silanization with Di- and Trichlorosilane in vapor phase.....	85
A-7 Water contact angle data (θ_A) of PVA-silanol fiber mats after silanization with Mono-, Di-, and Alkylrichlorosilane in solution.....	86
A-8 Water contact angle data (θ_A) of PVA-silanol beaded fiber mats after silanization with Mono-, Di- and Trichlorosilane in vapor phase.....	86
A-9 Water contact angle data (θ_A) of PVA-silanol beaded fiber mats after silanization with Mono-, Di- and Trichlorosilane in solution.....	86

LIST OF FIGURES

Figures	Pages
2.1 Droplet of water deposited on two surfaces of different energies: (a) wetting surface ($\theta < 90^\circ$), (b) nonwetting surface ($\theta > 90^\circ$).....	3
2.2 Surface tension on the three phase contact line of a liquid droplet deposited on a substrate	4
2.3 Advanced (θ_A) and receding (θ_R) angles of a liquid droplet on a tilted surface.....	6
2.4 The two superhydrophobic states: in the Wenzel state (a), the liquid follows the solid surface. In the Cassie state (b), it only contacts the top of the asperities, leaving air below.....	7
2.5 Millimetric water drops (of the same volume) deposited on a superhydrophobic substrate consisting of dilute pillars ($\phi_s = 0.01$). (a) The right drop has been pressed, which induced a Wenzel state, characterized by a smaller angle (the roughness is very low). The light passes below the left drop, indicating a Cassie state. (b) Ten minutes later, the drop volumes have decreased, owing to evaporation, and angles became receding ones. The difference of hysteresis between both states is clearly visible: the Wenzel drop even became hydrophilic.....	9
2.6 SEM images of carbon nanotube forest: before (a) and after coating (b) with PTFE.....	14
2.7 (a) SEM images of Au catalyzed ZnO thin film, (b) Water droplet on the superhydrophobic and superhydrophilic surface of ZnO.....	15
2.8 SEM images of anisotropic ACNT microstructures, (A, B and C) Periodic ACNT arrays with pillar height of 20, 15 and 10 μm , respectively. In the figure D, the ACNT array at A was magnified, and a, b, c represents vertical ACNT arrays on the top of pillars, horizontal ACNT array on the side walls of pillars, and ACNTs grown from the bottom of the templates, respectively.....	17

2.9	SEM images of the surfaces: (a) square (b) staggered rhombus, (c) star and (d) indented square reported by Öner and McCarthy.....	19
2.10	SEM images of polypropylene as a function of argon/PTFE plasma reaction time.....	20
2.11	(a) SEM image of the surface containing staggered rhombus posts. (b) SEM image of the surface shown in panel after being coated with a cross-linked hydrophobic polymer network.....	21
2.12	Scanning Electron Microscope (SEM) of a Lichao's Surface ($\theta_A/\theta_R = 180^\circ/180^\circ$).....	22
2.13	Schematic diagram shows polymer nanofibers forming by electrospinning process.....	24
2.14	Hydrolysis of PVAC to produce PVA: (a) partially hydrolyzed; (b) fully hydrolyzed.....	26
2.15	Contact angles and surface morphologies of four silica films with TFCS self-assembly monolayer. (a), (b), (c) and (d) are smooth surface, nanoparticles surface, nanorods surface and nanofibers surface and their corresponding contact angles after self-assembly respectively.....	30
2.16	SEM images of the PCL electrospun mats: (a1) fiber mats and (a2) beads fiber and (b) contact angles for PPFEMA-coated PCL mats.....	31
2.17	SEM images of electrospun mat, showing similar topography of (a) PS-PDMS/PS and (b) PS fibers.....	32
2.18	SEM images of (a) silica microspheres of 700 nm in size and (b) polystyrene latex spheres of 237 nm in size.....	33
2.19	SEM images of electrospun composite nanofibers and silica particles: (a, b) with monodisperse silica particles of 50 nm in size before and after calcinations, respectively; (c, d) with bidisperse silica particles of 50 and 700 nm in size before and after calcination, respectively.....	33
2.20	Possible products of the reaction of alkylchlorosilanes with silicon dioxide surfaces.....	36
2.21	Schematic representation of the Young's equation.....	39

2.22	Schematic representation of wettability.....	39
2.23	Schematic representation of the SEM work.....	41
2.24	Schematic representation of the directors collects of X-rays in SEM....	41
3.1	Experimental set-up for electrospinning (grounded target plat collector) :(a) a schematic drawing and (b) a real set-up.....	44
4.1	Relationship between viscosity and concentration of PVA solution.....	48
4.2	SEM micrographs of electrospun fiber mats from PVA solutions with different concentration: (a) 5%, (b) 6%, (c) 7%, (d) 8%, (e) 10%, and (f) 12%. Original magnification was 10,000x.....	49
4.3	Average diameters (nm) of PVA fibers electrospun from PVA solutions at various concentrations	50
4.4	Water contact angle (θ_A) of electrospun PVA fiber mats as a function of PVA concentration.....	52
4.5	SEM micrographs of electrospun PVA fiber mats after the reactions with (a) HFBC and (b) LC in solution for 3 h. Original magnification was 6,000x.....	53
4.6	SEM micrograph of electrospun PVA fiber mats after soaking in toluene for 3 h. Original magnification was 10,000x.....	53
4.7	SEM micrographs of PVA fiber mats after a reaction with acyl chlorides: (a) BC, (b) HC, (c) LC, and (d) HFBC.....	56
4.8	ATR-FTIR spectra of PVA fiber mats before (a) and after esterified with BC (b) and HFBC (c).....	57
4.9	Silicon/carbon ratio (■) and fiber diameter (□) of PVA fiber mats as a function of number of SiCl ₄ /H ₂ O reaction cycle.....	58
4.10	SEM micrographs of PVA fiber mats after a reaction with SiCl ₄ /H ₂ O: (a) 1 cycle, (b) 3 cycles, and (c) 5 cycles. Original magnification was 10,000x.....	59
4.11	ATR-FTIR spectra of PVA fiber mats (a) and PVA-silanol fiber mats before (b) and after silanized with CDODS (c), DDS (d) TOS (e), and TFOS (f).....	63

4.12 SEM micrographs of PVA-silanol fiber mats after silanization with DDS in solution with magnification of 10,000X (a1) and 50,000X (a2), in vapor phase with magnification of 10,000X (b1) and 50,000X (b2).....	65
4.13 SEM micrographs of PVA-silanol fiber mats after silanization in vapor with CDPS with magnification of 10,000X (a1) and 50,000X (a2), CDOS with magnification of 10,000X (b1) and 50,000X (b2), and CDODS with magnification of 10,000X (c1) and 50,000X (c2).....	66
4.14 SEM micrographs of PVA-silanol fiber mats after silanization in solution with CDPS with magnification of 10,000X (a1) and 50,000X (a2), CDOS with magnification 10,000X (b1) and 50,000X (b2), and CDODS with magnification of 10,000X (c1) and 50,000X (c2).....	67
4.15 SEM micrographs of PVA-silanol fiber mats after silanization in vapor phase with TMS with magnification of 10,000X (a1) and 50,000X (a2), TFOS with magnification of 10,000X (b1) and 50,000X (b2), and TOS with magnification of 10,000X (c1) and 50,000X (c2).....	69
4.16 SEM micrographs of PVA-silanol fiber mats after silanization with TMS in solution with magnification of 10,000X (a1) and 50,000X (a2).....	70
4.17 SEM micrographs of PVA-silanol bead fiber mats after silanization with DDS and TMS in solution with magnification of 10,000X (a1) and (a2), in vapor phase with magnification of 10,000X (b1) and (b2)..	72

LIST OF ABBREVIATIONS

BC	: Butyryl chloride
CAH	: Contact angle hysteresis
CDODS	: Chlorodimethyloctadecylsilane
CDOS	: Chlorodimethyloctylsilane
CDPS	: Chlorodimethylpropylsilane
DDS	: Dichlorodimethylsilane
HC	: Heptanoyl chloride
HFBC	: Heptafluorobutyryl chloride
LC	: Lauroyl chloride
PVA	: Poly(vinyl alcohol)
SEM	: Scanning Electron Microscope
TFOS	: Trichloro(1 <i>H</i> ,1 <i>H</i> ,2 <i>H</i> ,2 <i>H</i> -perflurooctyl)silane
TMS	: Trichloromethylsilane
TOS	: Trichloro(octyl)silane
WCA	: Water contact angle
θ_A	: Advancing contact angle
θ_R	: Receding contact angle

CHAPTER I

INTRODUCTION

1.1 Statement of Problem

The wettability of a solid surface is governed by both surface chemistry or surface energy and the geometrical microstructure of the surface, and important for various commercial applications. It is well known that when a surface exhibits a water contact angle exceeding 150° , it is considered “superhydrophobic”. Nature exhibits this phenomenon in “lotus leaf effect” to harness the roll-off action for self-cleaning of leaves which has been attributed to a combined micro and nanoscale morphology of its surface. In brief, the surface of the lotus leaf is textured with micron-sized hills and valleys (bumps) that are decorated with nanometer sized particles of a hydrophobic wax like material, which prevents the penetration of the water into valleys. As a result, water cannot wet the surface and therefore forms nearly spherical water droplets, leading to superhydrophobicity. Achieving superhydrophobicity is of great current interest in view of its diverse applications such as water repellency, self-cleaning and antifouling properties.

For the fabrication of artificial superhydrophobic surfaces, a combination of creating a rough structure on a hydrophobic surface and lowering the surface energy with a rough surface by chemical modification is required. Based on these two principles, many superhydrophobic surfaces have been prepared using various strategies including the generation of rough surfaces followed by the modification with low surface energy molecules such as fluorine-based or silicone-based silanes or roughening the surface of hydrophobic materials and creating well-ordered structures using micromachining such as mechanical abrasion, etching, anode oxidation, molding, and lithography.

Electrospinning is a simple but versatile method to produce continuous fibers having a size ranging from micrometer to nanometer (<100 nm). The method employs electrostatic forces to stretch a polymer jet and make superfine fibers. Numerous polymeric materials have been electrospun into continuous and uniform fibers. It has

been shown that charge density of the electrified jet, surface tension, and viscoelasticity of the polymer solution play important roles both in making the production of fibers possible and in controlling the size and uniformity of the fibers. Recent works has demonstrated a potential of the electrospinning process for introducing a rough surface coating of hydrophobic materials such as poly(styrene-*b*-dimethylsiloxane) (PS-PDMS), perfluoroalkyl ethyl methacrylate (PPFEMA).

Here we propose to generate hydrophobic coating by firstly creating a rough structure by electrospinning of poly(vinyl alcohol) (PVA) to produce PVA fiber mats. Taking advantage of hydroxyl group availability in PVA structure, hydrophobicity is thereafter introduced by esterification using acyl chloride and silanization using silane reagents. Unlike the previous work which mostly focused on either electrospinning of hydrophobic polymer or non-specific chemical treatment (i.e. plasma polymerization) of electrospun polymer, this study used hydrophilic PVA as a material for electrospinning and then fine tuned the hydrophobicity of the electrospun PVA fiber mats by varying reaction conditions and reagents that can react with the hydroxyl groups of PVA. It is anticipated that the information gained from this study will be useful for the development of superhydrophobic coating using electrospinning process.

1.2 Objective

To generate hydrophobic coating by a combination of electrospinning and chemical modification of poly(vinyl alcohol).

1.3 Scope of Investigation

The stepwise investigation was carried out as follows.

1. Literature survey for related research work
2. To prepare poly(vinyl alcohol) fiber mats by electrospinning
3. To modify the surface of poly(vinyl alcohol) fiber mats by chemical reaction of hydroxyl groups.
4. To characterize the surface-modified poly(vinyl alcohol) fiber mats

CHAPTER II

THEORY AND LITERATURE REVIEW

2.1 Surface Wetting

2.1.1 Wetting Theory

On the subject of wetting theory, dewetting and spreading, one can find extensive amount of theoretical and experimental articles. Even though these subjects are extensively studied, they are still attracting many researchers attention especially for industrial expectations [1]. The wetting properties of a surface is defined according to the angle θ , when we place a liquid droplet onto a solid substrate, there are three phases in contact (liquid-solid-air Figure 2.1(a)).

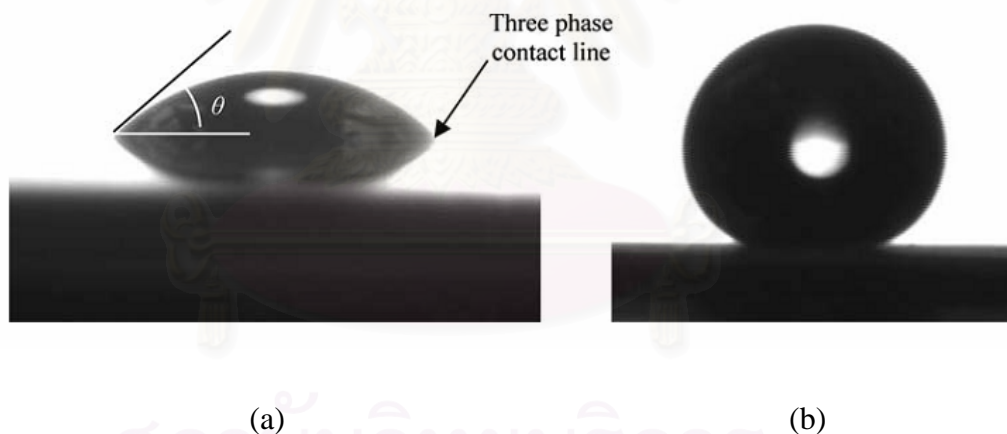


Figure 2.1 Droplet of water deposited on two surfaces of different energies: (a) wetting surface ($\theta < 90^\circ$), (b) nonwetting surface ($\theta > 90^\circ$) [6]

A surface is regarded as wetting when the contact angle, which forms a drop with this one, is lower than 90° (Figure 2.1(a)). In the opposite case (the contact angle is higher than 90°), the surface is nonwetting (Figure 2.1(b)). For water, the terms “hydrophilic” and “hydrophobic” are commonly used for wetting and nonwetting surfaces, respectively.

The contact angle of liquid on a surface according to the surface tension is given by the relation of Young [2].

$$\cos \theta = \frac{\gamma_{SV} - \gamma_{SL}}{\gamma_{LV}} \quad (2.1)$$

Where θ is the contact angle of liquid with solid, and γ_{SV} , γ_{SL} and γ_{LV} are the surface tensions at the interface of solid-vapor, solid-liquid and liquid-vapor, respectively (Figure 2.2). It is expressed in energy per unit of area (mJ.m^{-2}), but can also be regarded as a force per unit of length (mN.m^{-1}).

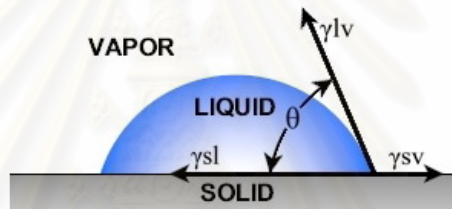


Figure 2.2 Surface tension on the three phase contact line of a liquid droplet deposited on a substrate [6].

When a liquid is placed in contact with the solid, capillary forces drive the interface spontaneously towards equilibrium. As the drop spreads, the contact angle relaxes from its initial maximum value of 180° at the moment of contact to its equilibrium angle θ in the case of partial wetting or 0° , if the liquid wets the solid completely [3].

According to the Young's equation, If $(\gamma_{SV} - \gamma_{SL})$ is larger than γ_{LV} , the drop tends to spread completely ($\theta = 0^\circ$) and wet the solid. Such behavior can be observed in the case of silicone oil on most solids. Conversely, a liquid film coating a solid will be stable if the same condition is satisfied. This explains why low surface tension liquids wet most surfaces. For this reason, surfactants, which lower the liquid/vapor surface tension, will often be added to a paint to make it wetting. In the second case, if $(\gamma_{SL} - \gamma_{SV})$ is larger than γ_{LV} , the drop should be in a pure drying

situation, sitting on the solid like a marble ($\theta = 180^\circ$). But there is no physical system which realizes this complete drying situation [2].”

2.1.2 Definition of Commonly Used Terms in Hydrophobicity

Indeed, the formula of Young considers that there is only one contact angle, the static contact angle. However, this configuration exists only for perfect surfaces. Generally, surfaces present imperfections related to physical defects like roughness or to chemical variations. The contact angle measurements are mainly divided into two, as static contact angle and dynamic contact angle measurements.

In the static contact angle measurement, a drop of liquid is gently deposited on a surface and its contact angle is measured. It is also termed as stationary “advancing” contact angle [4]. And the dynamic contact angle describes the happenings at the liquid-solid boundary during the wetting and dewetting processes. Dynamic contact angle can be measured either by moving the deposited liquid with a speed as constant as possible. A drop of liquid is deposited on the solid surface and the drop is slowly enlarged or advanced by addition of more liquid. The contact angle initially increases than the drop front starts to move as the drop advances. This is the maximum angle that can be achieved and this measurement is called the “advancing contact angle (θ_A)” measurement. By continuously wetting fresh surfaces, the advancing angle represents the contact angle which is formed directly on the contact of liquid and solid. This large droplet is drawn back into the syringe and the liquid front starts to recede. The contact angle measured during this event is termed as “receding contact angle (θ_R)”. The receding contact angle allows making a statement about the macroscopic roughness of the solid. The difference between these two angles ($\theta_A - \theta_R$) is called contact angle hysteresis (CAH). While this force is opposed to droplet motion, the small hysteresis is, the more it will be easy to move the liquid droplet.

An alternative dynamic contact angle measurement method is by slowly tilting the surface and measure the angle of inclined surface at which the drop starts to roll (slide). So, this result is published as “the sliding (tilt) angle” data [5].

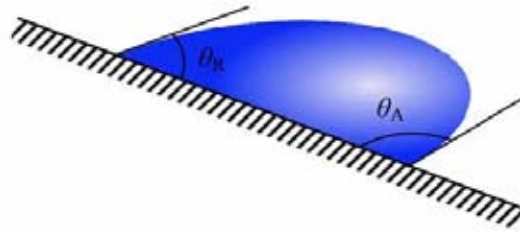


Figure 2.3 Advanced (θ_A) and receding (θ_R) angles of a liquid droplet on a tilted surface [6].

A superhydrophobic surface must possess both high static contact angle and low hysteresis or sliding angle. Only in this way, it can be named as superhydrophobic.

2.1.3 Theory of Superhydrophobicity [6,7]

Superhydrophobic surfaces can only be produced by generating sub-micron or micron level roughness on the inherently hydrophobic surfaces. The foundations of roughness induced hydrophobicity were developed by the articles of Wenzel [8] and Cassie-Baxter [9].

These two models were highlighted by the experiment of Johnson and Dettre [10]. Many research teams have tried to understand in more detail the superhydrophobicity phenomenon and particularly the difficulty of the wetting transition from Wenzel to Cassie configuration [11]. A drop on a rough and hydrophobic surface can adopt two configurations: a Wenzel (complete wetting) and a Cassie-Baxter configuration (partial wetting), as presented in Figure 2.4 (a) and (b), respectively. In both cases, even if locally, the contact angle does not change (angle of Young), an increase in the apparent contact angle θ^* of the drop is observed.

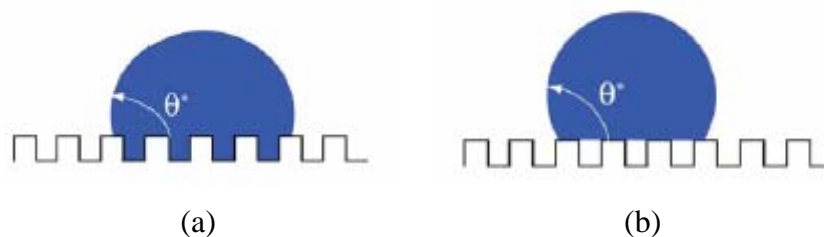


Figure 2.4 The two superhydrophobic states: in the Wenzel state (a), the liquid follows the solid surface. In the Cassie state (b), it only contacts the top of the asperities, leaving air below [6].

In the first case (Wenzel scenario), the increase of the surface area (due to the presence of the texture) amplifies the natural hydrophobicity of the material [8]. Thus the key parameter controlling the contact angle θ^* on this surface is the solid roughness, r .

$$r = \frac{\text{actual surface}}{\text{geometric projected surface}} \quad (2.2)$$

In other words, the solid surface energy can be seen as multiplied by the factor r , which yields:

$$\cos \theta^* = r \cos \theta \quad (2.3)$$

where θ is the Young contact angle, fixed by the chemical natures of the solid, liquid and vapor.

Equation 2.3 predicts that the contact angle on a hydrophobic material ($\theta > 90^\circ$) will increase with the roughness ($\theta^* > \theta$). This looks like a simple and attractive solution for inducing superhydrophobicity: the rougher the material, the higher the contact angle. However, this is not that simple, for two reasons: firstly, contact angles generally spread in quite a large interval, contrasting with equation 2.3 which predicts a unique angle. This interval, often referred to as the contact angle hysteresis, is responsible for the sticking of drops, an effect in contradiction with water repellency. In a Wenzel state, the hysteresis will be very large: trying to remove a

liquid makes it contact itself (owing to the fraction left in the textures), which yields a low “receding” contact angle—values as low as 40° were reported, making this state hydrophilic like in the receding stage. The second reason which makes it impossible to reach high values of θ^* , as expected from equation 2.3 for r large and $\theta > 90^\circ$, can be guessed quite easily: for very rough hydrophobic materials, the energy stored for following the solid surface is much larger than the energy associated with the air pockets sketched in Figure 2.4 (b) [12-14].

In this state (first suggested by Cassie and Baxter), the liquid only contacts the solid through the top of the asperities, on a fraction that we denote as ϕ_s . If only air were present between the solid and the liquid (as for a water drop on a very hot plate), the “contact angle” would be 180° : the smaller ϕ_s , the closer to this extreme situation, and thus the higher the hydrophobicity. More precisely, the contact angle θ^* of drop [Figure 2.4 (b)] is an average between the angles on the solid (of cosine $\cos\theta$), and on the air (of cosine -1), respectively weighed by the fractions ϕ_s and $1 - \phi_s$, which yields:

$$\cos \theta^* = -1 + \phi_s (\cos \theta + 1) \quad (2.4)$$

For $\theta = 110^\circ$ and $\phi_s = 10\%$, we find that θ^* is about 160° . In this case, 90% of the drop base contacts air. This makes it understandable that the corresponding hysteresis is observed to be very low (typically around 5 to 10°), as first reported by Johnson and Dettre [10]: the liquid has very little interactions with its substrate. Hence, this state will be the (only) repellent one, since it achieves both a large contact angle and a small hysteresis (Figure 2.5).

θ^* monotonously increases as ϕ_s decreases, suggesting that ϕ_s should be made as small as possible. But reducing ϕ_s also makes the roughness decrease, so that the critical roughness r_c can be reached below which the Wenzel state is favored [12, 13]. The quantity r_c is easily deduced from the intersection of equation 2.3 and 2.4, and is found to be $(\phi_s - 1)/\cos \theta + \phi_s$, which is generally close to $-1/\cos\theta$ (since we will often have: $\phi_s \ll 1$). For $\theta = 120^\circ$ (a high value for the Young angle, obtained on fluorinated substrates), the state will thus be favored for roughness

factors larger than 2. Conversely, Öner and McCarthy experimentally observed that below a critical density of defects (i.e. below a critical roughness), there is indeed a serious deterioration of the water-repellent properties [15].

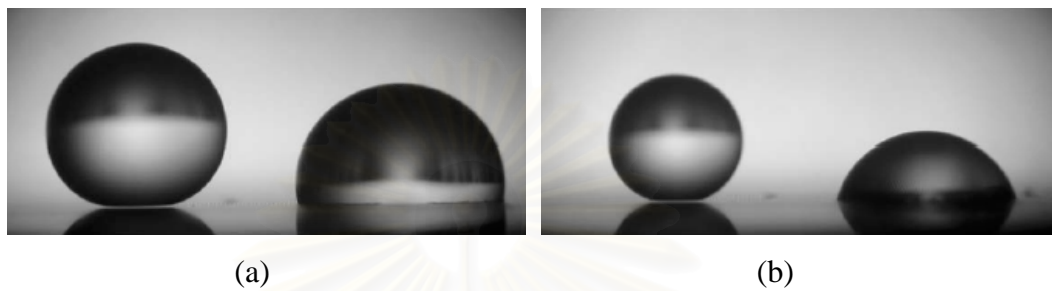


Figure 2.5 Millimetric water drops (of the same volume) deposited on a superhydrophobic substrate consisting of dilute pillars ($\phi_s = 0.01$). (a) The right drop has been pressed, which induced a Wenzel state, characterized by a smaller angle (the roughness is very low). The light passes below the left drop, indicating a Cassie state. (b) Ten minutes later, the drop volumes have decreased, owing to evaporation, and angles became receding ones. The difference of hysteresis between both states is clearly visible: the Wenzel drop even became hydrophilic [6].

In summary, Wenzel regime enhances water contact angle by pinning of the liquid to the surface, whereas Cassie-Baxter regime enhances water contact angle by minimum contact with the solid surface. This difference strongly affects contact angle hysteresis (CAH) of the regimes as for Cassie regime hysteresis is lower than in Wenzel mode. So, sliding angle is lower and self-cleaning property is better.

A question may arise: when does a homogeneous wetting (Wenzel) turn to the heterogeneous (Cassie-Baxter) wetting, what is its limit? This has been first simulated by Johnson and Dettre on sinusoidal surfaces [10]. They showed that as the surface roughness factor increased, both water contact angle and hysteresis enhanced. However, after a certain limit (~ 1.7), as the water contact angle continued to increase, hysteresis started to decrease. This decrease in hysteresis is a consequence of the switching of the dominant hydrophobicity mode from Wenzel to

Cassie-Baxter due to the increase of the air fraction at the interface between the solid and water.

2.1.4 Chemistry Driven Hydrophobicity

Chemical hydrophobicity is produced by employing hydrocarbon, fluorine or siloxane rich materials in the chemistry of the surface. A well known hydrophobic material is polytetrafluoroethylene (PTFE), which has trade name of Teflon. It has high water and oil resistance in addition to its organic solvents resistance. Here, because fluorine has a small atomic radius and the highest electronegativity in the periodic table, it forms a stable covalent bond with carbon, so significantly lowers surface free energy [16]. Water contact angles and surface energies of several plastics are listed in Table 2.1.

Table 2.1 Water contact angle and surface energies of common plastics.

Material	Surface energy (mJ m ⁻²)	Water Contact Angle (°)
Polyacrylonitrile (PAN)	40	73
Polymethylmethacrylate (PMMA)	41	74
Nylon 6,6	38	79
Polyethylene	33	96
Polypropylene	26	108
Paraffin	19	110
Teflon	18	112

Zisman *et al.* reported that in the case of hydrocarbon surface, the surface energy decreases in the following order: $-\text{CH}_2-$ (bulk polyethylene); a mixture of $-\text{CH}_2-$ and $-\text{CH}_3$ groups (thin films of hexadecane); $-\text{CH}_3$ groups in a monolayer (octadecylamine monolayer); $-\text{CH}_3$ groups in a crystal plane (hexatriacontane cleavage surface). A similar ordering is observed for fluorocarbon surfaces (just replace the hydrogen with the fluorine atom) [17]. Tsibouklis and Nevell has indicated similar ordering as $-\text{CH}_2-$ (36 mJ m⁻²) > $-\text{CH}_3$ (30 mJ m⁻²) > $-\text{CF}_2-$ (23 mJ

$\text{m}^{-2}) > -\text{CF}_2\text{H} > -\text{CF}_3$ (15 mJ m^{-2}) [18]. These indicate that the lowest surface energy can be obtained by closely packed $-\text{CF}_3$. Nishino *et al.* generated the closest hexagonal packed $-\text{CF}_3$ groups with epitaxially grown n-perfluoroeicosane, $\text{C}_{20}\text{F}_{42}$ and measured 122° advancing and 116° receding contact angle, and a surface energy of 6.7 mJ m^{-2} [16]. The maximum surface roughness was measured as 8 \AA on this surface.

Tsibouklis *et al.* had reported and experimentally proved several rule of thumbs of low surface energy surfaces especially for antifouling applications [18-21]. They suggested that “amorphous, comb-like polymers possessing a flexible linear backbone onto which side chains with low intermolecular interactions are attached will exhibit low values of surface energy”. The wetting behavior can be summarized by four structural features of the macromolecule: i) nature of the pendant chain; ii) length of the pendant chain; iii) nature of the linking moiety; and iv) nature of the polymer backbone. Their data showed that nature of the pendant chain did the most remarkable effect on surface energy. Such as, substitution of fluorinated groups as pendant chains yielded much lower surface energies than their alkyl-substituted counterparts. The length of the pendant perfluorinated moiety is also very crucial. As the length of the pendant moiety increases, the surface tension of the film decreases. However, roughness of the film increases as well. They published surface energy as low as 5.5 mJ m^{-2} , but the surface had the roughness of 8.25 nm , with 125° WCA and 30° hysteresis [18].

2.1.5 Literature Review

In this section, the recent publications on the field of superhydrophobicity were briefly reviewed, and their chief results were presented.

Otten and Herminghaus have studied two superhydrophobic plant surface with totally different surfaces morphologies in their article [22]. One is *Indian Cress*, which has a surface like Lotus leaf, with a surface decorated with three different length scales of micrometric roughness (First length scale is a few tens of microns by the epidermal cells, second, $\sim 1 \text{ }\mu\text{m}$ wax crystals on top of the cell surface, and the

last was the distance of the wax crystal bundles, $\sim 5 \mu\text{m}$). Other is Lady's Mantle, which has a hairy water-repellent surface. Both let water droplets run off easily over their surfaces. Also, a model system composed of a patterned substrate which was made up of carbon nanotube bundles with $10 \mu\text{m}$ high. In these bundles, each nanotube had a few nanometers diameter. First, they studied the Indian Cress surface. When a water droplet placed onto the rough surface of Indian Cress, $\sim 180^\circ$ water contact angle (WCA) was measured. However, when micron-scale water droplets were grown by cooling the solid surface, $\sim 140^\circ$ WCA was measured. The reason of this WCA loss is; when droplet is placed onto the surface, it traps air underneath the water between roughness, but when a droplet was slowly grown by condensing water on the surface, the condensed water fills the cavities during growing, thus no air pockets was generated and lower WCA was observed. The same behavior was observed for the carbon nanotube bundles decorated surface. Thus, the water repellence of micro-rough plant leaves is due to a specific surface comprising a hierarchy of length scales. The material of which the structure was made of must possess a contact angle $>90^\circ$, and air is entrapped below the water droplet resulting very high WCA.

However, the hairs of Lady's Mantle exhibited WCA well below than 90° both for advancing and receding WCA measurements. During the condensing of water droplet on the surface, first the droplets started to nucleate on the cuticula surface below the hairs, then after a certain volume suddenly the drop was lifted from the cuticula into the brush, and no decrease in WCA was measured between the condensed and normal water droplet cases. The lift of the droplet was explained energetically favorable situation of hydrophilic hairs than the hydrophobic cuticula. The water droplet prefers to pass to hydrophilic hairs. Their studies on the reason of high WCA has shown that when a water droplet was left or condensed on the surface, the hairs, which are underneath the droplet, prefer to create bundles, thus mechanically resists to the entrance of water droplet. This results a superhydrophobic surface. For hairy situation, the important parameters are the distance between the hairs (their density) and the hair's elastic modulus. So, a

different approach by nature to superhydrophobicity was presented and underlying mechanism was first presented.

A superhydrophobic surface via generating a vertically aligned multi-walled nanotube (MWNT) forest were created and coated with a nonwetting coating, PTFE. To deposit vertically aligned nanotubes, Lau *et al.* used a plasma enhanced chemical vapor deposition (PECVD) technique [23]. First, nickel (Ni) catalyst islands were formed on an oxidized (20 nm) silicon substrate through the sintering of a thin (5 nm) Ni film at 650°C. Second, nanotubes were grown from these islands of catalyst in a DC plasma discharge of acetylene and ammonia. The height of nanotubes was controlled by the plasma deposition time, where typical nanotube growth rate was 330 nm/min. A height of 2 μm nanotube forests with 10 MWNTs per μm^2 could be wetted by water easily. And when the samples were examined after drying, it was observed that the nanotubes forced into bundles under the surface tension effect of evaporating water. If taller (10-15 μm) nanotube forests were generated, WCA of 161° angle was observed for a short period of time. However, the droplets were not stable and with in a few minutes they swept into the forest voids. Then, the group coated the nanotubes in the forest with the PTFE, through a hot filament chemical vapor deposition (HFCVD) process.

In this respect, hexafluoropropylene oxide (HFPO) gas was thermally decomposed at 500°C to form difluorocarbene (CF_2) radicals, and radicals polymerized into PTFE with the aid of initiator. The advancing and receding WCA of PTFE coated nanotubes were found as 170° and 160°, respectively. In addition to static measurements, dynamic measurements were also performed. The bouncing of a water droplet on the forest surface was imaged by a high speed camera. Also, condensations of micrometer diameter droplets were investigated with ESEM and no wetting was observed. When the ϕ_S in Cassie-Baxter equation was calculated, it was found as 11% for 60 nm (coated) average radius 10 nanotubes per μm^2 surfaces. This ϕ_S value results 170° and 158°, respectively, which was in good agreement with the measured values. Finally, the group measured the advancing and receding WCA of the coated nanotube forests at different heights (0.2 to 1.1 μm). It was observed that

as the tube height increased, advancing did not change too much, but receding angles were increased, so hysteresis was decreased.

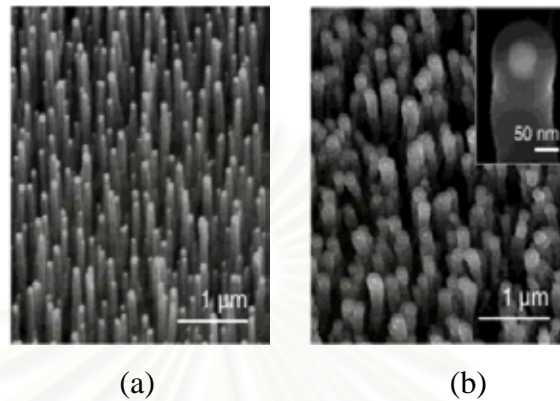


Figure 2.6 SEM images of carbon nanotube forest: before (a) and after coating (b) with PTFE [23].

Liu *et al.* synthesized a superhydrophobic surface, which could reversibly turn to superhydrophilic when exposed to UV illumination [24]. The superhydrophobic surface was synthesized by Au-catalyzed chemical vapor deposition of ZnO. Equal amount of carbon powder and ZnO powder were placed into a quartz boat which was placed into a furnace with Au-coated substrates. After heated to 600-650°C at a rate of 1° C/sec and kept for 60 minute at that temperature under Argon gas flow, the substrates were covered with ZnO. In the SEM images it was seen that, the surface was covered with many block-shaped protuberances with 320-560 nm which were decorated with many ZnO nanopillar with a size from 21.6 to 41 nm. The AFM roughness was found within the range of 600-1191 nm. On this surface, water droplets made 164.3 contact angles. When the surface was subjected to UV illumination, within 1000 minutes, the WCA were decreased <5°. If this illuminated surface was placed in the dark or was heated, within several days, superhydrophilic surface was reconverted to superhydrophobic. The reason of this reversible change was explained as: “the electron and hole generated by ZnO under band gap illumination will move to the surface to react with the lattice metal ions Zn^{+2} to form Zn defective sites and the lattice oxygen to form the surface oxygen

vacancies, respectively. When it was placed in the dark or was heated, oxygen atoms that result from the recovery of its initial state can replace these oxygen vacancies gradually”, so the wettability is reconverted.

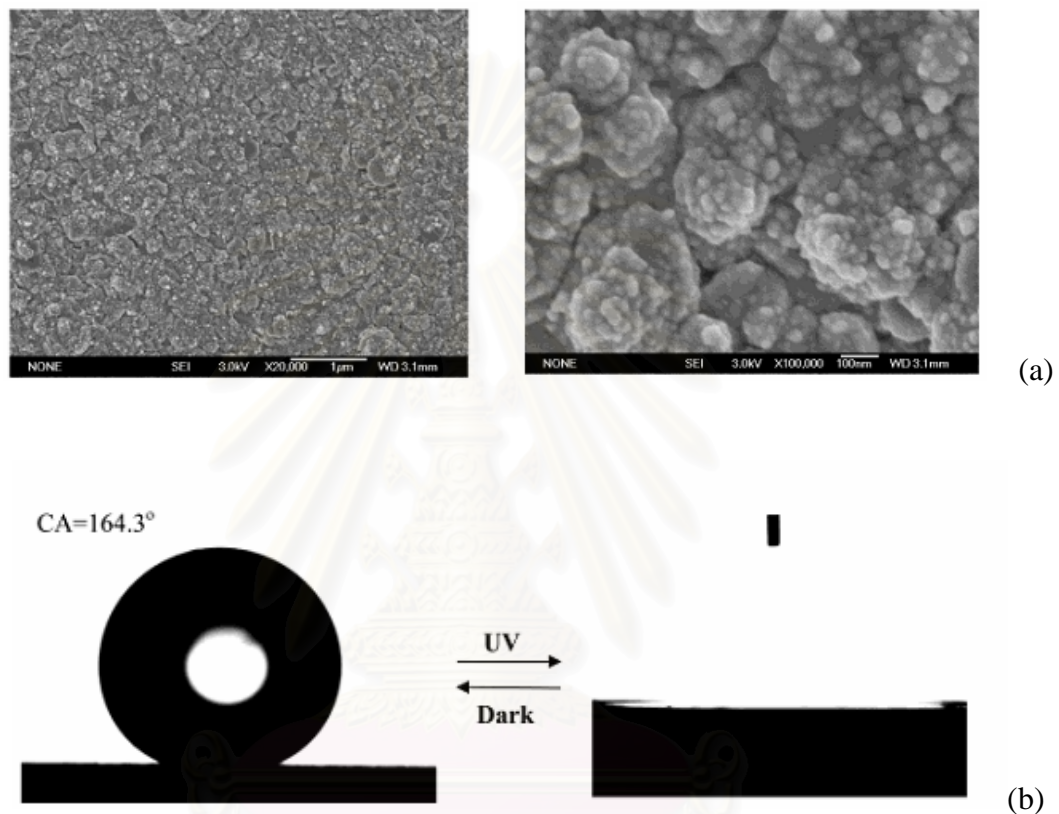


Figure 2.7 (a) SEM images of Au catalyzed ZnO thin film, (b) Water droplet on the superhydrophobic and superhydrophilic surface of ZnO [24].

A novel pattern for controlling the surface wettability is by adjusting the anisotropic structure of surface generated by aligned carbon nanotube (ACNT) films. ACNTs can be grown normal to the substrate by chemical vapor deposition (CVD) method. The nanotubes are dense and at the same length. By using ACNTs, Sun *et al.* proposed a method to control the wettability of surfaces [25]. They, first, manufactured patterned silicon templates with the square pillars of 30 μm in height, and 10 μm in width. As the spacing between pillars 6, 10, 13, 15 and 20 μm were selected. After this, by CVD, ACNTs were produced on the surface of silicon

template. At the horizontal sections of the template the ACNTs were grown vertically, whereas at the vertical regions (side-walls of pillars) the ACNTs were grown horizontally. The ACNTs diameters were ranging between 25 to 50 nm, and their length was around 10 μm . Thus, especially for the 6 and 10 μm spacing cases, the ACNTs on neighboring pillars touched each other and curled. Then, the ACNTs wettability was modified by vinyltrimethoxysilane (VTMS) and (2-(perfluorooctyl)ethyl)trimethoxy-silane (FETMS). The smooth films of VTMS and FETMS yielded WCA of $78.1 \pm 1.8^\circ$ and $111.9 \pm 2.1^\circ$, respectively. When the virgin silicon templates were covered with VTMS, the WCA was measured as $158 \pm 1.5^\circ$. For VTMS modified ACNT covered surfaces, the WCA was measured for 20, 15, 13, 10 and 6 μm spacing samples as $21.2 \pm 1.5^\circ$, $153.3 \pm 3.3^\circ$, $154.9 \pm 1.5^\circ$, $27.2 \pm 1.8^\circ$ and $20.8 \pm 2.3^\circ$, respectively.

While the wetting in 6 and 10 μm cases happened immediately, for 20 μm case, first, the droplet made a high contact angle, but it lowers within the time, and after about 10 seconds, it immediately spreaded. The reason of wetting at 6 and 10 μm were explained by the curling of ACNTs, and they facilitated the reach of water droplet to the horizontal ACNTs. Thus, the water droplet was spreaded in the horizontal segments due to the capillary effect. Because the ACNTs were not hydrophobic, in 13, 15 and 20 μm cases, there were less or no curling, so the vertical ACNTs restricted the reach of water to the horizontal sections. However, because the number of vertical ACNTs was lower in 20 μm spacing case, after a certain period the water could reach the horizontal segments and immediately spreads. In FETMS treated case, the WCAs were all measured higher than 150° . Because the ACNTs were intrinsically hydrophobic, when the water droplet reached the horizontal sections, wetting did not occur. These results showed that anisotropic microstructures can bring a better control over the surface wettability. By simply varying the spacing between the micropillars or coating of ACNTs, the transition between superhydrophobicity and high hydrophilicity can be induced.

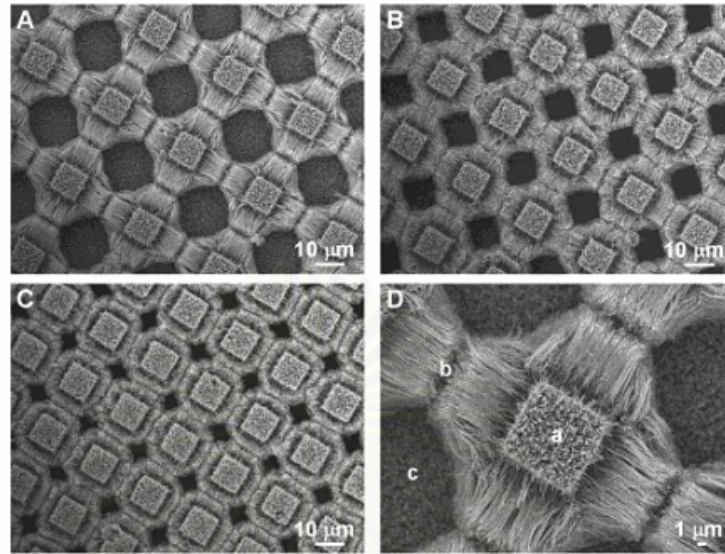


Figure 2.8 SEM images of anisotropic ACNT microstructures, (A, B and C) Periodic ACNT arrays with pillar height of 20, 15 and 10 μm , respectively. In the figure D, the ACNT array at A was magnified, and a, b, c represents vertical ACNT arrays on the top of pillars, horizontal ACNT array on the side walls of pillars, and ACNTs grown from the bottom of the templates, respectively [25].

Chen *et al.* prepared ultrahydrophobic and ultralyophobic surfaces using two different types of surface [26]. Plasma polymerization of 2,2,3,3,4,4,4-heptafluorobutyl acrylate on poly(ethylene terephthalate) yields surfaces with water contact angles of $\theta_A/\theta_R = 174^\circ/173^\circ$. And Argon plasma etching of polypropylene in the presence of poly(tetrafluoroethylene) renders surfaces with water contact angles as high as $\theta_A/\theta_R = 172^\circ/169^\circ$. Surfaces of compressed pellets of submicrometer, variable-diameter spherical particles of PTFE oligomers exhibit water contact angles of $\theta_A/\theta_R = 177^\circ/177^\circ$. These surfaces are rough at the micrometer and submicrometer scales, and water drops roll easily on all of them. The contact angle hysteresis is more important in characterizing lyophobicity than the maximum achievable contact angle and suggests that the terms ultrahydrophobic and ultralyophobic be reserved for materials upon which drops move spontaneously or easily on horizontal or near-horizontal surfaces. Moreover, They reported that

smooth ultralyophobic surfaces can be prepared by silanization of silicon wafers with $\text{Cl}(\text{SiMe}_2\text{O})_n\text{SiMe}_2\text{Cl}$ ($n = 0, 1, 2,$ and 3), $(\text{Me}_3\text{SiO})_3\text{SiCH}_2\text{CH}_2\text{Si}(\text{CH}_3)_2\text{Cl}$, and $(\text{Me}_3\text{SiO})_2\text{Si}(\text{CH}_3)\text{CH}_2\text{CH}_2\text{Si}(\text{CH}_3)_2\text{Cl}$. These surfaces exhibit much lower contact angles but little or no hysteresis, and droplets of water. And covalently attached monolayers are flexible and liquid-like and that droplets in contact with surface experience very low energy barriers between metastable states.

Öner and McCarthy discuss dynamic hydrophobicity from the perspective of the force required to move a water droplet on a surface and argue that the structure of the three-phase contact line is important [15]. They studied the wettability of a series of silicon surfaces that were prepared by photolithography and hydrophobized using silanization reagents. Hydrocarbon, siloxane, and fluorocarbon surfaces were prepared. The surfaces contain posts of different sizes, shapes, and separations. Surfaces containing square posts with X - Y dimensions of $32\ \mu\text{m}$ exhibited less ultrahydrophobic behavior with high advancing and receding water contact angles. Water droplets moved very easily on these surfaces and rolled off with slightly tilted surfaces. Contact angles were independent of the post height from 20 to $140\ \mu\text{m}$ and independent of surface chemistry. Water droplets were pinned on surfaces containing square posts with larger dimensions. Increasing the distance between posts and changing the shape of the posts from square to staggered rhombus, star, or indented square (Figure 2.9) caused increases in receding contact angles. They ascribe these contact angle increases to decreases in the contact length and increases in tortuosity of the three-phase contact line. The maximum length scale of roughness that imparts ultrahydrophobicity is $\sim 32\ \mu\text{m}$.

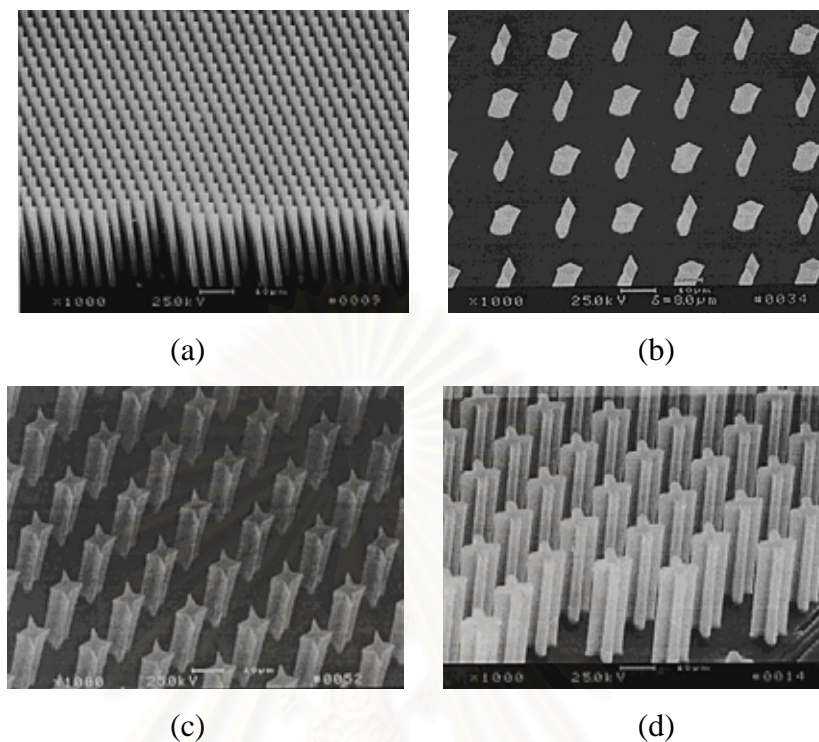


Figure 2.9 SEM images of the surfaces: (a) square (b) staggered rhombus, (c) star and (d) indented square reported by Öner and McCarthy [15]

Youngblood and McCarthy reported that the preparation of ultrahydrophobic surfaces, which exhibit both high advancing (θ_A) and high receding (θ_R) water contact angles, by simultaneous etching of polypropylene and sputtering of poly(tetrafluoroethylene) (PTFE) using inductively coupled radio frequency argon plasmas [27]. The semicrystalline polypropylene surface is roughened due to the differential rates at which the crystalline and amorphous regimes ablate and is also fluorinated by the fluorocarbon plasma that results from the ablation/depolymerization of PTFE. The roughness of the polypropylene is controlled by the time of plasma etching; features become smaller, more pronounced, more contorted and closer together with increasing reaction time. After a critical reaction time (between 60 and 90 min) (Figure 2.10), the surfaces became ultrahydrophobic, water droplets rolled easily on horizontal surfaces. The presence of PTFE increases the rate of polypropylene roughening by reactive ion etching. Wettability was found to depend on the size scale and topology of the roughness.

The most hydrophobic surfaces exhibited advancing and receding water contact angles of $\theta_A/\theta_R = 172^\circ/169^\circ$ and hysteresis was very low.

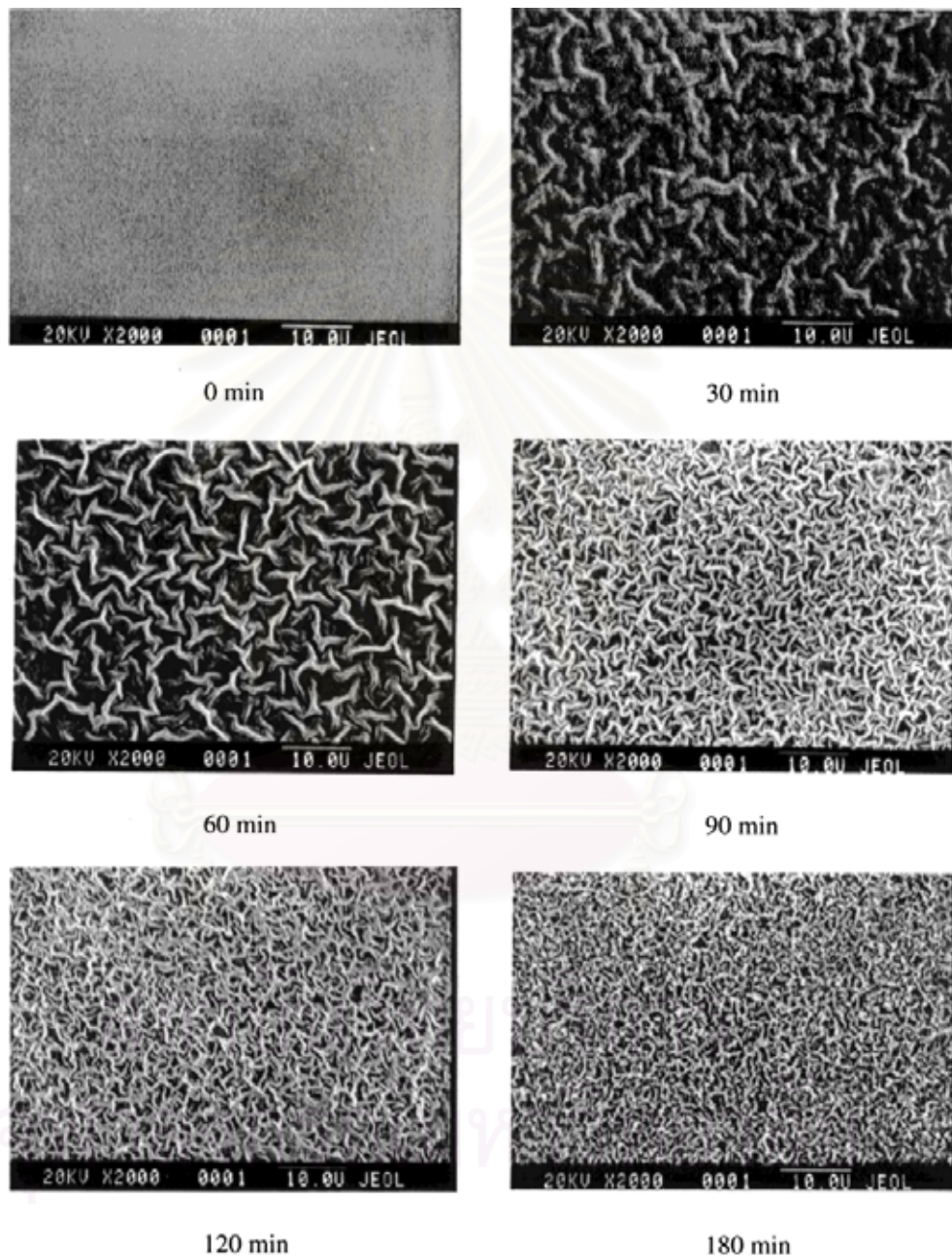


Figure 2.10 SEM images of polypropylene as a function of argon/PTFE plasma reaction time [27].

Gao and McCarthy explained: two reasons why two length scales of topography were important by hydrophobized surfaces containing staggered rhombus posts using two method [28]. One, using a dimethyldichlorosilane reaction in the vapor phase, introduces a smooth modified layer (Figure 2.11 (a)), and the other, a solution reaction using methyltrichlorosilane, imparts a second (nanoscopic) length scale of topography (Figure 2.11 (b)). The smooth modified surface exhibits contact angles of $\theta_A/\theta_R = 176^\circ/156^\circ$. Arguments are made that the pinning of the receding contact line by the post tops (with $\theta_A/\theta_R = 104^\circ/103^\circ$) is responsible for the hysteresis. The second level of topography raises the contact angles of the post tops and the macroscopic sample to $\theta_A/\theta_R = >176^\circ/>176^\circ$ and eliminates hysteresis. The increase in Laplace pressure due to the increase in the advancing contact angle of the post tops is a second reason that two length scales of topography are important.

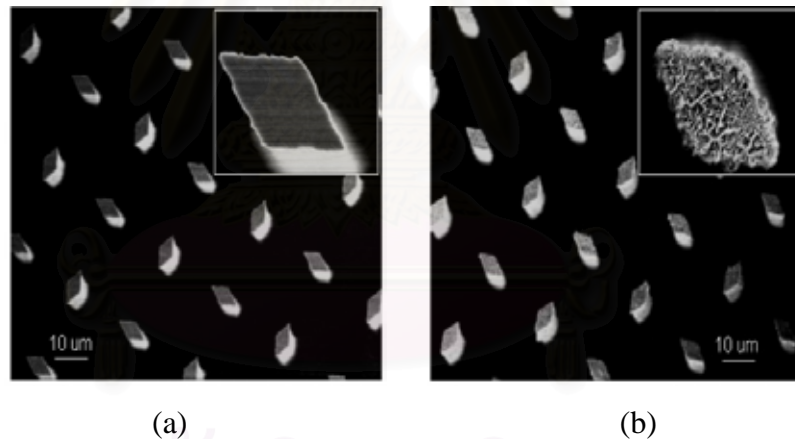


Figure 2.11 (a) SEM image of the surface containing staggered rhombus posts. (b) SEM image of the surface shown in panel after being coated with a cross-linked hydrophobic polymer network [28].

In the same year, the first perfectly hydrophobic surface that exhibits advancing and receding water contact angles of 180° were prepared by Gao and McCarthy [29]. To obtain convincing evidence that the contact angles of this surface are indeed 180° and to distinguish them from 179° , a new technique for testing extreme hydrophobicity was devised. The conditions used for this modification promote “vertical polymerization” [30] of MeSiCl_3 into a covalently attached

toluene-swollen 3-D methylsiloxane network. Rapid extraction of toluene by ethanol induces the phase separation observed. This procedure has been reproduced over 100 times, and extremely hydrophobic surfaces are always formed. “Perfectly hydrophobic” ($\theta_A/\theta_R = 180^\circ/180^\circ$, Lichao’s Surface) samples are formed in 70% of the cases. When the humidity is not sufficiently high or the reaction is not allowed to proceed for a sufficient length of time, smoother surfaces with lower contact angles form. When the humidity is too high, phase separation causes spherical-shaped particles and these surfaces exhibit lower contact angles.

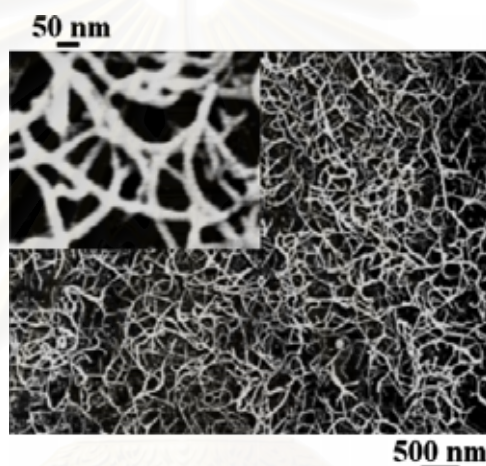


Figure 2.12 Scanning Electron Microscope (SEM) of a Lichao’s Surface ($\theta_A/\theta_R = 180^\circ/180^\circ$) [29].

Quarmyne and Chen reported the preparation of robust nanoscale inorganic layers on polymer film substrates [31]. Poly(tetrafluoroethylene-co-hexafluoropropylene) (FEP), poly(4-methyl-1-pentene) (PMP), and poly(ethylene terephthalate) (PET) were “activated” by the spontaneous adsorption of poly(vinyl alcohol); silica and titania were subsequently condensed on these surfaces by subsequent vapor phase reaction with either silicon tetrachloride (SiCl_4) or titanium tetrachloride (TiCl_4) and water (H_2O). The thickness and wettability of the inorganic layers can be controlled by the number of SiCl_4 or TiCl_4 and H_2O reaction cycles. Reactions between the nanoscale inorganic layers and monochlorosilanes for

silica and hydridosilanes for titania indicate that these surfaces have silica-like and titania-like reactivities.

2.2 Electrospinning Process

A number of processing techniques such as drawing, template synthesis, phase separation, self-assembly, electrospinning have been used to prepare polymer nanofibers in recent years. The electrospinning process seems to be the only method which can be further developed for mass production of one-by-one continuous nanofibers from various polymers [32].

Electrospinning is a unique process that used an electrical field to create an electrically charged jet of polymer solution or melt, which dries or solidifies to leave a polymer fiber. The first patent on electrospinning process was issued to Anton Formhals in 1934 [33]. Formhals' patent claimed the novelty of capable of producing parallel filaments in continuous length, enabling the filaments to be used in textile applications. Formhals modified the existing electrostatic spinning apparatus to allow collection of continuous fibers through the used of a drum take-up. At that time the produced fibers were still in the micrometers in diameters. Formhals's invention did not gain much attention since the concept was beyond his time and other available fiber spinning methods were more efficient and practical.

The electrospinning process can be described (based on the current trends of nanofiber development) thusly: when a high voltage is applied to a polymer solution, a high electric field is generated between a polymer fluid (contained in a spinning dope reservoir with a capillary tip or a spinneret) and a metallic fiber collection ground surface. As the intensity of the electric field is increased, the hemispherical surface of the fluid at the tip of the capillary tube elongates to form a conical shape known as the Taylor cone. Further increasing the electric field, a critical value is attained with which the repulsive electrostatic force overcomes the surface tension and the charged jet of the fluid is ejected from the tip of the Taylor cone. The electrically charged jet undergoes a series of electrically included bending instabilities during its passage to the collection surface which results in the hyperstretching of the jet. This stretching process is accompanied by the rapid

evaporation of the solvent molecules, further reducing the diameter of the polymer jet. The dry fibers are accumulated on the surface of the collection plate, resulting in a non-woven mesh of nano-to-micro diameter fibers. The process can be adjusted to control the fiber diameter by varying the electric field strength and polymer solution concentration, whereas the duration of the electrospinning controls fiber deposition thickness. A schematic drawing of the electrospinning process is shown in Figure 2.13.

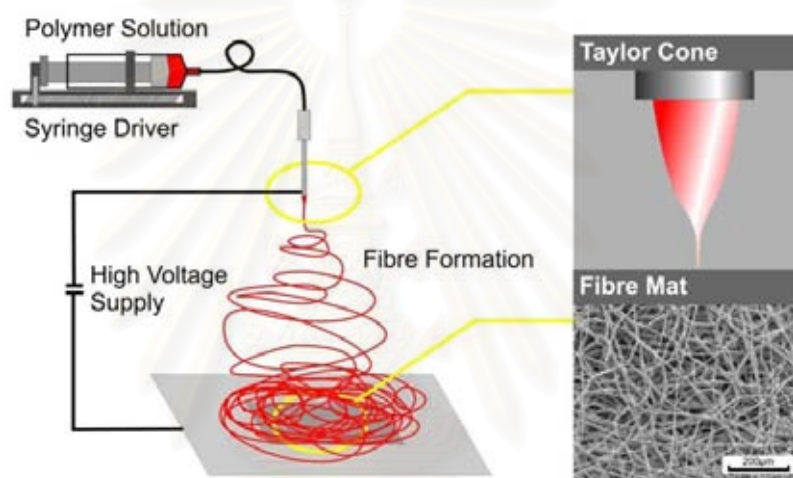


Figure 2.13 Schematic diagram shows polymer nanofibers forming by electrospinning process.

The properties of fiber obtained from this process depend on two types of parameter; the first is system parameters including molecular weight, molecular weight distribution, and architecture of the polymer e.g. branched or linear chain and solution properties (viscosity, conductivity and surface tension). The second one is processing parameters including electrical field strength, flow rate, solution concentration, distance between the capillary and the collector, and ambient parameters (temperature, humidity and air velocity in the chamber) [34].

The advantages of electrospinning process are simple equipment, requiring a short time, cost effective process and producing a very high orientation fiber with very small pore sizes. Therefore, electrospun fibers from electrospinning have

regained more attention probably due in part to interest in many applications such as in the field of filtration systems [35], medical prosthesis mainly grafts and vessels, tissue template [36], electromagnetion shielding, protective clothing [37], composite delamination resistance , and chemical and biochemical sensor [38].

2.3 Poly(vinyl alcohol) (PVA)

Poly(vinyl alcohol) (PVA), a water-soluble polyhydroxy synthetic polymer, is the largest volume synthetic resin produced in the world. It has been used since the early 1930s in a wide range of industrial, commercial, medical and food applications including resins, lacquers, surgical threads and food-contact applications because of its excellent chemical resistance, physical properties, and completes biodegradability [39, 40].

Table 2.2 General chemical identity and physical properties of poly(vinyl alcohol)

Identity/Properties	Detail
Structure formula	$(-\text{CH}_2\text{CHOH}-)_n(-\text{CH}_2\text{CHOCOCH}_3)_m$
Empirical formula	$(\text{C}_2\text{H}_4\text{O})_n(\text{C}_4\text{H}_6\text{O}_2)_m$
Physical appearance	White to off-white powder
Specific gravity	1.19 – 1.31
Solubility	Insoluble in aliphatic and aromatic hydrocarbons, esters, ketones, and oils; water soluble

General chemical and physical properties of PVA are summarized in Table 2.2. It is known that, the physical characteristics of PVA are dependent on its method of preparation from the hydrolysis, or partial hydrolysis, of poly(vinyl acetate) (Figure 2.14). PVA is generally classified into two groups, partial hydrolyzed (a) and fully hydrolyzed (b).

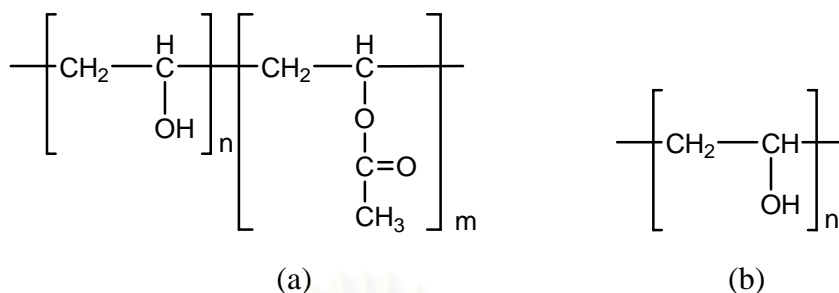


Figure 2.14 Hydrolysis of PVAC to produce PVA: (a) partially hydrolyzed; (b) fully hydrolyzed.

Varying the length of the initial vinyl acetate polymer and the degree of hydrolysis under alkaline or acidic conditions yields PVA products of differing molecular weights (20,000-400,000), solubility, flexibility, tensile strength and adhesiveness. Various properties are measured to characterize PVA such as pH, viscosity, loss on drying, melting point, reflective index, heavy metals and residue on ignition. These properties vary based on molecular weight and % hydrolysis for the grade of PVA [41].

PVA has grown hand in hand with fiber ‘Vinylon’ [42]. Vinylon is said to be the most similar to cotton fibers since this fiber is most moisture absorbent among synthetic fibers. Vinylon fiber is widely used for industrial, agricultural, fishing uses, because it is light in weight, durable and resistant to weathering. Vinylon was first developed in Japan before the Second World War, but was not commercial laboratories; much of the research was directed towards the synthesis of PVA as a raw material for Vinylon and towards the elucidation of the properties of PVA. The major emphasis in research was placed on the improvement of Vinylon fiber, including a search for polymers with higher degrees of polymerization, more uniform distribution, and higher degrees of crystallinity, to obtain the improvements of mechanical strength and water resistance needed for fiber applications [43]. In addition, PVA has also been widely used in non-fiber applications such as paper-coating, wrap sizing, adhesives (including protective colloids), film, etc [44].

2.4 Electrospinning of Poly(vinyl alcohol)

There are many researchers reported that PVA was successfully fabricated into ultrafine fiber by electrospinning and was used in several applications.

Ding *et al.* reported that nanoscale PVA fiber aggregates were successfully prepared with an electrospinning technique [42]. The average diameter of as-spun PVA ($M_w = 65,000$ Da; degree of hydrolysis (DH) = 96%) fibers ranged between about 100 and 500 nm [over the PVA concentration range of 8 to 16% w/v and the applied electrostatic field strength (EFS) of 19 kV/8 cm]. Additionally, a chemical crosslink method (using glyoxal) was successfully used to crosslink those nanoscale PVA fiber aggregates to obtain the better antiwater solubility and mechanical properties than the noncrosslinked PVA fiber aggregates.

Effects of molecular weight (M_w) on fibrous PVA produced by electrospinning were studied by Koski *et al.* [43], Lee *et al.* [44], and Jun *et al.* [45]. The first group reported that the average diameter of as-spun PVA ($M_w = 9,000$ -186,000 g/mol; DH = 98-99%) fibers ranged between about 250 nm and 2 μm (for the PVA concentration of 25% w/v and the applied electric field strength of 30 kV/10.2 cm). The concentration of the polymer in the solution was depending on the molecular weight and the fiber diameters increased with M_w and concentration. The second group reported that the average diameters of as-spun PVA (degree of polymerization = 4,000) fibers ranged between about 270 and 280 nm (for the PVA concentration of 7% w/v; the applied EFS of 20 kV/10 cm; flow rate = 1 mL/h). The higher molecular weight of PVA showed the results that the obtained fiber diameter and the superior the physical properties of PVA nanofabrics were higher. Another group reported that the average diameter of as-spun PVA ($M_w = 100,000$ -195,000 g/mol) fibers ranged between about 50 and 700 nm (for the PVA concentration of 6 and 8% w/v; the applied EFS of 55 kV/12 cm). Formation of beaded fiber combined with decrease fiber diameters was observed for low PVA concentration. Electrospinning of beads of PVA of different molecular weight resulted in less formation and smaller fiber diameter as compared to corresponding homopolymers of similar viscosity.

Wu *et al.* prepared nanofibrous PVA membranes by electrospinning and used these membranes for immobilization of enzymes cellulose [46]. PVA (degree of polymerization = 1750; DH = 98%) and cellulose were dissolved together (in an acetic buffer (pH 4.6) and electrospun (over the tip to target distance = 10 cm; the applied potential = 10 kV ; flow rate = 0.2 mL/h) into nanofibers with diameter of around 200 nm. The nanofibrous membrane was crosslinked by glutaraldehyde vapor and examined catalytic efficiency for biotransformations. Nanofibers were superior to casting films from the same solution for immobilization of cellulose.

Zeng *et al.* fabricated PVA fibers by electrospinning and reported that the as-spun PVA (Mw = 195,000 Da; DH = 98%) fibers ranged between about 250 and 300 nm (for the PVA concentration of 5% w/v; the applied EFS of 55 kV/12 cm; flow rate = 1 mL/h) [47]. These electrospun fibers were used as the protein delivery system and the retardation of enzyme release by additional polymer coating.

Zhang *et al.* studied various parameters that affect morphology of electrospun PVA mats and reported that the average diameter of as-spun PVA (degree of polymerization = 1700; DH = 98%; flow rate = 0.2 mL/h) fibers ranged between about 90 and 250 nm (over the PVA concentration range of 6 to 8% w/v and the applied EFS of 8 kV/15 cm) [48]. They found that, tip to target distance exhibited no significant effect on the fiber morphology; however the morphological structure can be slightly changed by changing the solution flow rate. At high voltages above 10 kV, electrospun PVA fibers exhibited a broad diameter distribution. With increasing solution concentration, the morphology was changed from beaded fiber to uniform fiber and the average fiber diameter could be increased from 87 ± 14 to 246 ± 50 nm. Additions of sodium chloride and ethanol had significant effects on the fiber diameter and the morphology of electrospun PVA fibers because of the different solution conductivity, surface tension and viscosity. When the DH value of PVA was increased from 80 to 99 %, the morphology electrospun PVA fibers was changed from ribbon-like fibers to uniform fibers and then to beaded fibers. Moreover, the addition of aspirin and bovine serum albumin also resulted in the appearance of beads.

Son *et al.* studied the effect of pH on electrospinning of PVA and reported that the average diameter of as-spun PVA ($M_w = 78,000$ Da; DH = 99.7%) fibers ranged between about 240 and 425 nm (for the PVA concentration of 7wt%; the applied EFS of 19 kV/10 cm; flow rate = 1 mL/h) [49]. Electrospun PVA fibers became straighter and finer with increasing pH under basic conditions, whereas the electrospinning solution was not continuous and PVA fibers with beads-on-string structures were obtained due to the protonation of PVA under acidic conditions.

2.5 Using Electrospinning for Generating Superhydrophobic

Electrospinning is a powerful technique to make ultrafine fibers and has been found by several groups to provide sufficient surface roughness for introducing superhydrophobicity.

Shang *et al.* reported a study on superhydrophobic silica surfaces based on roughness created by assembling various nanostructure materials [50]. Four different surface structures were created (as shown in Figure 2.15): (1) a smooth surface achieved by dip-coating sol-gel films, (2) an assembly of uniformly sized spherical nanoparticles, (3) a uniformly sized nanorod array unidirectionally aligned perpendicular to surface, and (4) an open mesh of nanofibers lying parallel on a substrate. All surface structures were created on a silica base material, which was subsequently covered with a self-assembled monolayer of tridecafluoro-1,1,2,2-tetrahydrooctyldimethylchlorosilane (TFCS, $\text{CF}_3(\text{CF}_2)_5(\text{CH}_2)_2(\text{CH}_3)_2\text{SiCl}$). All of the four films changed from hydrophilic to hydrophobic with static contact angles ranging from 118° , in films (a), to 160° , in films (d), when a TFCS self-assembly monolayer was applied to the surface. The contact angles increased respectively in films (a), (b), (c) and (d). Such increased contact angles were in accordance with the increased surface roughness.

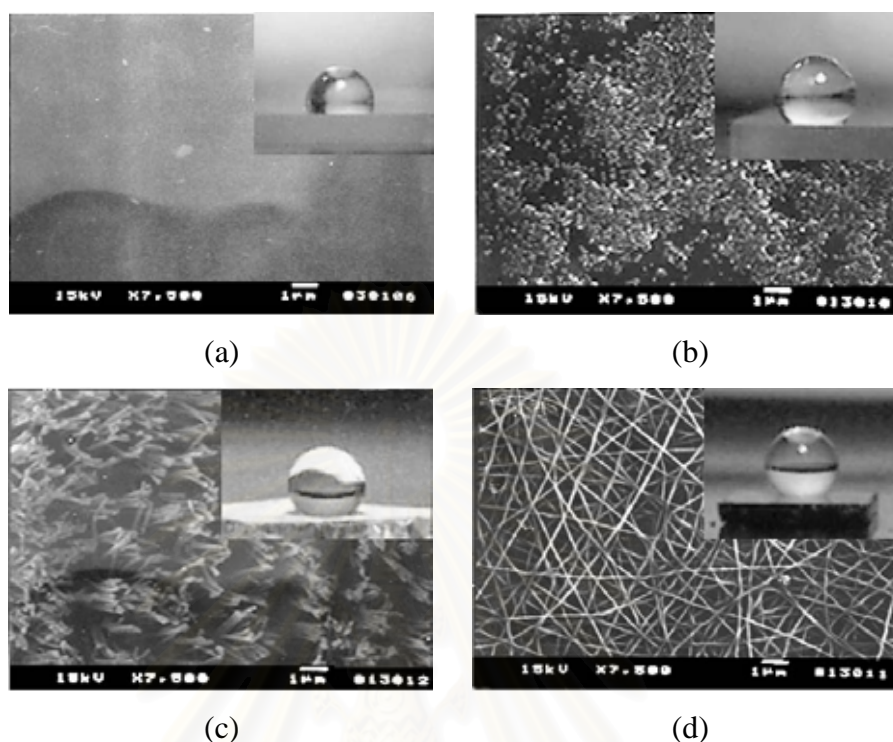


Figure 2.15 Contact angles and surface morphologies of four silica films with TFCS self-assembly monolayer (a), (b), (c) and (d) are smooth surface, nanoparticles surface, nanorods surface and nanofibers surface [50].

Ma *et al.* showed that an even higher superhydrophobicity with WCA up to 175° could be obtained from hydrophobic poly(caprolactone) (PCL), first electrospun and then applying a thin layer of conformal coating of a perfluoroalkyl ethyl methacrylate (PPFEMA) to electrospun mats by initiated chemical vapor deposition (iCVD) [51]. The hierarchical surface roughness inherent in the PCL electrospun mats and the extremely low surface free energy of the coating layer obtained by iCVD yields stable superhydrophobicity with a contact angle of 175° and a threshold sliding angle less than 2.5° . This PPFEMA-coated PCL mat was also shown to exhibit oleophobicity. Hydrophobicity was demonstrated to increase monotonically with a reduction in diameter among bead-free fibers and with the introduction of a high density of relatively small diameter beads. The systematic effect of fiber morphology on superhydrophobicity was also investigated

theoretically and experimentally using both beaded and bead-free fibers with diameters ranging from 600 to 2200 nm.

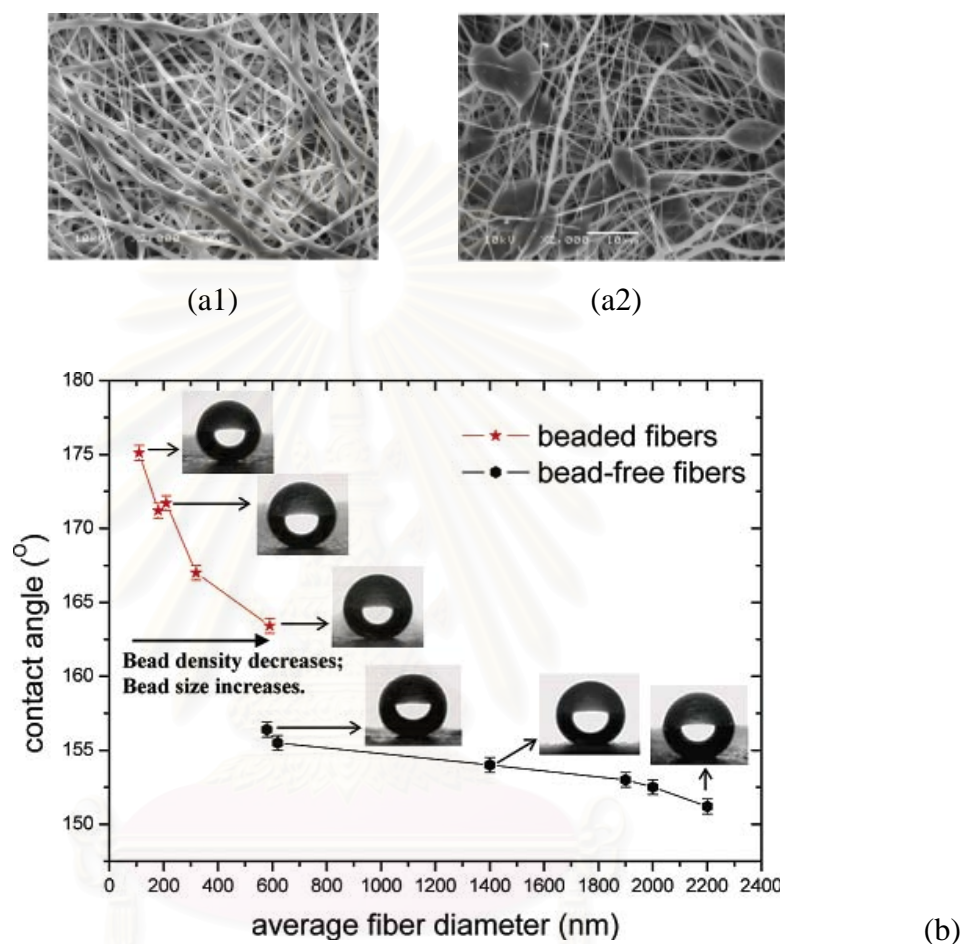


Figure 2.16 SEM images of the PCL electrospun mats: (a1) fiber mats and (a2) beads fiber and (b) contact angles for PPFEMA-coated PCL mats [51].

Ma *et al.* reported that the superhydrophobicity of electrospun nonwoven mats composed of submicrometer diameter fibers of poly(styrene-*b*-dimethylsiloxane) block copolymers blended with homopolymer polystyrene (PS-PDMS/PS) [52]. Fibers with average diameters in the range of 150-400 nm were fabricated. Contact angle measurements indicated that the nonwoven fibrous mats are superhydrophobic, with a contact angle of 163° and contact angle hysteresis of 15°. The superhydrophobicity was attributed to the combined effects of surface

enrichment in siloxane and surface roughness of the electrospun mat itself. The high surface tension at the air/polymer interface, the confinement of the microphase-separated structures to the fiber geometry, and the aligning effect of the elongational flow are believed to have some effects on the morphologies of the block copolymers. Proper annealing protocols might even enhance the regularity of the microphases and the hydrophobicity for these fibers.

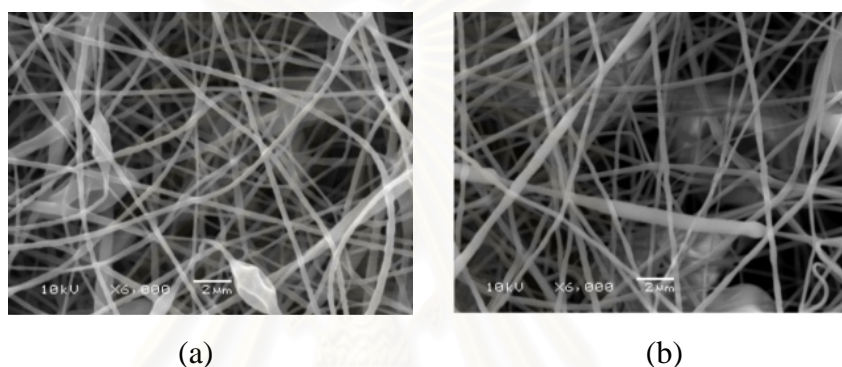


Figure 2.17 SEM images of electrospun mat, showing similar topography of (a) PS-PDMS/PS and (b) PS fibers [52].

Lim *et al.* fabricating multiple-scale nanofiber films via an electrospinning process using aqueous solutions which contained water-soluble polymers and different colloids: monodisperse silica or polystyrene microspheres for larger particles and monodisperse silica nanoparticles for smaller particles [53]. Various types of fibrous films were produced depending on the properties of the dispersing medium, the effects of additives, and the compositions of the bidisperse colloids. When polystyrene microspheres were used as sacrificial templates, macropores were left behind in the nanofibers during the removal of polystyrene microspheres. The multiple-scale roughness from bidisperse colloids of 700 and 50 nm silica particles (as shown in Figure 2.18) or macropores templated from polystyrene particles and 50 nm silica particles (as shown in Figure 2.19) was essential to generate higher contact angles and lower water sliding angles compared to the nanofiber films without multiple-scale roughness. In both cases, stable superhydrophobic multiple-scale

fibrous films with large contact angle ($>150^\circ$) and low sliding angle ($<2^\circ$) were successfully produced.

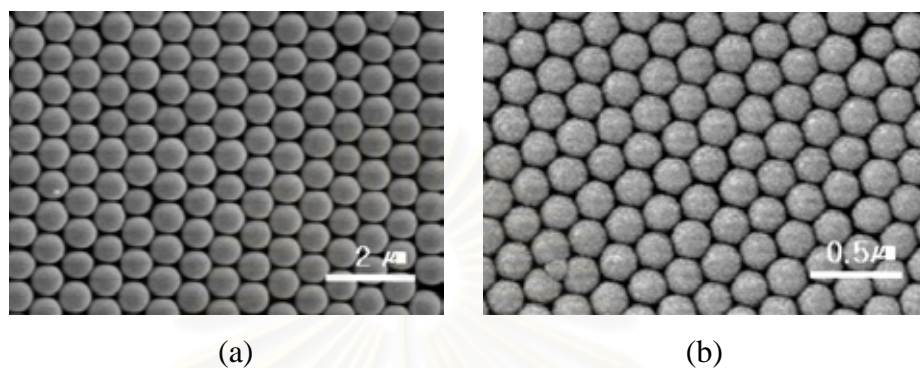


Figure 2.18 SEM images of (a) silica microspheres of 700 nm in size and (b) polystyrene latex spheres of 237 nm in size [53].

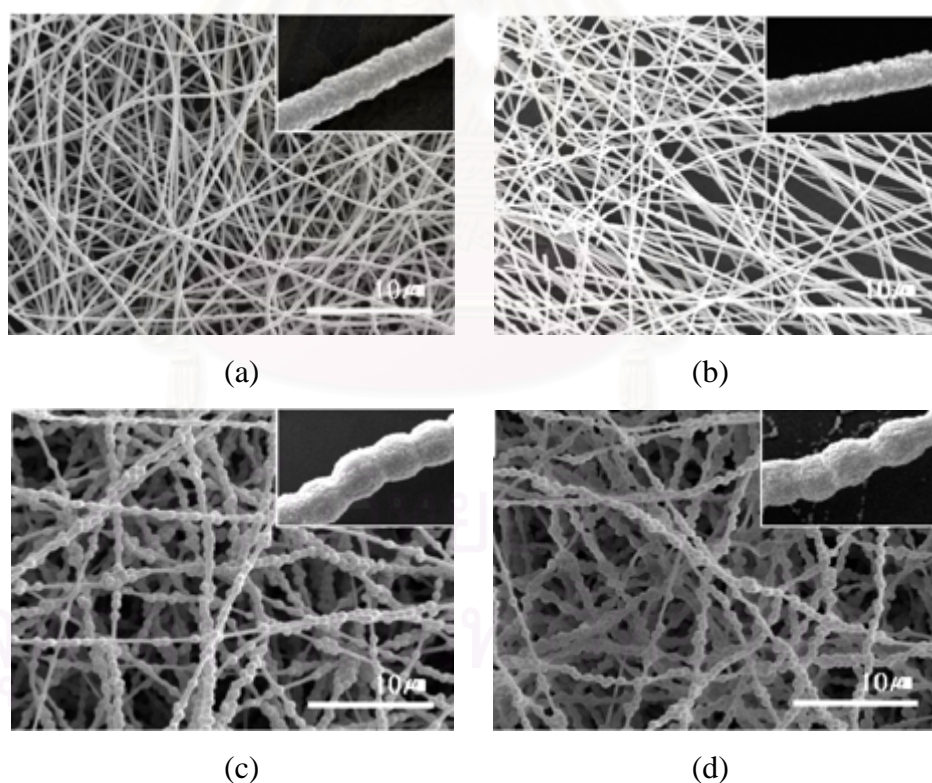


Figure 2.19 SEM images of electrospun composite nanofibers and silica particles: (a, b) with monodisperse silica particles of 50 nm in size before and after calcinations, respectively; (c, d) with bidisperse silica particles of 50 and 700 nm in size before and after calcination, respectively [53].

2.6 Esterification [54]

There is perhaps no organic functional group more important than the carboxyl group with its activated derivatives (acid chlorides, anhydrides, methyl esters, etc.). The carboxyl group is found in numerous compounds and polymers of biological, industrial, and academic significance. It has important acid-base properties, and its activated react to form carboxylic acids, amides, esters, thioesters, ketones, alcohols.

Esterification is the chemical process for making esters, which are compounds of the chemical structure $R-COOR'$, where R and R' are either alkyl or aryl groups. The most common method for preparing esters is to heat a carboxylic acid, $R-CO-OH$, with an alcohol, $R'-OH$, while removing the water that is formed.

Esters can also be formed by various reactions. These include the reaction of an alcohol with an acid chloride ($R-CO-Cl$). Early studies into the chemical mechanism of esterification concluded that the ester product ($R-CO-OR'$) is the union of the acyl group ($R-C=O-$) from the acid, $R-CO-OH$, with the alkoxide group ($R'O-$) from the alcohol, $R'-OH$, rather than other possible combinations.

The chemical structure of the alcohol used in the esterification reaction all affects its rate. Simple alcohols such as methanol (CH_3OH) and ethanol (CH_3CH_2OH) can react very fast because they are relatively small and contain no carbon atom side chains that would hinder their reactions.

2.7 Silanization [30,55]

The use of reactive organosilicon compounds to modify the surface properties of inorganic materials is a process that is widely used in both research and technology. Depending on reaction conditions, chemistry of the organosilane, and surface prehistory, a number of different structures can be produced on the surface. The complexity of this chemistry is illustrated in Figure 2.20.

Monofunctional organosilanes (R_3SiX) having only one hydrolysable group in the molecule (usually $X = Cl, OR, NMe_2$) are attractive in terms of the reproducibility of surface structures because only one type of grafting is possible in

the systems by covalent attachment to the surface by chemical bonds ($\text{Si}_s\text{-O-Si}$) Figure 2.20. The structure of these monolayers has been studied extensively, primarily for porous and nonporous highly dispersed silicas, and these results are discussed in a number of publications: reaction conditions [56], bonded layer structure and dynamics [56, 57], phase transitions of bonded layers, use as chromatographic stationary phases [58, 59].

The maximum bonding density is limited by the size of the dimethylsilyl group and decreases slightly with larger alkyl groups. The cross-sectional area of alkyldimethylsilyl groups in a densely packed monolayer is 32-38 Å, which is almost twice the area peralkyl chain observed in dense monolayers of fatty acids [60], alkanethiols [61], and self-assembled alkyltrichlorosilane-derived monolayers [62] (molecules in these monolayers exhibit cross-sectional areas of $\sim 20\text{Å}$). A survey of wettability studies of monolayers prepared with monofunctional silanes on single surfaces has been published [30]. The reactions of monofunctional silanes at the solution-solid interface are very slow in the later stages of the reaction, and long reaction times (tens of hours/several days) are necessary to achieve maximum bonding density, even for a single surface substrate like a silicon wafer [30].

Wettability studies indicate that dense monolayers of contact angles ($\theta_A/\theta_R = \sim 105^\circ/\sim 94^\circ$) are independent of chain length [30], indicating that these surfaces project disordered methyl groups toward the probe fluid and that water does not penetrate monofunctional silanes project disordered alkyl chains toward the probe fluids. Hydrophobization is achieved topologically: the monolayers prevent water from penetrating and interacting with residual silanols.

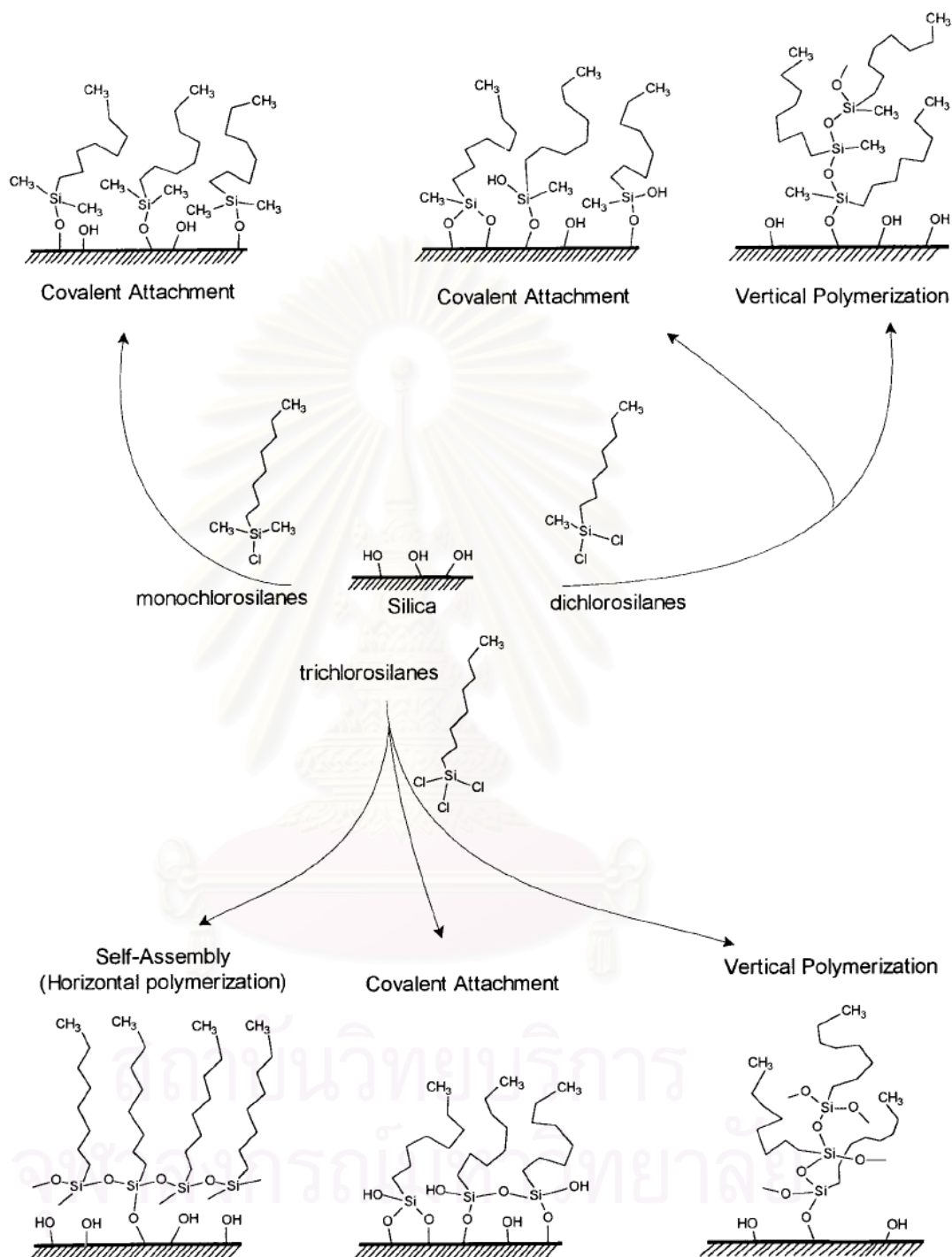


Figure 2.20 Possible products of the reaction of alkylchlorosilanes with silicon dioxide surfaces [30].

Trifunctional organosilanes (R_3SiX_3), compared to their monofunctional analogues, are more reactive and are capable of polymerizing in the presence of water, which gives rise to a number of possible surface structures. Along with covalent attachment, 2-D (self-assembly) and 3-D surface-induced polycondensation are possible (Figure 2.20). The self-assembly process of long-chain alkyltrichlorosilanes (primarily octadecyltrichlorosilane, OTS) has received the major attention of researchers in this area. The deposition process is now reasonably well understood, and the importance of temperature [63, 64], solvent, and surface water has been appreciated [65].

The structure of these supported films has been investigated using a range of techniques, and the best monolayers are composed of close-packed (~ 4.5 - 5 groups/nm²), close to vertical chains in an extended all-trans conformation [66]. The strong bonding between molecules in this system (lateral siloxane bonds and van der Waals interactions between alkyl chains) and to a small extent bonding with the surface is a distinctive property of these monolayers. This allows the preparation of monolayers of the same quality on different substrates, whether or not covalent bonds can form with the substrate, for example, silicon, glass, mica, and gold [67, 68]. The self-assembly mechanism of bonding (horizontal polymerization) has been reported as well for the reaction of several alkyltrichlorosilanes with porous and high surface area nonporous silica [69].

Obviously, self-assembly is not the only reaction possible between alkyltrichlorosilanes and the silica surface. Under certain conditions, alkyltrichlorosilanes react with surface silanols predominately in a covalent attachment manner, which has been referred to as poor self-assembly because of the substantially lower bonding density. Covalent attachment takes place in the reaction of trichlorosilanes with dry silica at elevated temperatures [70] or in the presence of adsorbed amine at room temperature. The stoichiometry of the covalent attachment of trichlorosilanes, that is, the average number of bonds with the silica surface per silane molecule, is not completely clear yet. According to NMR, IR, and other methods [71], 1:1 (one Si-O-Si bond) as well as 1:2 (two Si-O-Si bonds) grafted structures are present on the surface. Structures (1:3) with three Si-O-Si bonds are

not formed due to steric reasons. After exposure to the ambient atmosphere, unreacted Si-Cl bonds undergo hydrolysis to form Si-OH groups. The latter were shown to have a significant impact on adsorption [72] and chromatographic properties [73] of silicas modified with alkyltrichlorosilanes.

If there is a sufficient amount of water in the system, the polycondensation of trifunctional silanes into 3-D siloxanes grafted to the surface can become the dominant process. Polymeric grafted layers were reported for the reaction of methyltrichlorosilane with glass in the vapor phase [74] and the reaction of alkyltrichlorosilanes with high surface area silicas. Trialkoxysilanes with the general formula $Z(CH_2)_nSi(OR)_3$, where R = Me or Et (often used Z are amino, epoxy, acryloyl, vinyl, bromo), which are often referred to as “silane coupling agents” and are used for adhesion improvement, also form relatively thick polymeric layers on the surface when applied from aqueous-based solvents.

Difunctional organosilanes (R_2SiX_2) are the least studied reactive silanes in respect to their reaction with hydrated silica. Covalent attachments as well as surface induced polymerization to form grafted polysiloxane are conceivable reactions with silica (Figure 2.20). Dimethyldichlorosilane and octadecylmethyldichlorosilanes the most studied alkyldichlorosilanes were shown to react with silica surfaces yielding either covalently attached monolayers [57,70,71] or polymeric layers [73] depending on the reaction conditions used.

2.8 Characterization Techniques

2.8.1 Contact Angle Measurement [74]

Contact angle measurements are often used to assess changes in the wetting characteristics of a surface and hence indicate a change in surface energy. The technique is based on the three-phase boundary equilibrium described by Young's equation.

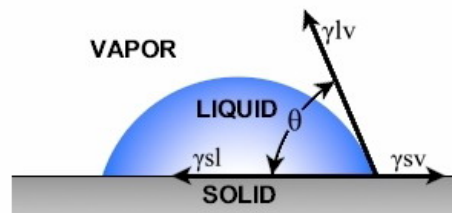


Figure 2.21 Schematic representation of the Young's equation [6].

$$\cos \theta = \frac{\gamma_{SV} - \gamma_{SL}}{\gamma_{LV}} \quad (2.5)$$

where γ_{LV} , γ_{SV} and γ_{SL} are the interfacial tension between the phases with subscripts L, V, S corresponding to liquid, gas, and solid phase, respectively and θ refers to the equilibrium contact angle. The Young's equation applies for a perfectly homogeneous atomically flat and rigid surface. In the case of real surfaces, the contact angle value is affected by surface roughness, heterogeneity, vapor spreading pressure, and chemical contamination of the wetting liquid. Although the technique to measure contact angles is easy, data interpretation is not straightforward and the nature of different contributions to the surface is a matter of discussion. Generally, we can define the complete wetting, wetting, partial wetting, and nonwetting according to Figure 2.22.

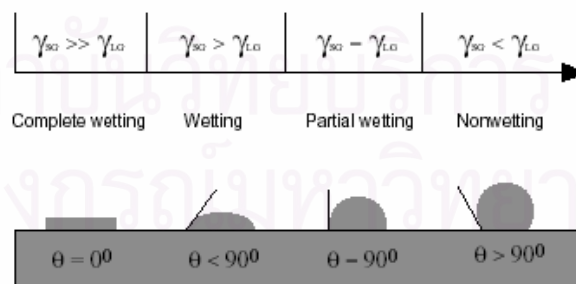


Figure 2.22 Schematic representation of wettability [74].

2.8.2 Scanning Electron Microscope (SEM) [75]

SEM stands for scanning electron microscope. The SEM is a microscope that uses electrons instead of light to form an image. Since their development in the early 1950's, scanning electron microscopes have developed new areas of study in the medical and physical science communities. The SEM has allowed researchers to examine a much bigger variety of specimens.

The scanning electron microscope has many advantages over traditional microscopes. The SEM has a large depth of field, which allows more of a specimen to be in focus at one time. The SEM also has much higher resolution, so closely spaced specimens can be magnified at much higher levels. Because the SEM uses electromagnets rather than lenses, the researcher has much more control in the degree of magnification. All of these advantages, as well as the actual strikingly clear images, make the scanning electron microscope one of the most useful instruments in research today.

The SEM is an instrument that produces a largely magnified image by using electrons instead of light to form an image. A beam of electrons is produced at the top of the microscope by an electron gun. The electron beam follows a vertical path through the microscope, which is held within a vacuum. The beam travels through electromagnetic fields and lenses, which focus the beam down toward the sample. Once the beam hits the sample, electrons and X-rays are ejected from the sample.

สถาบันวิทยบริการ
จุฬาลงกรณ์มหาวิทยาลัย

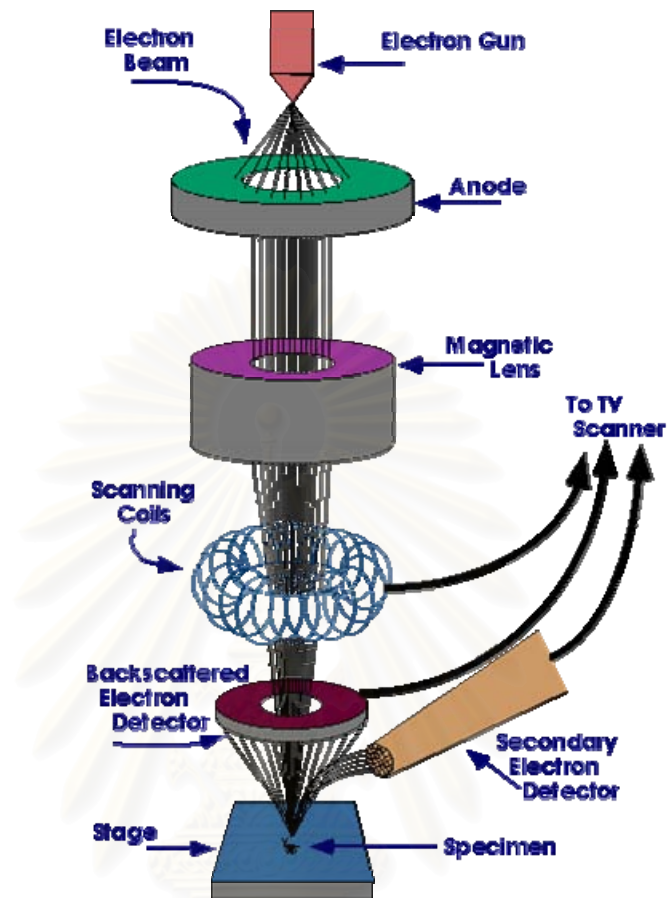


Figure 2.23 Schematic representation of the SEM works [75].

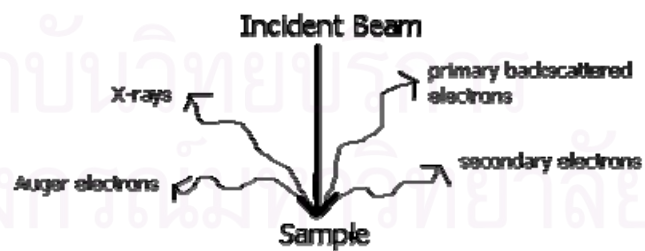


Figure 2.24 Schematic representation of the detectors collect of X-rays in SEM [75].

Detectors collect these X-rays, backscattered electrons, and secondary electrons and convert them into a signal that is sent to a screen similar to a television screen. This produces the final image.

CHAPTER III

EXPERIMENTAL

3.1 Materials

All reagents and materials are analytical grade and used without further purification.

1. Butyryl chloride	: Fluka
2. Calcium hydride	: Fluka
3. Chlorodimethyloctadecylsilane	: Aldrich
4. Chlorodimethyloctylsilane	: Fluka
5. Chlorodimethylpropylsilane	: Fluka
6. Dichlorodimethylsilane	: Fluka
7. Ethanol	: Merck
8. Heptafluorobutyryl chloride	: Fluka
8. Heptanoyl chloride	: Fluka
9. Lauroyl chloride	: Fluka
10. Poly(vinyl alcohol)	: Aldrich
11. Silicon tetrachloride	: Riedel-de Haën
12. Toluene	: Merck
13. Trichloro(1 <i>H</i> ,1 <i>H</i> ,2 <i>H</i> ,2 <i>H</i> -perfluorooctyl)silane	: Aldrich
14. Trichloromethylsilane	: Fluka
15. Trichlorooctylsilane	: Aldrich
16. Triethylamine	: Carlo

3.2 Equipment

3.2.1 Contact Angle Measurements

Contact angle goniometer model Ramé-Hart 200-F1 was used for the determination of water contact angles. The measurements were carried out in air at room temperature. A droplet of water is placed on the tested surface by bringing the

surface into contact with a droplet suspended from a needle of the syringe. A silhouette image of droplet was projected on the screen and the angle is measured. Dynamic advancing and receding angles were recorded while water was added to and withdrawn from the drop, respectively. The reported angle is an average of 5 measurements on different area of each sample.

3.2.2 Scanning Electron Microscopy (SEM)

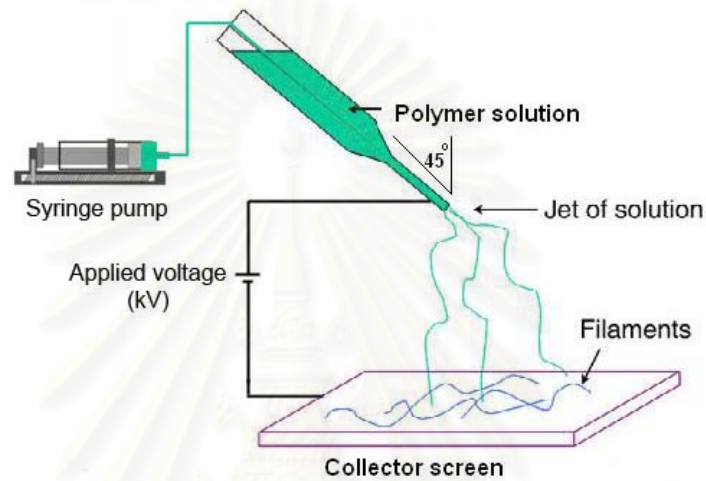
The morphological appearances of the as-spun PVA fibers before and after chemical modification, were investigated using a scanning electron microscope (SEM) model JSM-6480LV. Each sample was placed on the holder with an adhesive tape and coated with a thin layer of gold. The scanning electron images were obtained by using an acceleration voltage of 15 kV with a magnification of 6,000, 10,000 and 50,000x. The average fiber diameter of the electrospun fibers was measured by Semafore software directly from SEM images.

3.3 Preparation of Electrospun Poly(vinyl alcohol) Fiber Mats

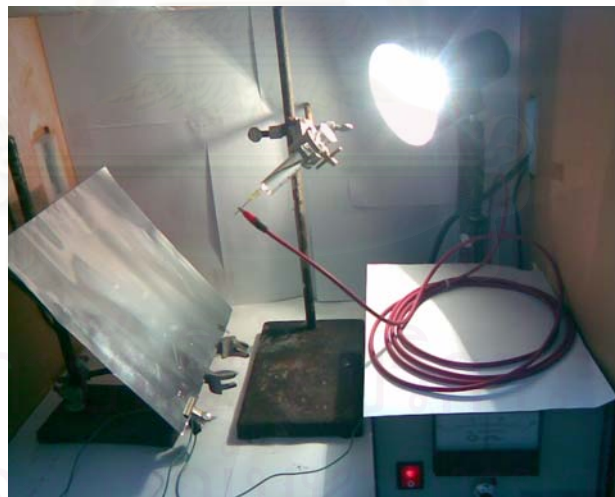
A weighed amount of PVA powder ($M_w = 89,000-98,000$) was dissolved in 50-mL warm distilled water at 80°C in a 250-mL round bottom flask under slight stirring for 3 h to prepare a poly(vinyl alcohol) solution with a desired concentration (6, 7, 8, 10, and 12% (w/v)) prior to electrospinning.

A set-up for electrospinning is schematically shown in Figure 3.1. Each of the as-prepared solutions was placed in a 10-mL syringe. A 1.5-cm long, blunt-end stainless-steel gauge 20 needle (i.e. outside diameter = 0.91 mm) was used as a nozzle. The tilt angle of the syringe and the needle was 45° from a horizontal baseline to ascertain a constant presence of a solution droplet at the tip of the nozzle. A sheet of aluminum foil on a plastic backing was used as the grounded target plate collector. A Gamma High Voltage Research DES30PN/M692 power supply was used to generate a high DC potential across the needle (connected to the positive emitting electrode) and the collector (connected to the grounding electrode). The applied potential was fixed at 15 kV over a fixed collection distance between the tip of the nozzle and the screen collector of 15 cm. The feed rate of the solutions for

most experiments was controlled by means of a Kd Scientific syringe pump at 1 mL/h. The collection time was also fixed at 12 h. The as-spun fibers mats were kept in an oven at 95°C for 24 h to ensure the complete drying of the fibers prior to further characterization.



(a)

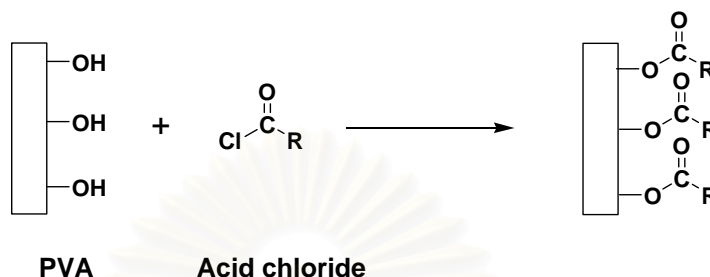


(b)

Figure 3.1 Experimental set-up for electrospinning (grounded target plate collector): (a) a schematic drawing and (b) a real set-up.

3.4 Chemical Modification of Poly(vinyl alcohol) Fiber Mats

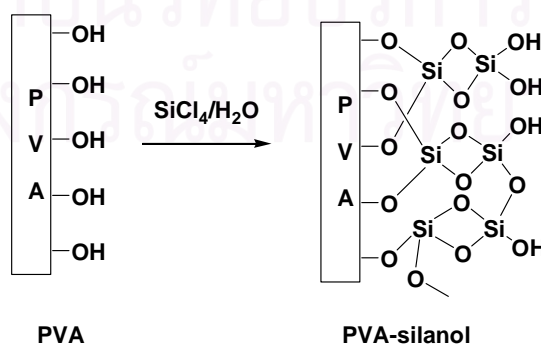
3.4.1 Esterification with Acyl Chlorides



where $R = -(\text{CF}_2)_2\text{CF}_3, -(\text{CH}_2)_2\text{CH}_3, -(\text{CH}_2)_5\text{CH}_3, -(\text{CH}_2)_{10}\text{CH}_3$

Dried PVA fiber mats were suspended using a sample holder in a Schlenk flask containing 0.5 mL of acyl chloride. There was no direct contact between liquid and the fiber mats during the reaction. The reaction time was chosen on the basis of kinetics studies to maximize conversion at a predetermined temperature. A reaction with heptafluorobutyl chloride (HFBC) and butyryl chloride (BC) was carried out at ambient temperature and 70–80°C, respectively. Reactions with hexanoyl chloride (HC) and lauroyl chloride (LC) were performed at 120°C. All of the modified PVA fiber mats were rinsed with copious amounts of water and dried in a clean oven at 120°C for 10 min. The modified PVA fiber mats were then kept in covered flasks prior to contact angle and SEM analyses.

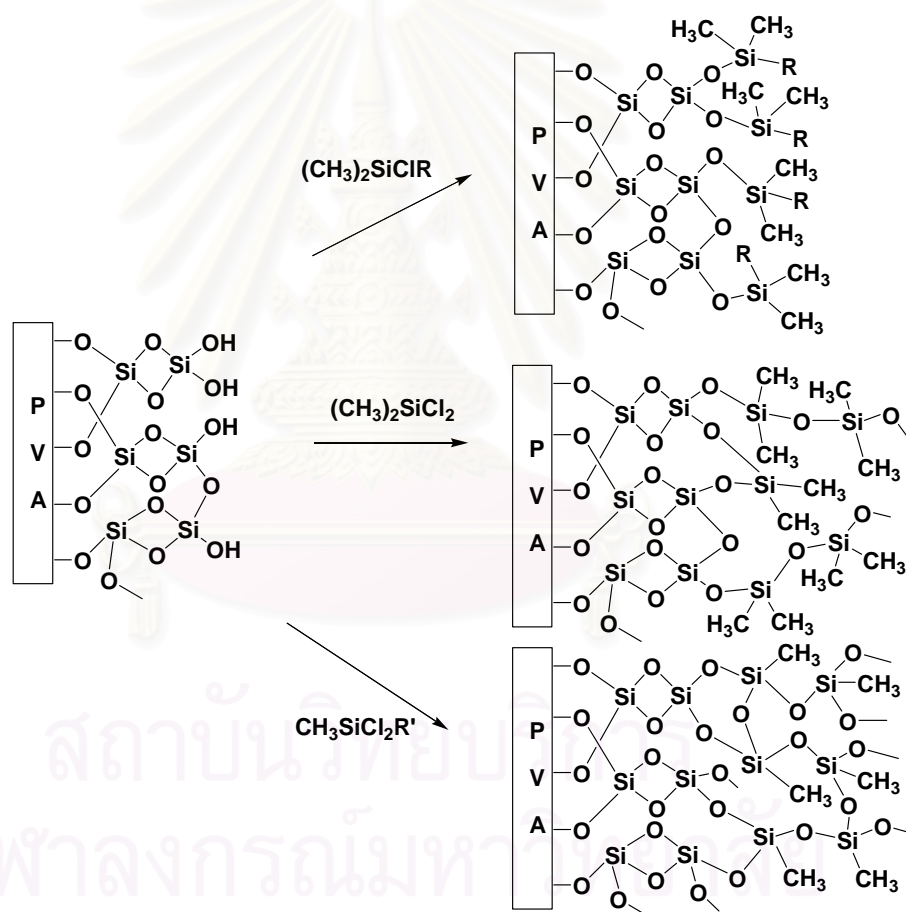
3.4.2 Preparation of PVA-silanol Fiber Mats



PVA fiber mats were dried in a Schlenk flask for 2 h under reduced pressure and purged with N_2 (g). The fiber mats were then exposed to SiCl_4 vapor via a

cannula connecting the reaction flask and a SiCl_4 reservoir in a steady stream of N_2 (g) at ambient temperature for 15 min. At the end of the reaction, residual SiCl_4 in the flask was purged with N_2 (g) before the fiber mats were exposed to air for 5 min to allow hydrolysis to take place. Before the next cycle, the sample flask was pumped down under reduced pressure and filled with N_2 (g).

3.4.3 Vapor-phase Silanization of PVA-silanol Fiber Mats with Alkylchlorosilane



where $\text{R} = -(\text{CH}_2)_2\text{CH}_3, -(\text{CH}_2)_7\text{CH}_3, -(\text{CH}_2)_{10}\text{CH}_3$

$\text{R}' = -\text{CH}_3, -(\text{CH}_2)_7\text{CH}_3, -(\text{CH}_2)_2(\text{CF}_2)_5\text{CF}_3$

Dried PVA-silanol fiber mats obtained from 3.4.2 were suspended using a sample holder in a Schlenk flask containing 0.5 mL of alkylchlorosilane. There was no direct contact between liquid and the fiber mats during reaction. Reactions were

carried out at 70°C for chlorodimethylpropylsilane (CDPS), dichlorodimethylsilane (DDS) and trichloromethylsilane (TMS) and at 120°C for chlorodimethyloctadecylsilane (CDODS), chlorodimethyloctylsilane (CDOS), trichloro(1*H*,1*H*,2*H*,2*H*-perfluorooctyl)silane (TFOS), and trichloro(octyl)silane (TOS). The modified fiber mats were rinsed with 2×10 mL of toluene, 2×10 mL of ethanol, 2×10 mL of ethanol-water (1:1), 2×10 mL of water and were dried in a clean oven at 120°C for 10 min. The fiber mats were then kept in covered flasks prior to contact angle and SEM analyses.

3.4.4 Solution-phase Silanization of PVA-silanol Fiber Mats with Alkylchlorosilane

Dried PVA-silanol fiber mats obtained from 3.4.2 were suspended using a sample holder in a Schlenk flask and covered with anhydrous toluene (15-20 mL) containing triethylamine (0.15 mL, 10⁻³ mol). A selected alkylchlorosilane was added by syringe to render a 1.0 M solution. Reactions were run at ambient temperature for a desired period of time. The modified fiber mats were rinsed with 2×10 mL of toluene, 2×10 mL of ethanol, 2×10 mL of ethanol-water (1:1), 2×10 mL of water and dried in a clean oven at 120°C for 10 min. The fiber mats were then kept in covered flasks prior to contact angle and SEM analyses.

CHAPTER IV

RESULTS AND DISCUSSION

This chapter is divided into 2 parts. The first part concentrates on the preparation of PVA fiber mats. The second part is dedicated to chemical modification of PVA fiber mats using esterification and silanization. Morphological appearance and surface wettability of the modified fiber mats were assessed by scanning electron microscopy (SEM) and water contact angle (WCA) measurements.

4.1 Preparation of Electrospun Poly(vinyl alcohol) Fiber Mats

4.1.1 Effect of Solution Concentration on Fiber Size and Morphology

Changing the polymer concentration could alter the solution viscosity. As shown in Figure 4.1, the PVA viscosity increased monotonously with increasing solution concentration. It is well known that to prepare fibers by electrospinning, a proper solution concentration and hence the resulting viscosity is required. Therefore, a series of pristine PVA solutions at various PVA concentrations in a range of 5-12% (w/v) were electrospun, resulting in various fiber morphology and diameter as shown in Figures 4.2.

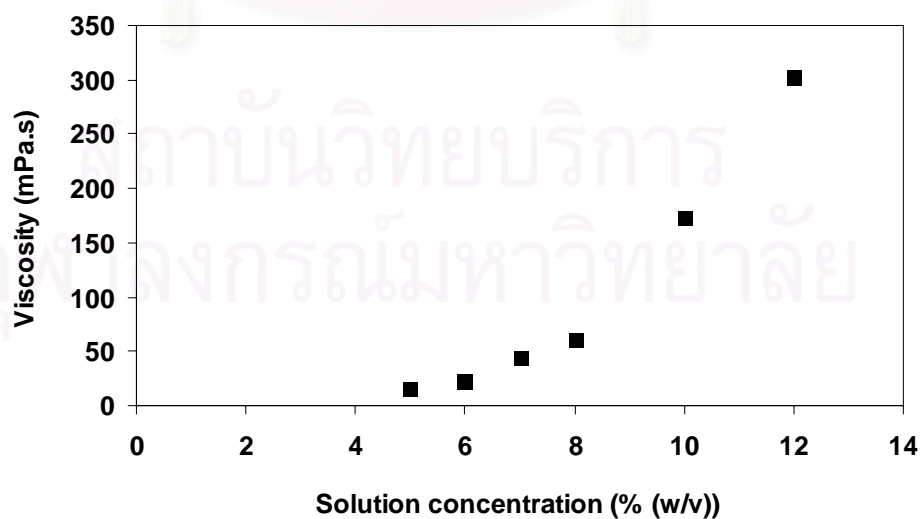


Figure 4.1 Relationship between viscosity and concentration of PVA solution

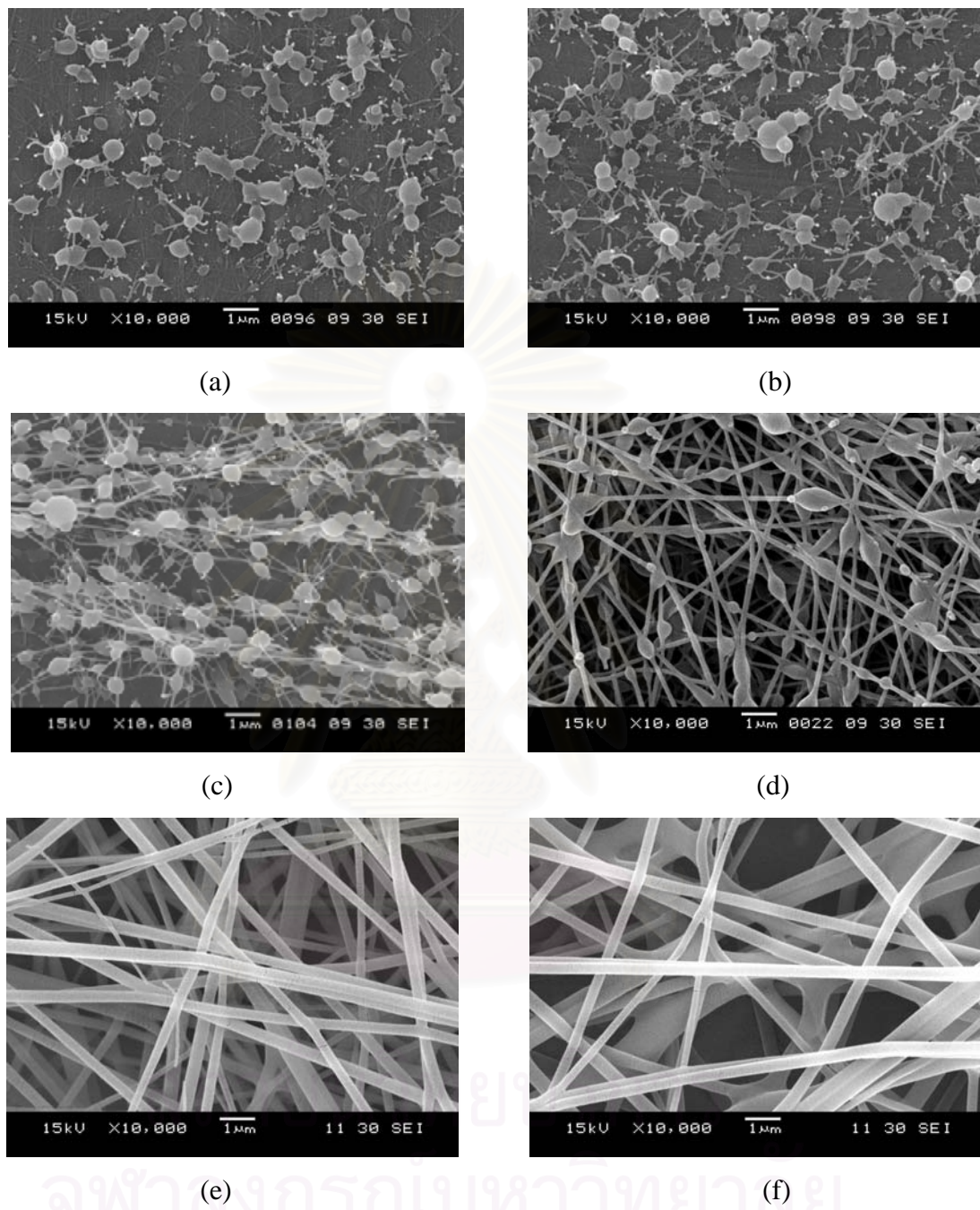


Figure 4.2 SEM micrographs of electrospun fiber mats from PVA solutions with different concentration: (a) 5%, (b) 6%, (c) 7%, (d) 8%, (e) 10%, and (f) 12%. Original magnification was 10,000x.

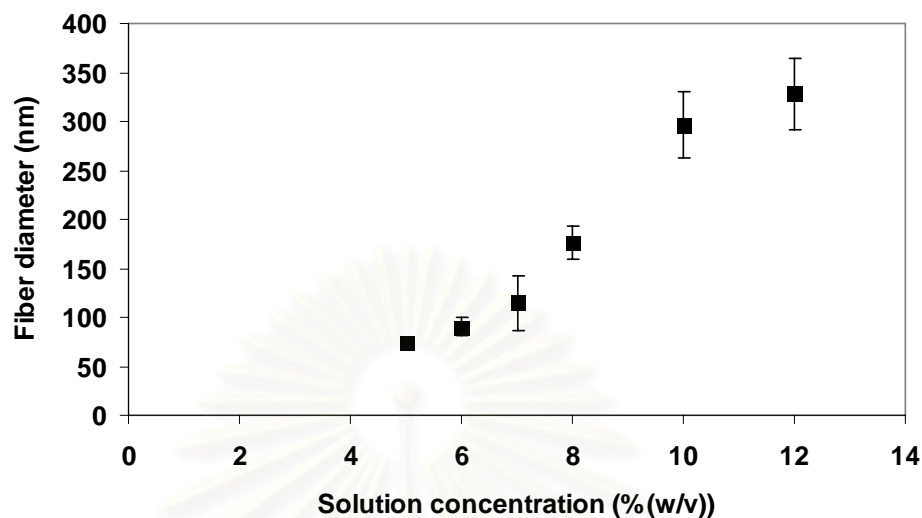


Figure 4.3 Average diameters (nm) of PVA fibers electrospun from PVA solution with different concentration

In principle, the morphology of the electrospun fibers are in the form of beads, fibers or a combination of beads and fibers, depending on the concentration of solution used during the experiment. If the concentration of the solution is too low, a continuous stream of the charged liquid (i.e., charged jet) cannot be formed, as the charged jet undergoes a flow instability leading to the formation of droplets (i.e., electrospaying) [76]. In other words, the solution concentration should be above a certain critical concentration at which there are enough chain entanglements so that continuous fibers can be formed.

In electrospinning, the coiled macromolecules in solution were transformed by the elongational flow of the jet into oriented entangled networks that persisted with fiber solidification. Below this concentration, chain entanglements were insufficient to stabilize the jet and the contraction driven by the surface tension caused the solution to form beads or beaded fibers. However, if the solution concentration becomes too great, electrospinning is also prohibitive as a continuous flow of the polymer liquid from the nozzle tip is somewhat restricted. As a result, there is a limited concentration or viscosity range within which a polymer solution can be electrospinnable. Beyond this range (either higher or lower), discrete droplets are likely to occur [77].

In our case, at the lowest concentration [5% (w/v)], many beads were observed in the structure along with fibers, as seen in Figure 4.2 (a). The shapes of the beads varied from spherical to spindle-like due to low entanglement of polymer chains and average fiber diameters between beads were very small. They are in a range of 74.53 ± 1.63 nm. With increasing concentration, the morphology of fibers was changed from beaded fiber to uniform fiber structure and the fiber diameter was also gradually increased to the range of 328.60 ± 36.25 nm at the high concentration [12% (w/v)], as seen in Figure 4.3. These data indicate that as high as 10% (w/v) PVA solution is necessary to obtain sufficient chain entanglements, yielding continuous fibers.

4.1.2 Effect of Solution Concentration on Wettability of Fiber Mats

Wettability of the PVA fiber mat was expressed in term of water contact angle. The results presented in Figure 4.4 suggest that the advancing water contact angle (θ_A) decreased as the PVA concentration increased. The θ_A of the electrospun PVA fiber mats was in a range of $49.41 - 59.34^\circ$, which is in a hydrophilic region. It can be explained by the variation of bead and fiber density. The fibers lying on a surface created a tortuous surface in x-y plane. However, they are smooth in amplitude (z-axis). When the beads, bigger than fibers, were introduced into the micro-texture, they increased the roughness in amplitude. So, the roughness in three dimensions was obtained. This resulted in a longer and discontinuous three-phase interface at the bottom of the water droplet. As a result, the presence of beads increased the variation in roughness amplitude, so higher WCA is attained especially when the fiber morphology was in the form of beads and beads with short fibers. It should be noted that it was not possible to measure receding water contact angles (θ_R) in all cases. The droplets did not recede after the water was withdrawn from the drops. This behavior implies that the surface roughness may be so high that the water was trapped within the space (in a micron range) between adjacent beads or fibers.

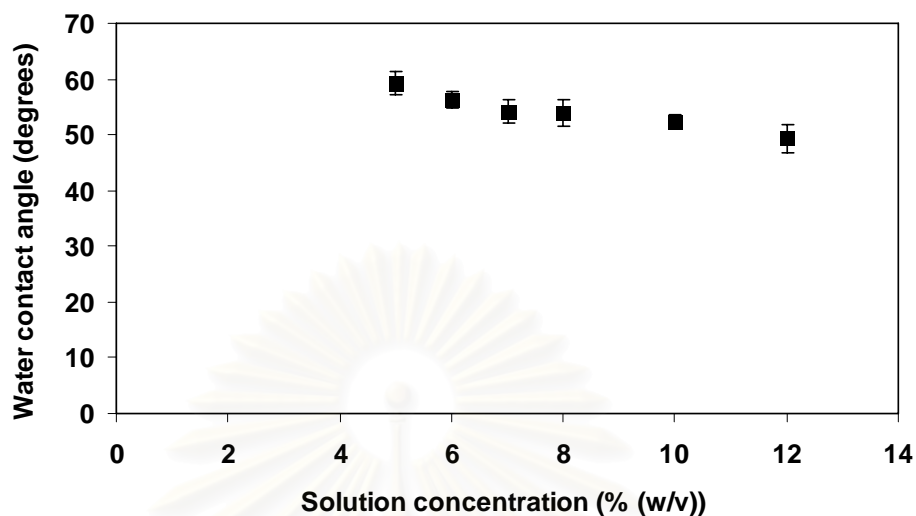
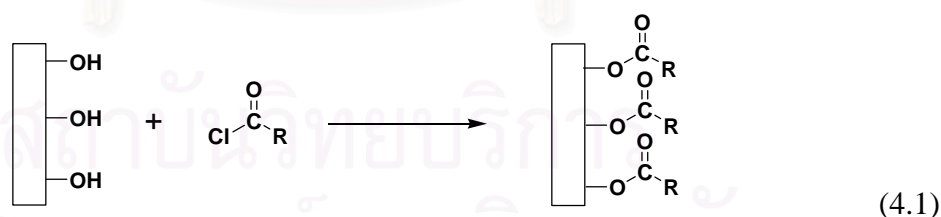


Figure 4.4 Water contact angle (θ_A) of electrospun PVA fiber mats as a function of PVA concentration.

4.2 Chemical Modification of Poly(vinyl alcohol) Fiber Mats

Most chemical modification reactions were conducted on PVA fiber mats electrospun from 10%(w/v) PVA solution. The fiber diameter was in a range of $297.05 \pm 33.59^\circ$. The θ_A of the fiber mats was $52.31 \pm 1.22^\circ$.

4.2.1 Esterification with Acyl Chlorides



where R = $-(\text{CF}_2)_2\text{CF}_3$, $-(\text{CH}_2)_2\text{CH}_3$, $-(\text{CH}_2)_5\text{CH}_3$, $-(\text{CH}_2)_{10}\text{CH}_3$

Esterification of PVA fiber mats was first performed in a solution phase in the presence of triethylamine. It was found that the PVA fiber mats became collapsed and lost their original morphologies after the reactions with acid chlorides. Figure 4.5 (a, b) illustrate the morphology of PVA fiber mats after the reaction with heptafluorobutyryl chloride (HFBC) and lauroyl chloride (LC) for 3 h.

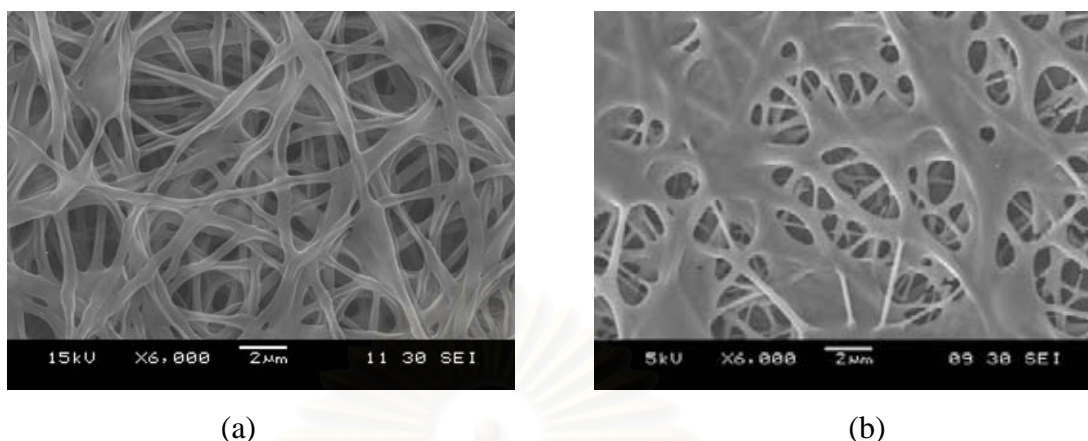


Figure 4.5 SEM micrographs of electrospun PVA fiber mats after the reactions with (a) HFBC and (b) LC in solution for 3 h. Original magnification was 6,000x.

To determine whether the deformation of the fibers was caused by the intrinsically low integrity of the hydrophilic PVA itself against organic solvent or the reagents (acyl chloride, triethylamine), we conducted a controlled experiment by soaking a PVA fiber mat in toluene, the solvent used for reaction, for 3 h. As seen in Figure 4.6, the fiber mat still maintained its original morphology. No deformation was observed. This result implied that the deformation may be caused by the reagents, not the solvent.

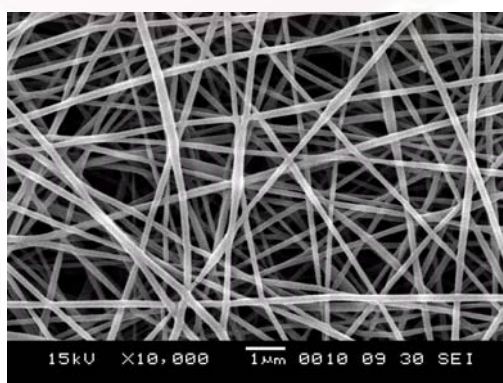


Figure 4.6 SEM micrograph of electrospun PVA fiber mats after soaking in toluene for 3 h. Original magnification was 10,000x.

We then attempted to increase the integrity of the PVA fiber mats by a pre-treatment with glutaraldehyde which can act as a crosslinking agent. It was found that the exposure to glutaraldehyde vapor caused the θ_A of the PVA fiber mats to drop from 46.14 ± 1.09 to 30.14 ± 0.86 indicating that the crosslinking was not successful. We also failed to crosslink the PVA fiber mats in solution. The fibers could not tolerate the strong acidity of H_2SO_4 which was used as a solvent. The fiber mats collapsed and dissolved in the solution of 0.075 M glutaraldehyde in 0.2 M H_2SO_4 .

Despite the failure to esterify the PVA fiber mats in solution, we further explored the possibility to conduct the esterification in vapor. Table 4.1 shows the conditions used for the esterification in vapor phase along with the water contact angle data of the PVA fiber mats. Since the reaction was performed in vapor phase, the extent of reaction, which was varied as a function of vapor pressure of acid chloride, should be greatly affected by the temperature used for the reaction. In these studies, the temperature chosen for each acid chloride was above ambient temperature (except for HFBC), but below the boiling point. The reaction time shown in the table is the period of time that yielded the highest θ_A . The water contact angles unexpectedly turned out to be almost the same independent of the acid chloride. The highest θ_A was in a range of $115 \pm 6^\circ$. It is suspected that the greater hydrophobic influence from the longer alkyl chains of HC and LC may be counteracted by the lower reactivity of the acid chlorides themselves against the hydroxyl nucleophile of PVA. However, the same speculation could not be used in the case of HFBC, of which reactivity should even be higher than BC.

Table 4.1 Conditions used for the esterification in vapor phase and water contact angle data of PVA fiber mats

Acyl chloride	R	Boiling Point (°C)	Reaction temperature (°C)	Reaction time (h)	Water contact angle (θ_A , degree)
PVA fiber mats	-	-	-	-	52.31 ± 1.22
control	-	-	70	3	54.37 ± 2.82
BC	$(\text{CH}_2)_2\text{CH}_3$	98-102	70	1	115.67 ± 5.67
HC	$(\text{CH}_2)_5\text{CH}_3$	173	120	3	114.28 ± 4.44
LC	$(\text{CH}_2)_{10}\text{CH}_3$	264	120	3	115.55 ± 6.42
HFBC	$(\text{CF}_2)_2\text{CF}_3$	39	RT	1	114.01 ± 5.54

Although the PVA fiber mats can be hydrophobized, their morphologies were also damaged (Figure 4.7) upon the exposure to acid chlorides and also to HCl release as a by-product from the reactions. These data demonstrated the drawback of using the esterification of acid chloride as a tool to hydrophobized the surface.

สถาบันวิทยบริการ
จุฬาลงกรณ์มหาวิทยาลัย

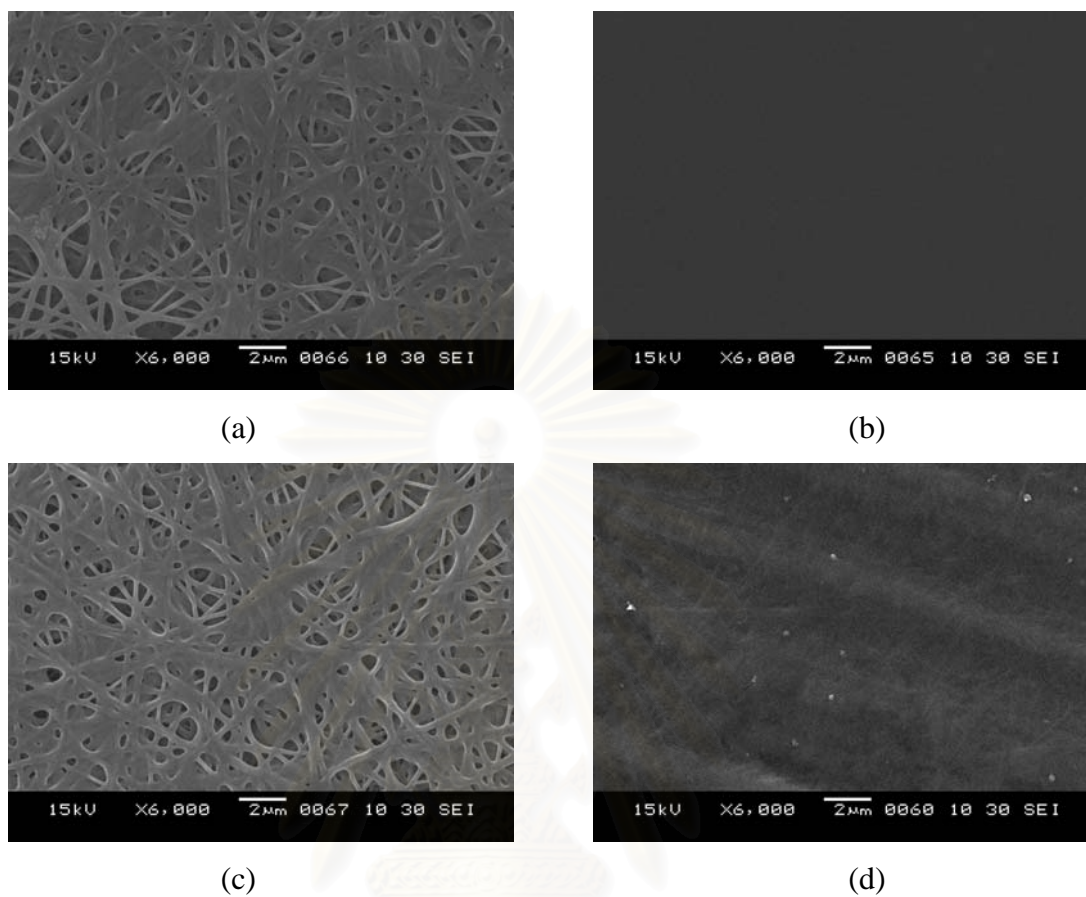


Figure 4.7 SEM micrographs of PVA fiber mats after a reaction with vapor phase of acyl chlorides: (a) BC, (b) HC, (c) LC, and (d) HFBC.

สถาบันวิทยบริการ
จุฬาลงกรณ์มหาวิทยาลัย

4.2.2 Confirmation of Esterification

Esterification on the PVA fiber mats was confirmed by the presence of C=O stretching of ester groups in ATR-FTIR spectra shown in Figure 4.8. As expected, the signal of the PVA fiber mats esterified by fluorinated acid chloride, HFBC appeared at 1774 cm^{-1} as opposed to that of the PVA fiber mats esterified by BC which appeared at 1730 cm^{-1} . The higher energy (higher wavenumber) is required for the vibration of C=O bond connected to electronegative fluorocarbon.

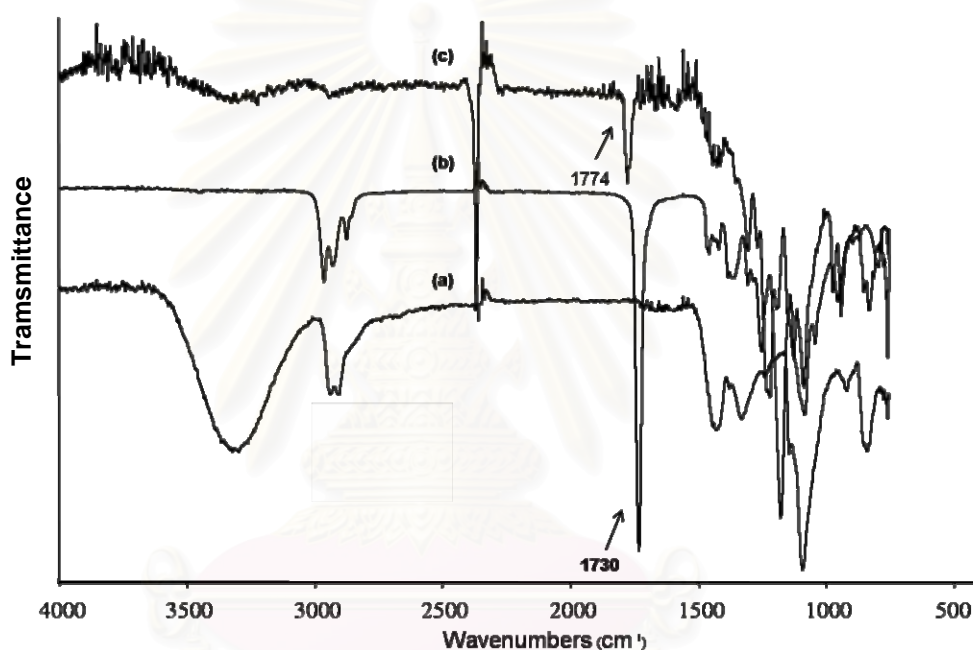
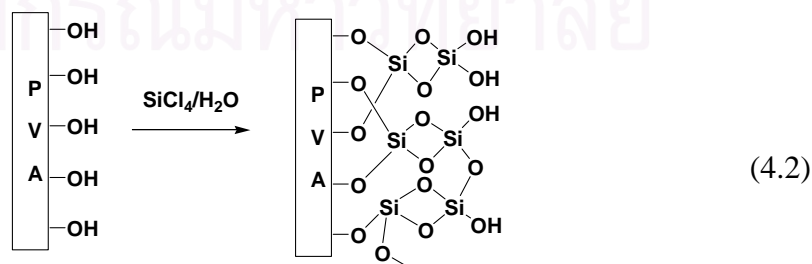


Figure 4.8 ATR-FTIR spectra of PVA fiber mats before (a) and after esterified with BC (b) and HFBC (c)

4.2.3 Preparation of PVA-silanol Fiber Mats



In light of the success to introduce an inorganic layer of silicon oxide/silanol to an ultrathin film of PVA adsorbed on polymer substrates, recently reported by

Quarmyne and Chen [31], we used the same approach to introduce the inorganic character to the PVA fibers in order to increase the strength and integrity of the PVA fiber mats. It was later found that not only can this inorganic layer prevent the PVA fibers from deforming, but it also makes the PVA fiber mats extremely hydrophilic with 0° water contact angle. This is much higher than the water contact angle of the virgin PVA fiber mats. Also, the silanol groups generated are readily available for subsequent silanization with acid chlorides.

The method involves sequential reactions between SiCl_4 and water (present in air). According to Figure 4.9 Si/C ratio determined by SEM-EDX analysis, increased linearly as a function of the number of reaction cycles. The ratio increases from 0 of PVA to 1.34, 3.38, and 6.04 after 1, 3, and 5 reaction cycles, respectively. The hydroxyl groups of the PVA fiber mats allows more SiCl_4 to react and thus more silica to grow during each cycle [31]. All PVA-silanol fiber mats exhibited 0° water contact angle regardless of the number of $\text{SiCl}_4/\text{H}_2\text{O}$ cycle. As seen in Figures 4.9 and 4.10, the fiber diameter was also enhanced after the formation of SiO_2/SiOH layer. It increased from 297.05 ± 33.59 nm of PVA to 305.50 ± 31.71 , 364.75 ± 33.05 , and 440.20 ± 36.03 nm after 1, 3, and 5 reaction cycles, respectively. The condition that was used for further studies was 3 cycles.

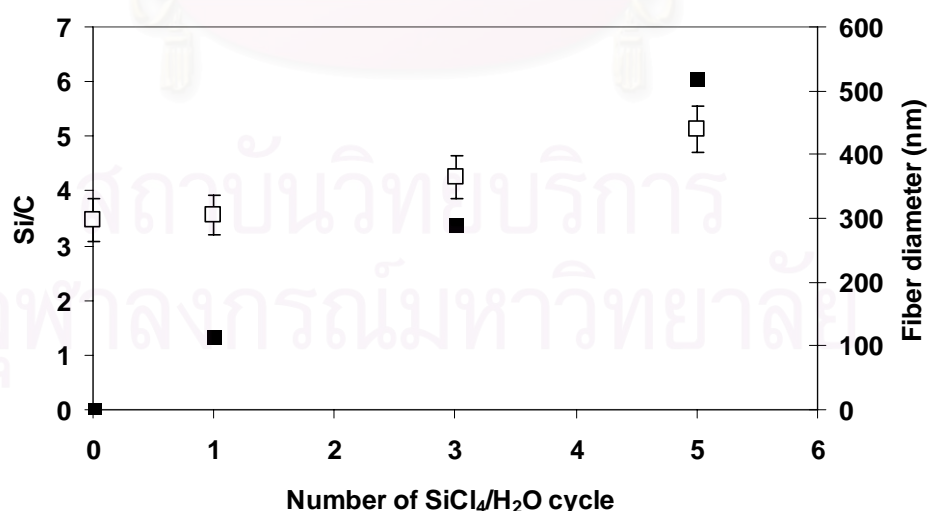


Figure 4.9 Silicon/carbon ratio (■) and fiber diameter (□) of PVA fiber mats as a function of number of $\text{SiCl}_4/\text{H}_2\text{O}$ reaction cycles.

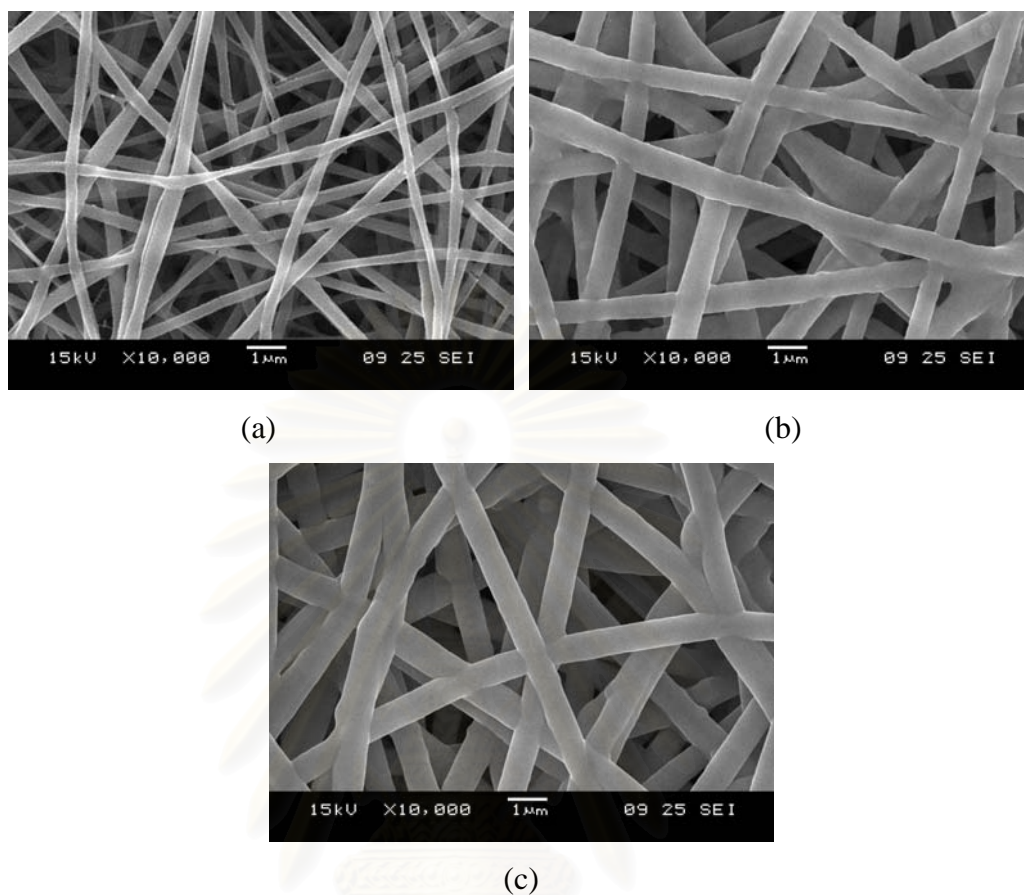
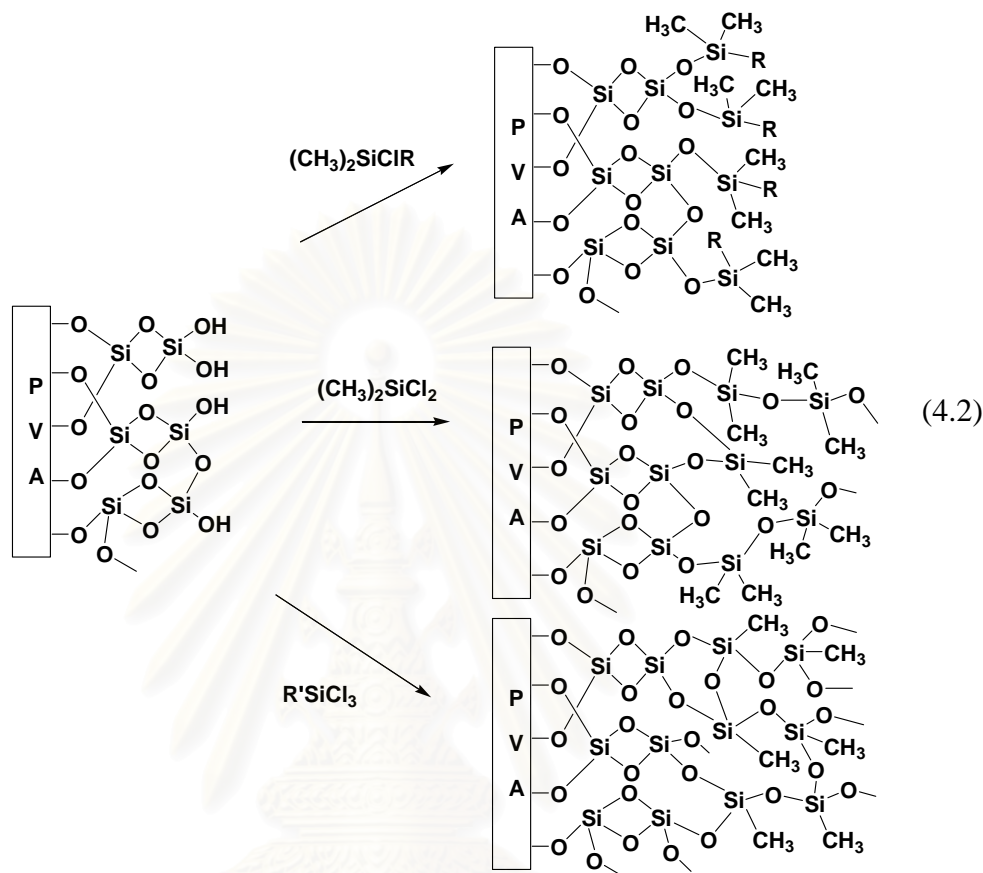


Figure 4.10 SEM micrographs of PVA fiber mats after a reaction with $\text{SiCl}_4/\text{H}_2\text{O}$: (a) 1 cycle, (b) 3 cycles, and (c) 5 cycles. Original magnification was 10,000x.

สถาบันวิทยบริการ
จุฬาลงกรณ์มหาวิทยาลัย

4.2.4 Silanization of PVA-silanol Fiber Mats



where $R = -(CH_2)_2CH_3, -(CH_2)_7CH_3, -(CH_2)_{10}CH_3$

$R' = -CH_3, -(CH_2)_7CH_3, -(CH_2)_2(CF_2)_5CF_3$

Comparative studies on silanization of the PVA-silanol fiber mats were conducted both in solution and vapor phases. The reactions in the solution phase were performed at ambient temperature in the presence of triethylamine which acts as a base for neutralizing HCl by-product. The reactions in the vapor phase, on the other hand, were conducted at higher temperatures. A temperature of 70°C was used for the silane reagents having moderate boiling points: chlorodimethylpropylsilane (CDPS, bp = 113°C), dichlorodimethylsilane (DDS bp = 69-70°C), and trichloromethylsilane (TMS, bp = 64-66°C). A temperature of 120°C was used for the silane reagents having high boiling points: chlorodimethyloctadecylsilane (CDODS, bp = 158-160°C), chlorodimethyloctylsilane (CDOS, bp = 217-220°C)

Water contact angle data (θ_A) of all silanized PVA-silanol fiber mats are displayed in Table 4.2. The reaction time listed in the table corresponds to the period of time that yielded the highest θ_A for each silane reagent. The samples in a series of monochlorosilane having two methyl substituents and one alkyl groups varying in chain length from 3 to 11 were first considered. In the solution phase, the surface wettability was not much affected by the alkyl chain length. The θ_A of the PVA-silanol fiber mats after reacting with CDOS was somehow lower than the other two reagents in the same series. In the vapor phase, the θ_A of the fiber mats was gradually increased as the alkyl chain length became longer.

Evidently, the fiber mats modified by DDS and TMS exhibited higher water contact angles than those modified with the monochlorosilanes. In principle, the difunctional organosilanes can form covalent attachment as well as surface-induced polymerization (vertical and/or horizontal) to form grafted polysiloxane while trifunctional organosilanes, as compared to monofunctional organosilanes, are more reactive and are capable of polymerizing in the presence of water and forming crosslinked three dimensional networks. As a result, these can give rise to a number of possible surface structures of which the anchored alkyl groups may be denser than the surfaces modified by monofunctional organosilanes.

In all cases, the contact angles are higher for the fiber mats silanized in the vapor phase than for those silanized in the solution. This behavior is in accordance with the work previously described by Fadeev and McCarthy [30]. They have suggested that the silanization in vapor phase is cleaner than that in the solution. Neither base nor solvent are necessary so the reactions can presumably give better yields. In particular, for monochlorosilanes, the molecule can pack more efficiently in the monolayer with less holes and defects in the vapor phase as opposed to the liquid phase. The longer the alkyl chain length is, the more efficient the monolayer packs. This can be evidenced from the fact that the water contact angle increases as a function of alkyl chain length.

Table 4.2 Water contact angle data of PVA-silanol fiber mats after silanization with alkylchlorosilanes

Series	Silane reagent R	Reaction time (h)	Water contact angle (θ_A)	
			Solution	Vapor
Monochlorosilane	CDPS (CH ₂) ₂ CH ₃	3	131.02 ± 0.50	135.96 ± 2.27
	CDOS (CH ₂) ₇ CH ₃	1	120.76 ± 2.14	141.83 ± 4.04
	CDODS (CH ₂) ₁₀ CH ₃	3	131.64 ± 1.40	144.06 ± 5.22
Dichlorosilane	DDS CH ₃	0.5	141.20 ± 1.01	150.60 ± 1.43
Trichlorosilane	TMS CH ₃	0.5	137.50 ± 3.78	145.10 ± 2.18

To further increase the hydrophobicity of the PVA-silanol fiber mats, other two trichlorosilanes, trichloro(octyl)silane (TOS) and trichloro(1*H*,1*H*,2*H*,2*H*-perfluorooctyl)silane (TFOS) were also investigated to form $-(\text{CH}_2)_7\text{CH}_3$ and $-(\text{CH}_2)_2(\text{CF}_2)_5\text{CF}_3$ containing surfaces. Using a reaction time of 8 h, TFOS and TOS yielded a surface with θ_A of $167.64 \pm 3.83^\circ$ and $160.28 \pm 1.71^\circ$. As expected, the fluorocarbon silane gave the surface with greater hydrophobicity than that of its hydrocarbon analog. It is well-known that fluorine is effective for lowering the surface free energy chemically because fluorine has a small atomic radius and the bigger electronegativity among atoms, so it forms a stable covalent bond with carbon [16].

4.2.5 Confirmation of Silanization

Figure 4.11 shows ATR-FTIR spectra of selected silanized PVA fiber mats. The absorption bands due to the Si-O stretching ($1100-1200\text{ cm}^{-1}$) are clearly visible in all samples indicating the success of silanization.

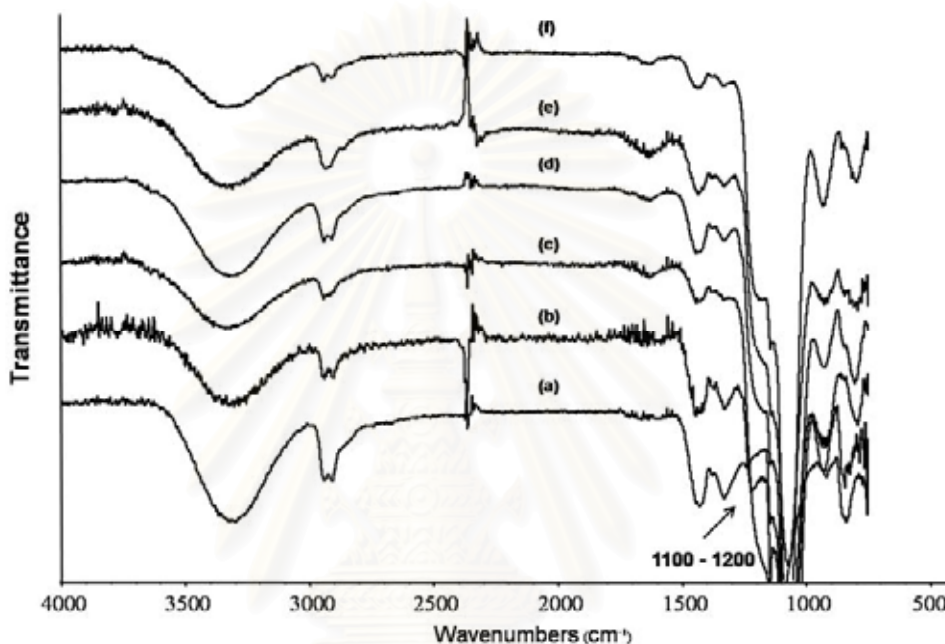


Figure 4.11 ATR-FTIR spectra of PVA fiber mats (a) and PVA-silanol fiber mats before (b) and after silanized with CDODS (c), DDS (d) TOS (e), and TFOS (f)

4.2.6 Morphology of PVA-silanol Fiber Mats after Silanization

To demonstrate the effect of reaction phase (solution vs vapor) on the morphology of fiber mats, SEM micrographs of the PVA-silanol fiber mats subjected to silanization with the dichlorosilane, DDS are displayed for comparison. As seen in Figure 4.12, the silanization introduced coating to the surface of fibers. The modified layer obtained in vapor is obviously smoother than that obtained in solution. This agrees well with the observation reported by Gao and McCarthy [29]. The incomplete coverage of the silanized layer in solution resulted in additional nanoscopic roughness to the fibers. This feature did not affect the water contact angle the way it was predicted based on previous work reported by others [29, 55].

Gao and McCarthy [29] showed that the second level of topography (three dimension of network having a diameter less than 50 nm) of hydrophobized surfaces containing staggered rhombus posts of silica raises the contact angles of the post tops and the macroscopic sample to $\theta_A/\theta_R = >176^\circ/>176^\circ$ and eliminates hysteresis. Using the electrospinning process, Lim *et al.* [53] fabricated multiple-scale nanofiber films which contained water-soluble polymers and different colloids: monodisperse silica or polystyrene particles. The multiple-scale roughness from bidisperse colloids of 700 and 50 nm silica particles or macropores templated from polystyrene particles and 50 nm silica particles was essential to generate higher contact angles and lower water sliding angles as compared with the nanofiber films without multiple-scale roughness. In both cases, stable superhydrophobic multiple-scale fibrous films with large contact angle ($>150^\circ$) and low sliding angle ($<2^\circ$) were successfully produced.

It was expected that the water contact angle would have been raised when the secondary roughness was introduced and that would help reducing the contact angle hysteresis as well as the sliding angle. Apparently, that was not the case. The receding water contact angle remained 0, leading to an extremely high contact angle hysteresis. The water drop remained intact with the fiber mats and did not roll off although the fiber mats were flipped up-side down. The issues related to both contact angle hysteresis and sliding angle will be later discussed in more detail.

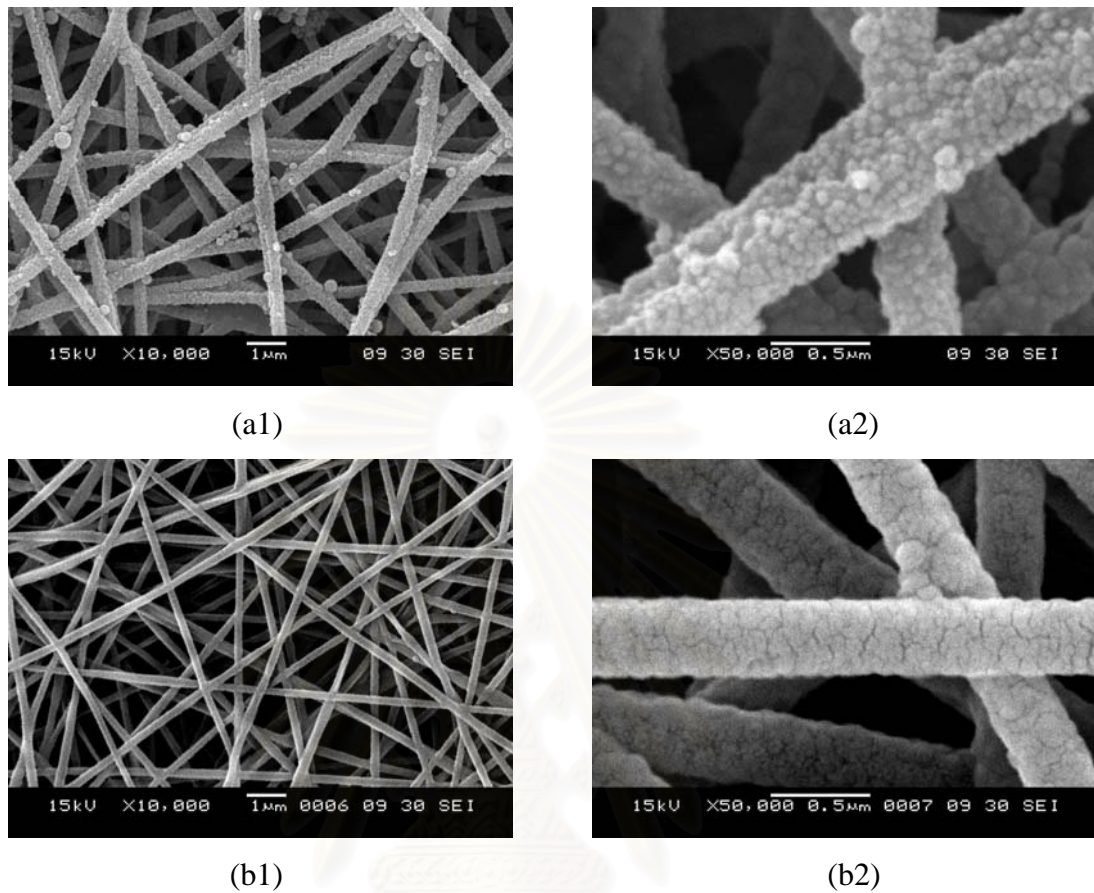


Figure 4.12 SEM micrographs of PVA-silanol fiber mats after silanization with DDS in solution with magnification of 10,000X (a1) and 50,000X (a2), in vapor phase with magnification of 10,000X (b1) and 50,000X (b2).

A similar trend was also observed for the PVA-silanol fiber mats modified by monochlorosilanes. The modified layer obtained in vapor (Figure 4.13) is obviously smoother than that obtained in solution (Figure 4.14).

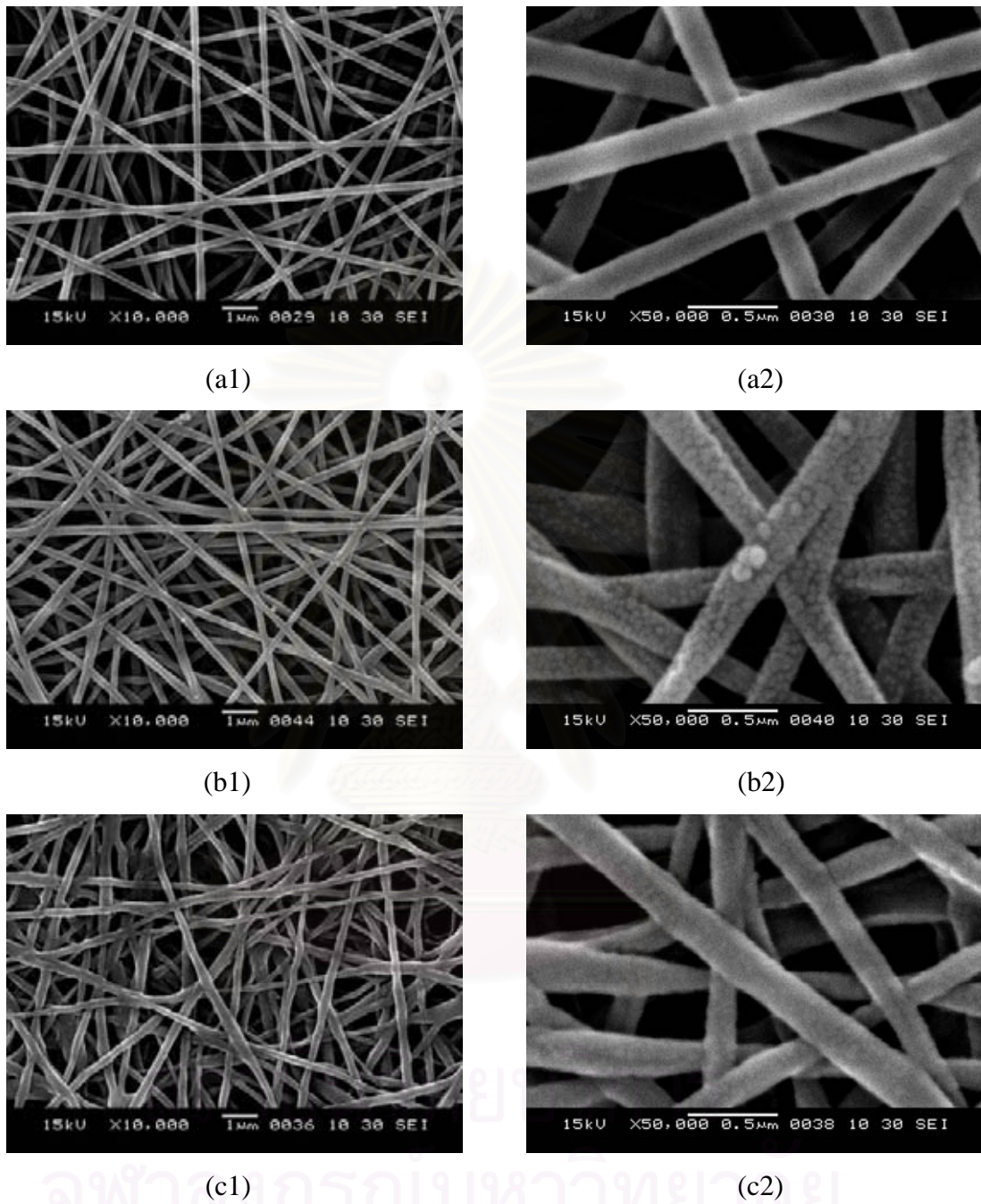


Figure 4.13 SEM micrographs of PVA-silanol fiber mats after silanization in vapor with CDPS with magnification of 10,000X (a1) and 50,000X (a2), CDOS with magnification of 10,000X (b1) and 50,000X (b2), and CDODS with magnification of 10,000X (c1) and 50,000X (c2)

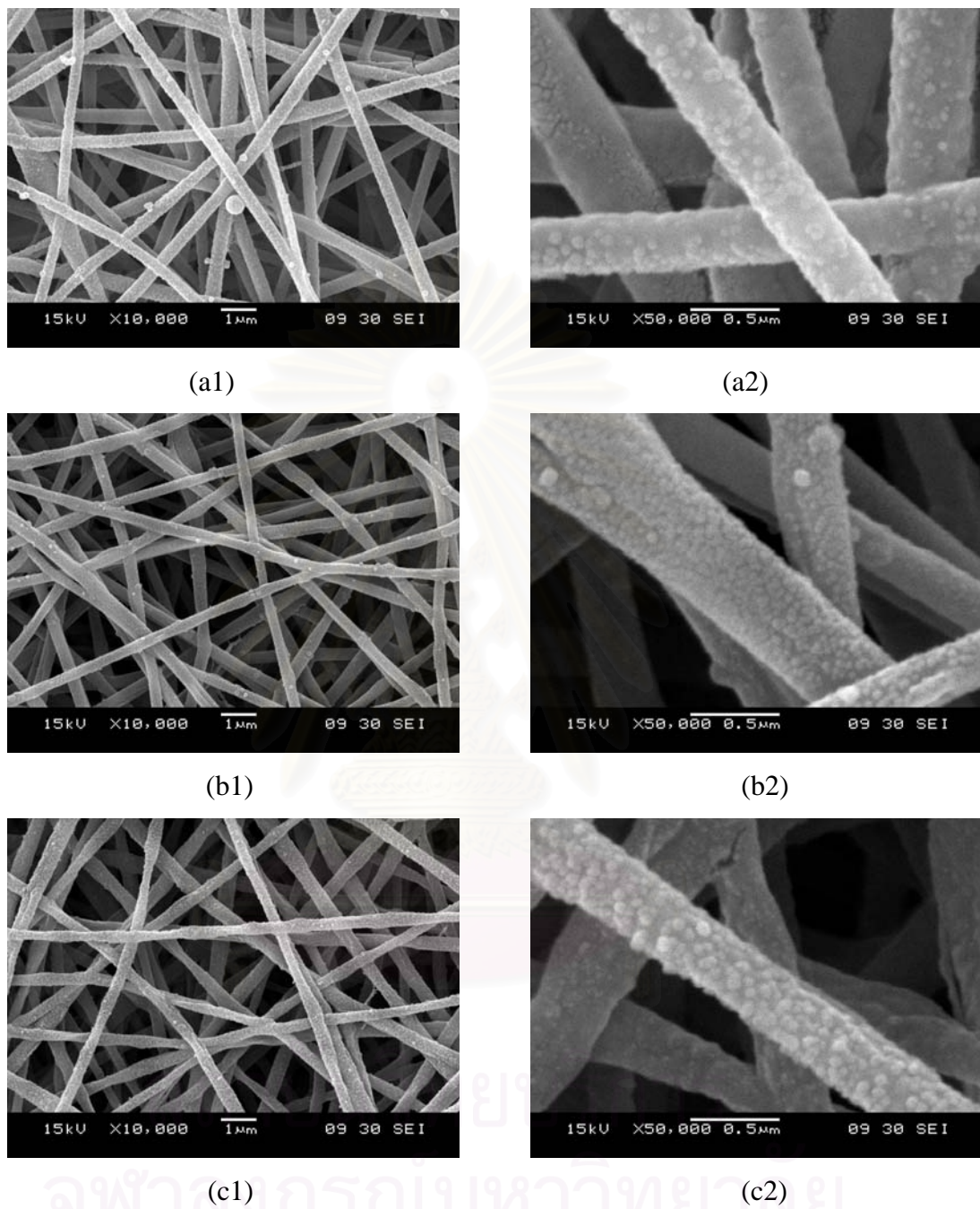


Figure 4.14 SEM micrographs of PVA-silanol fiber mats after silanization in solution with CDPS with magnification of 10,000X (a1) and 50,000X (a2), CDOS with magnification 10,000X (b1) and 50,000X (b2), and CDODS with magnification of 10,000X (c1) and 50,000X (c2)

Another observation that needs an explanation is a change of fiber diameter. In comparison with the PVA-silanol fibers whose diameter was as high as almost 1 μm , the fiber diameter became smaller after the silanization regardless of the type of silane reagent. The diameters of the modified fibers fall in the similar range (50-400 nm) as those of the virgin electrospun PVA fibers before the introduction of silanol layer. We suspect that the subsequent silanization made the overall modified layer denser and caused the PVA fibers to collapse back to their original size. Furthermore, it was found that the reduction of fiber diameter was even more pronounced when the structure of the silanized layer was more complex, especially in vapor phase. The fibers obtained after the modification with dichlorosilanes (grafted polysiloxane, 2D, Figure 4.11 (b)) and trichlorosilanes (crosslinked polysiloxane, 3D, Figure 4.14) were smaller in diameter than those modified by monochlorosilanes (monolayer, 1D, Figure 4.13).

In principle, the contact angle hysteresis is more important in characterizing hydrophobicity than the maximum achievable contact angle. Thus, the term and superhydrophobic should be reserved for materials upon which drops move spontaneously or easily on horizontal or near-horizontal surfaces liquid-like and that droplets in contact with surface experience very low energy barriers between metastable states. These contact angle increases to decreases in the contact length and increases in tortuosity of the three-interphase contact line. Although some of the silanized PVA fiber mats exhibit higher advancing contact angles (θ_A) higher than 150° , their receding contact angles were 0 and the contact angle hysteresis was exceedingly high. These characteristics suggest that all silanized PVA fiber mats cannot be considered superhydrophobic.

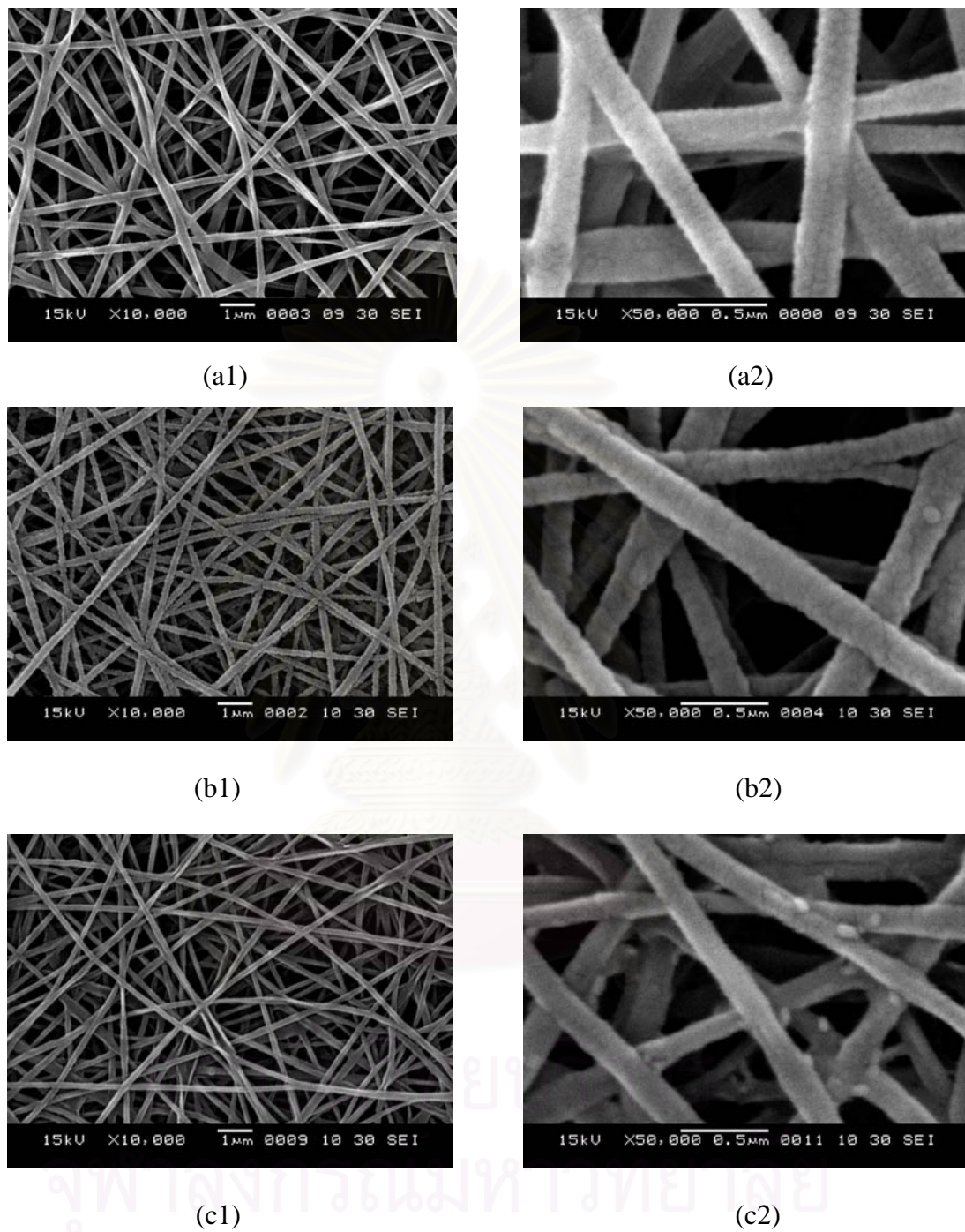


Figure 4.15 SEM micrographs of PVA-silanol fiber mats after silanization in vapor phase with TMS with magnification of 10,000X (a1) and 50,000X (a2), TFOS with magnification of 10,000X (b1) and 50,000X (b2), and TOS with magnification of 10,000X (c1) and 50,000X (c2)

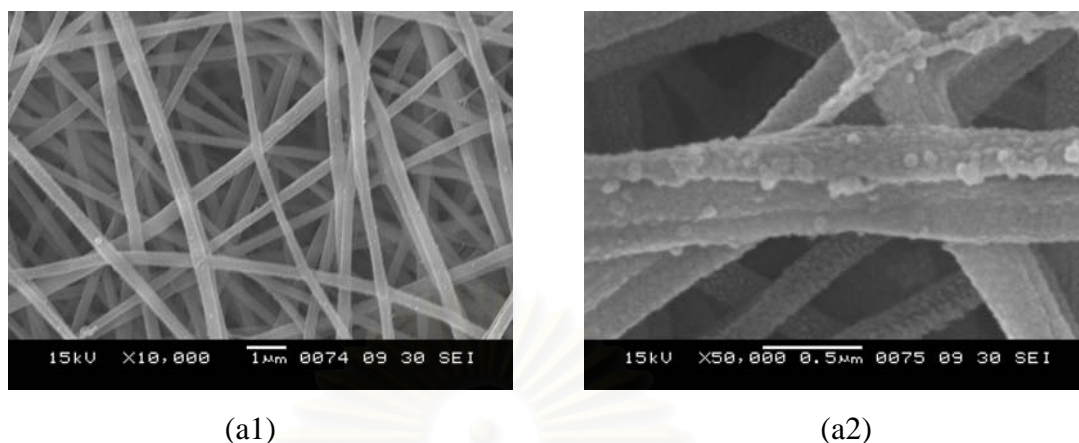


Figure 4.16 SEM micrographs of PVA-silanol fiber mats after silanization with TMS in solution with magnification of 10,000X (a1) and 50,000X (a2)

The fiber sizes of all silanized PVA fiber mats have an average diameter of 304.62 ± 42.74 nm. This range is, in fact, similar to or even less than the ranges of electrospun superhydrophobic fiber mats reported by Ma and co-workers [51, 52]. They prepared two series of superhydrophobic surfaces by electrospinning. One series was electrospun polycaprolactone (PCL) that was coated with a thin layer of poly(perfluoroalkyl ethyl methacrylate) by initiated chemical vapor deposition. The highest water contact angle obtained in this series was 175° and a threshold sliding angle was less than 2.5° . Their beaded and bead-free fibers have diameters ranging from 600 to 2200 nm. The other series was electrospun fibers of poly(styrene-*b*-dimethylsiloxane) block copolymers blended with homopolymer polystyrene [52]. The fabricated fibers had average diameters in the range of 150-400 nm. The highest water contact angle achieved was 163° with a contact angle hysteresis of 15° . Considering these data, the fiber size should not be the parameter that limits the ability to make the PVA fiber mats superhydrophobic.

Ma *et al.* also suggested that the water contact angle can be enhanced by an introduction a high density of relatively small diameter beads to the fiber. Alternatively, Lim *et al.* [53] have used monodisperse silica nanoparticles or polystyrene microspheres and monodisperse silica nanoparticles as templates to generate nanofiber films with multiple-scale roughness in order to generate higher contact angles ($>150^\circ$) and low water sliding angles ($<2^\circ$). In light of their success,

we also attempted to add the secondary roughness by using PVA mats containing beaded fibers. The PVA fiber mats were electrospun from 8% (w/v) PVA solution. The bead on fiber has an average diameter of 594.90 ± 59.08 nm. As displayed in Table 4.3, the θ_A of the silanized beaded fiber mats were not much different from those of the silanized fiber mats. In all cases, the receding water contact angles remained 0° and the water drop remained intact with the fiber mats and did not roll off although the fiber mats were flipped up-side down. SEM micrographs shown in Figure 4.16 demonstrate that the morphology of the beaded fiber mats remained unchanged after the silanization.

Table 4.3 Water contact angle data of PVA-silanol beaded fiber mats after silanization with alkylchlorosilanes

Series	Silane reagent R	Reaction time (h)	Water contact angle (θ_A)	
			Solution	Vapor
Monochlorosilane	CDPS (CH ₂) ₂ CH ₃	3	132.86±2.81	134.25 ±3.21
	CDOS (CH ₂) ₇ CH ₃	3	130.23±1.51	131.69±2.10
	CDODS (CH ₂) ₁₀ CH ₃	3	133.65±3.44	132.12±1.52
Dichlorosilane	DDS CH ₃	1	140.71±2.54	142.09±1.83
	Trichlorosilane	TMS CH ₃	1	151.30±2.77

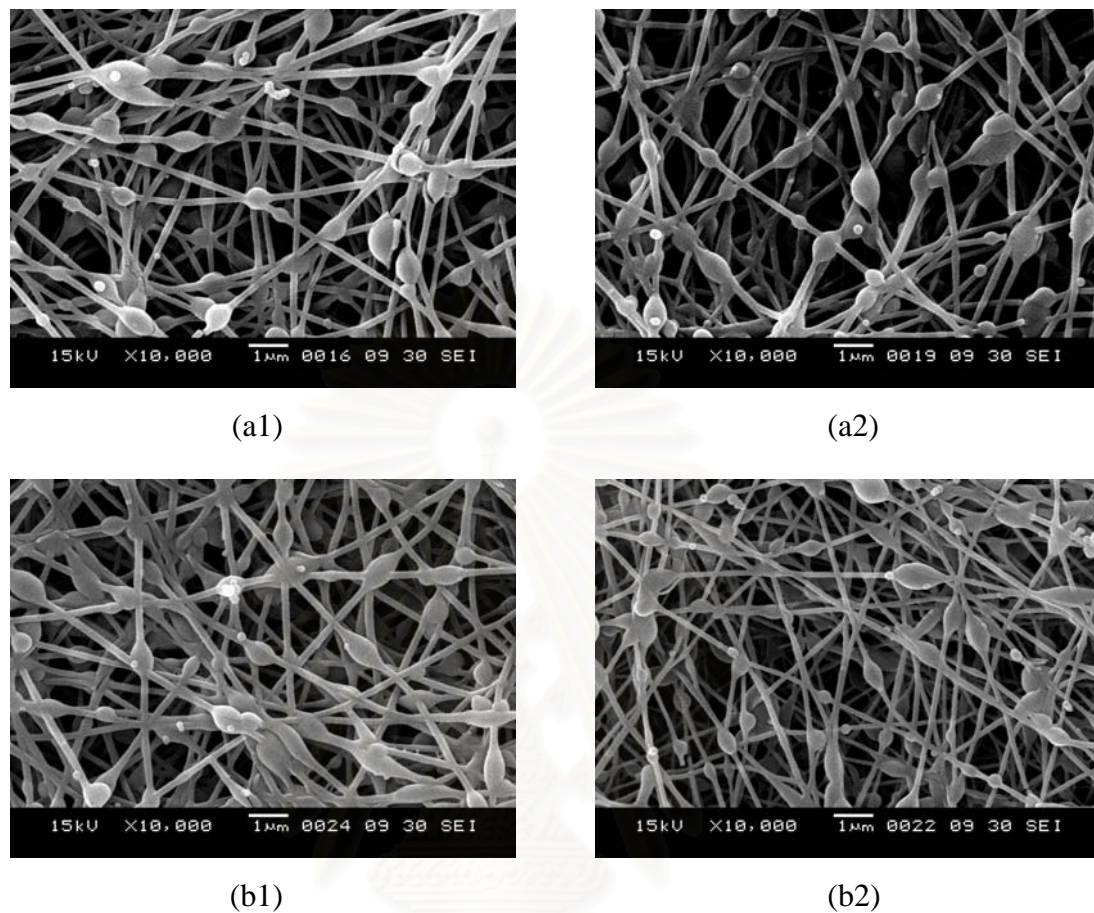


Figure 4.17 SEM micrographs of PVA-silanol beaded fiber mats after silanization with DDS and TMS in solution with magnification of 10,000X (a1) and (a2), in vapor phase with magnification of 10,000X (b1) and (b2).

We suspect that the failure to make the electrospun PVA fibers superhydrophobic may be caused by the low packing density of the fibers. If the packing density of the fibers is not high enough, there is a large tendency that the water does not only contact with the top surface of the fibers, but is also trapped in the air pocket between fibers. If that is the case, the water droplet in contact with the surface of fiber mats experiences very high energy barriers between metastable states and is pinned upon the withdrawing of the water. As a result, the receding angle is very low and the hysteresis becomes very high. In other words, the fiber mats adopt a Wenzel state. Although the introduction of additional roughness from the beads was attempted, that was not enough to minimize the contact between the water drop and the inter-space of the fibers.

CHAPTER V

CONCLUSION AND SUGGESTION

In this study, poly(vinyl alcohol) (PVA) were fabricated by electrospinning. The morphological appearance and diameter of the electrospun PVA fiber mats were varied as a function of PVA concentration. Upon increasing the PVA concentration, The fiber diameter became larger with less bead formation. The transition from beaded fibers to the bead-free fibers occurred at the concentration of 10% w/v. The fiber diameter was in a range of 74-328 nm. The electrospun PVA fiber mats exhibited a water contact angle in a range of 49.41°–59.34°, which was in a hydrophilic region. Most chemical modification reactions were conducted on PVA fiber mats electrospun from 10%(w/v) PVA solution, having a diameter of 297.05 ± 33.59 nm and water contact angle of $52.31^\circ \pm 1.22^\circ$.

Esterification of PVA fiber mats with acyl chlorides was performed both in solutions in the presence of triethylamine and in vapor. Although the water contact angle of the fiber mats was raised to as high as 115°, it was found that the PVA fiber mats became collapsed and lost their original morphologies after the reactions. It was suspected that the deformation of the fibers was caused by the intrinsically low integrity of the hydrophilic PVA itself against the reagents (acyl chloride, triethylamine) and the by-product (HCl).

Therefore, an inorganic layer of SiO₂/SiOH was introduced to the PVA fiber mats in order to increase the strength and integrity of the PVA fiber mats. It was later found that not only could this inorganic layer prevent the PVA fibers from deforming, but it also made the PVA fiber mats extremely hydrophilic with 0° water contact angle. This was much lower than the water contact angle of the virgin PVA fiber mats. Also, the silanol groups generated are readily available for subsequent silanization with acid chlorides. The fiber diameter was also enhanced after the formation of SiO₂/SiOH layer. It increased from 297.05 ± 33.59 nm of PVA to 305.50 ± 31.71 , 364.75 ± 33.05 , and 440.20 ± 36.03 nm after 1, 3, and 5 reaction cycles, respectively. The condition that was used for further studies was 3 cycles.

Subsequent silanization of PVA-silanol fiber mats was also conducted both in solutions in the presence of triethylamine and in vapor. It was found that the modified layers obtained in vapor were smoother and gave higher water contact angles than those obtained in solution. This stems from the fact that the silanization in vapor phase is cleaner than that in the solution. Neither base nor solvent are necessary so the reactions can presumably give better yields. The fiber mats modified by dichlorosilane and trichlorosilanes exhibited higher water contact angles than those modified with monochlorosilanes. The highest water contact angle ($167.64 \pm 3.83^\circ$) obtained from the silanization with trichloro(1*H*,1*H*,2*H*,2*H*-perfluorooctyl)silane (TFOS), the fluoro-containing trichlorosilane. It was also found that the subsequent silanization made the overall modified layer denser and caused the PVA fibers to collapse back to their original size independent of the silane reagent.

We also attempted to add the secondary roughness by using PVA mats containing beaded fibers electrospun from 8% (w/v) PVA solution. The bead on fiber has an average diameter of 594.90 ± 59.08 nm. Nonetheless, it was found that the water contact angles of the silanized beaded fiber mats were not much different from those of the silanized fiber mats. In all cases, the receding water contact angles remained 0; leading to an extremely high contact angle hysteresis and the water drop remained intact with the fiber mats and did not roll off although the fiber mats were flipped up-side down. These characteristics suggest that all silanized PVA fiber mats cannot be considered superhydrophobic.

It is suspected that the failure to make the electrospun PVA fibers superhydrophobic may be caused by the low packing density of the fibers. If the packing density of the fibers is not high enough, there is a large tendency that the water does not only contact with the top surface of the fibers, but is also trapped in the air pocket between fibers. The water droplet in contact with the surface of fiber mats experiences very high energy barriers between metastable states and is pinned upon the withdrawing of the water. As a result, the receding angle is very low and the hysteresis becomes very high. In other words, the fiber mats adopt a Wenzel state. Although the introduction of additional roughness from the beads was

attempted, that was not enough to minimize the contact between the water drop and the inter-space of the fibers.

It is advisable to investigate the effect of packing density of the fiber mats on the wettability of the fiber mats. It is anticipated that increasing the fiber packing density may reduce the contact between the water drop and the fiber mats and the fiber mats may be close to be in Cassie-Baxter regime. An introduction of secondary roughness by adding nano-sized fillers along with the PVA solution before electrospinning may be another way to make the PVA fiber mats superhydrophobic after surface silanization.



สถาบันวิทยบริการ
จุฬาลงกรณ์มหาวิทยาลัย

REFERENCES

1. Bonn, D. "Wetting Transitions" *Current Opinion in Colloid and Interface Science*. **2001**, 6, 22-27.
2. Quéré, D. "Rough Ideas on Wetting" *Physica A*. **2001**, 313, 32-46.
3. Coninck, J. D.; de Ruijter, M. J.; Voué, M. "Dynamics of Wetting" *Current Opinion in Colloid and Interface Science*. **2001**, 6, 49-53.
4. Chen, W.; Fadeev, A. Y.; Hsieh, M. C.; Öner, D.; Youngblood, J.; McCarthy, T. J. "Ultrahydrophobic and Ultralyophobic Surfaces: Some Comments and Examples" *Langmuir* **1999**, 15, 3395-3399.
5. Miwa, M.; Nakajima, A.; Fujishima, A.; Hashimoto, K.; Watanabe, T. "Effects of the Surface Roughness on Sliding Angles of Water Droplets on Superhydrophobic Surfaces" *Langmuir* **2000**, 16, 5754-5760.
6. Callies, M.; Quéré, D. "On Water Repellency" *Soft Matter* **2005**, 1, 55-61.
7. Verplanck, N., Coffinler, Y.; Thomy, V.; Boukherroub, R. "Wettability Switching Techniques on Superhydrophobic Surfaces" *Nanoscale Research Letter* **2007**, 2, 577-596.
8. Wenzel, R. N. "Surface Roughness and Contact Angle" *Industrial Engineering Chemistry* **1936**, 28, 988-994.
9. Cassie, A. B. D.; Baxter, S. "Wettability of Porous Surfaces" *Transactions of Faraday Society* **1944**, 40, 546-551.
10. Johnson, R. E. J.; Dettre, R. H. "In Contact angle, Wettability, and Adhesion" *Journal of the American Chemical Society* **1964**, 112-135.
11. Nosonovsky, M. "Multiscale Roughness and Stability of Superhydrophobic Biomimetic Interfaces" *Langmuir* **2006**, 23, 3157-3161.
12. Bico, J.; Thiele, U.; Quéré, D. "Wetting of Textured Surfaces" *Colloid and Surfaces A: Physicochemical and Engineering Aspects* **2002**, 206, 41-46.
13. Patankar, N. A. "On the Modelling of Hydrophobic Contact Angles on Rough Surface" *Langmuir* **2003**, 19, 1249-1253.
14. Marmur, A. "Wetting on Hydrophobic Rough Surfaces: To Be Heterogeneous or Not To Be?" *Langmuir* **2003**, 19, 8343-8348.

15. Öner, D.; McCarthy, T. J. "Ultrahydrophobic Surfaces. Effects of Topography Length Scale on Wettability" *Langmuir* **2000**, *16*, 7777-7782.
16. Nishino, T.; Meguro, M.; Nakamae, K.; Matsushita, M.; Ueda, Y. "The Lowest Surface Free Energy Based on $-CF_3$ Alignment" *Langmuir* **1999**, *15*, 4321-4323.
17. Hare, E. F.; Shafrin, E. G.; Zisman, W. A. "Properties of Films of Adsorbed Fluorinated Acids" *Journal of Physical Chemistry* **1954**, *58*, 236-239.
18. Tsibouklis, J.; Nevell, T. G. "Ultra-Low Surface Energy Polymers: The Molecular Design Requirements" *Advanced Materials* **2003**, *15*, 647-650.
19. Graham, P.; Stone, M.; Thorpe, A. A.; Nevell, T. G.; Tsibouklis, J. "Fluoropolymers with Very Low Surface Energy Characteristics" *Journal of Fluorine Chemistry* **2000**, *104*, 29-36.
20. Pullin, R. A.; Nevell, T. G.; Tsibouklis, J. "Surface Energy Characteristics and Marine Antifouling Performance of Poly(1H,1H,2H,2H-perfluorodecanoyl diitaconate) Film Structures" *Materials Letter* **1999**, *39*, 142-148.
21. Tsibouklis, J.; Stone, M.; Thorpe, A. A.; Graham, P.; Nevell, T. G.; Ewen, R. J. "Inhibiting Bacterial Adhesion onto Surfaces: the Non-stick Coating Approach" *International Journal of Adhesion and Adhesives* **2000**, *20*, 91-96.
22. Otten, A.; Herminghaus, S. "How Plants Keep Dry: A Physicist's Point of View" *Langmuir* **2004**, *20*, 2405-2408.
23. Lau, K. K. S.; Bico, J.; Teo, K. B. K.; Chhowalla, M.; Amaratunga, G. A. J.; Milne, W. I.; McKinley, G. H.; Gleason, K. K. "Superhydrophobic Carbon Nanotube Forests" *Nano Letters* **2003**, *3*, 1701-1705.
24. Liu, H.; Feng, L.; Zhai, J.; Jiang, L.; Zhu, D. "Reversible Wettability of a Chemical Vapor Deposition Prepared ZnO Film between Superhydrophobicity and Superhydrophilicity" *Langmuir* **2004**, *20*, 5659-5661.
25. Sun, T.; Wang, G.; Liu, H.; Feng, L.; Jiang, L.; Zhu, D. "Control over the Wettability of an Aligned Carbon Nanotube Film" *Journal of the American Chemical Society* **2003**, *125*, 14996-14997.

26. Chen, W.; Fadeev, A. Y.; Hsieh, M. C.; Öner, D.; Youngblood, J.; McCarthy, T. J. "Ultrahydrophobic and Ultrayophobic Surfaces: Some Comments and Examples" *Langmuir* **1999**, *15*, 3395-3399.
27. Youngblood, J.; McCarthy, T. J. "Ultrahydrophobic Polymer Surfaces Prepared by Simultaneous Ablation of Polypropylene and Sputtering of Poly(tetrafluoroethylene) Using Radio Frequency Plasma" *Langmuir* **1999**, *32*, 6800-6806.
28. Gao, L.; McCarthy, T. J. "The "Lotus Effect" Explained: Two Reasons Why Two Length Scales of Topography Are Important" *Langmuir* **2006**, *22*, 2966-2967.
29. Gao, L.; McCarthy, T. J. "A Perfectly Hydrophobic Surface ($\theta_A/\theta_R = 180^\circ/180^\circ$)" *Journal of the American Chemical Society* **2006**, *128*, 9052-9053.
30. Fadeev, A. Y.; McCarthy, T. J. "Self-Assembly Is Not the Only Reaction Possible between Alkyltrichlorosilanes and Surfaces: Monomolecular and Oligomeric Covalently Attached Layers of Dichloro- and Trichloroalkylsilanes on Silicon" *Langmuir* **2000**, *16*, 7268-7274.
31. Quarmyne, M.; Chen, W. "General Approach for the Preparation of Nanoscale Inorganic Layers on Polymeric Materials Surfaces" *Langmuir* **2003**, *19*, 2533-2535.
32. Huang, Z. M.; Zhang, Y. Z.; Kotaki, M.; Ramakrishna, S. "A Review on Polymer Nanofibers by Electrospinning and Their Applications in Nanocomposites" *Composite Science and Technology* **2003**, *63*, 2223-2253.
33. Formhals, A. **1934** US Patent No. 1,975,504.
34. Doshi, J.; Reneker, D. H. "Electrospinning Process and Applications of Electrospinning" *Polymer* **1995**, *40*, 4585-4592.
35. Tsai, P. P.; Schreuder-Gibson, H.; Gibson, P. "Different Electrostatic Method for making Electricity Magnet filters" *Journal of Electrostatics* **2002**, *54*, 333-341.

36. Hafemann, B.; Ensslen, S.; Erdmann, C.; Niedballa, R.; Zühlke, A.; Ghofrani, K.; Kirkpatrick, C. J. "Use of Collagen/Elastin-membrane for the Tissue Engineering of Dermis" *Burns* **1999**, *25* 373-384.
37. Gibson, P. W.; Schreuder-Gibson, H. L.; Rivin, D. "Electrospun Fiber Mats: Transport Properties" *American Institute of Chemical Engineers* **1999**, *45*, 90-195.
38. Gouma, P. I. "Nanostructured Polymorphic Oxides for Advanced Chemosensors" *Review of Advanced Materials Science* **2003**, *5*, 147-154.
39. Martien, F. L. "Encyclopedia of polymer science and engineering" *Wiley, New York*. **1986**.
40. DeMerlis, C. C.; Schoneker, D. R. "Review of the Oral Toxicity of Poly(vinyl alcohol) (PVA)" *Food and Chemical Toxicology* **2003**, *41*, 319-326.
41. Sui, G. X.; Yao, G.; Zhou, B. L. "Influence of Artificial! Pre-stressing during the Curing of VIRALL on its Mechanical Properties" *Composites Science and Technology* **1995**, *53*, 361-364.
42. Ding, B.; Kim, H. Y.; Lee, S. C.; Shao, C. L.; Lee, D. R.; Park, S. J.; Kwag, G. B.; Choi, K. J. "Preparation and Characterization of a Nanoscale Poly(vinyl alcohol) Fiber Aggregate Produced by an Electrospinning Method" *Journal of Polymer Science: Part B: Polymer Physics* **2002**, *40*, 1261-1268.
43. Koski, A.; Yim, K.; Shivkumar, S. "Effect of Molecular Weight on Fibrous PVA Produced by Electrospinning" *Materials Letter* **2004**, *58*, 493-497.
44. Lee, J. S.; Choi, K. H.; Ghim, H. D.; Kim, S. S.; Chun, D. H.; Kim, H. Y.; Lyoo, W. S. "Role of Molecular Weight of Atactic Poly(vinyl alcohol) (PVA) in the Structure and Properties of PVA Nanofabric Prepared by Electrospinning" *Journal of Applied Polymer Science* **2004**, *93*, 1638-1646.
45. Jun, Z.; Hou, H.; Wendroff, H. J.; Greiner, A. "Poly(vinyl alcohol) Nanofibers by Electrospinning: Influence of Molecular Weight on Fibre Shape" *e-Polymer* **2005**, *38*, 1-7.
46. Wu, L.; Yuan, X.; Sheng, J. "Immobilization of Cellulose in Nanofibrous PVA Membranes by Electrospinning" *Journal of Membrane Science* **2005**, *250*, 167-173.

47. Zeng, J.; Aliger, A.; Czubayko, F.; Kissel, T.; Wendorff, J. H.; Greiner, A. "Poly(vinyl alcohol) Nanofibers by Electrospinning as a Protein Delivery System and the Retardation of Enzyme Release by Additional Polymer Coatings" *Biomacromolecules* **2005**, *6*, 1484-1488.
48. Zhang, C.; Yuan, X.; Wu, L.; Han, Y.; Sheng, J. "Study on Morphology of Electrospun Poly(vinyl alcohol) Mats" *European Polymer Journal* **2005**, *41*, 423-432.
49. Son, W. K.; Youk, J. H.; Lee, T. S.; Park, W. H. "Effect of pH on Electrospinning of Poly(vinyl alcohol)" *Materials Letters* **2005**, *59*, 1571-1575.
50. Shang, H. M.; Wang, Y.; Takahashi, K.; Cao, G. Z. "Nanostructured Superhydrophobic Surfaces" *Journal of Materials Science* **2005**, *40*, 3587-3591.
51. Ma, M.; Mao, Y.; Gupta, M.; Gleason, K. K.; Rutledge, G. C. "Superhydrophobic Fabrics Produced by Electrospinning and Chemical Vapor Deposition" *Langmuir* **2005**, *38*, 9742-9748.
52. Ma, M.; Hill, R. M.; Lowery, J. L.; Fridrikh, S. V.; Rutledge, G. C. "Electrospun Poly(Styrene-*block*-dimethylsiloxane) Block Copolymer Fibers Exhibiting Superhydrophobic" *Langmuir* **2005**, *21*, 5549-5554.
53. Lim, J. M.; Yi, G. R.; Moon, J. H.; Heo, C. J.; Yang, S. M. "Superhydrophobic Films of Electrospun Fibers with Multiple-Scale Surface Morphology" *Langmuir* **2007**, *23*, 7981-7989.
54. <http://science.jrank.org/pages/2573/Esterification.html>
55. Fadeev, A. Y.; McCarthy, T. J. "Trialkylsilane Monolayers Covalently Attached to Silicon Surfaces: Wettability Studies Indicating that Molecular Topography Contributes to Contact Angle Hysteresis" *Langmuir* **1999**, *15*, 3759-3766.
56. Boksanyi, L.; Liardon, O.; Kovats, E. S. "Chemically modified silicon dioxide surfaces. Reaction of n-Alkyldimethylsilanols and n-Oxaalkyldimethylsilanols with the Hydrated Surface of Silicon Dioxide. Question of the Limiting Surface Concentration" *Advances in Colloid and Interface Science* **1976**, *6*, 95-137.

57. Berendsen, G. E.; Pikaart, K. A.; de Galan, L. "Preparation of Various Bonded Phases for HPLC using Monochlorosilanes" *Journal of Liquid Chromatography* **1980**, *3*, 1437-1464.
58. Kinkel, J. N.; Unger, K. K. "Role of Solvent and Base in the Silanization Reaction of Silicas for Reversed-phase High-performance Liquid Chromatography" *Journal of Chromatography* **1984**, *316*, 193-200.
59. Zeigler, R. C.; Maciel, G. E. "A Study of the Structure and Dynamics of Dimethyloctadecylsilyl-modified Silica Using Wide-line ^2H NMR Techniques" *Journal of the American Chemical Society* **1991**, *113*, 6349-6358.
60. Miltenburg, J. C.; Hammers, W. E. "Transitions in Chemically Bonded Organic Phases on Silica. Specific Heat Measurements by Adiabatic Calorimetry" *Journal of Chromatography* **1983**, *268*, 147-155.
61. Claudy, P.; Letoffe, J. M.; Gaget, C.; Morell, D.; Serpinet, J. J. "Long-chain Alkyl Grafts and Mixed Alkyl-Alkane Layers at the Surface of Macroporous Silicas. Their Gas Chromatographic Properties below and above the Phase Transition" *Journal of Chromatography A* **1985**, *329*, 331-349.
62. Bain, C. D.; Troughton, E. B.; Tao, Y. T.; Evall, J.; Whitesides, G. M.; Nuzzo, R. G. "Formation of Monolayer Films by the Spontaneous Assembly of Organic Thiols from Solution onto Gold" *Journal of the American Chemical Society* **1989**, *111*, 321-335.
63. Wasserman, S. R.; Whitesides, G. M.; Tidswell, I. M.; Ocko, B. M.; Pershan, P. S.; Axe, J. D. "The Structure of Self-assembled Monolayers of Alkylsiloxanes on Silicon: a Comparison of Results from Ellipsometry and Low-angle X-ray Reflectivity" *Journal of the American Chemical Society* **1989**, *111*, 5852-5861.
64. Rye, R. R. "Transition Temperatures for *n*-Alkyltrichlorosilane Monolayers" *Langmuir* **1997**, *13*, 2588-2590.
65. Carraro, C.; Yauw, O. W.; Sung, M. M.; Maboudian, R. "Observation of Three Growth Mechanisms in Self-Assembled Monolayers" *Journal of Physical Chemistry B* **1988**, *102*, 4441-4445.

66. Rye, R. R.; Nelson, G. C.; Dugger, M. T. "Mechanistic Aspects of Alkylchlorosilane Coupling Reactions" *Langmuir* **1997**, *13*, 2965-2972.
67. Allara, D. L.; Parikh, A. N.; Rondelez, F. "Evidence for a Unique Chain Organization in Long Chain Silane Monolayers Deposited on Two Widely Different Solid Substrates" *Langmuir* **1995**, *11*, 2357-2360.
68. Kessel, C. R.; Granick, S. "Formation and Characterization of a Highly Ordered and Well-anchored Alkylsilane Monolayer on Mica by Self-assembly" *Langmuir* **1991**, *7*, 532-538.
69. Brandriss, S.; Margel, S. "Synthesis and Characterization of Self-assembled Hydrophobic Monolayer Coatings on Silica Colloids" *Langmuir* **1993**, *9*, 1232-1240.
70. Grange, J. D. L.; Markham, J. L.; Kurkjian, C. R. "Effects of Surface Hydration on the Deposition of Silane Monolayers on Silica" *Langmuir* **1993**, *9*, 1749-1753.
71. Hair, M. L.; Hertl, W. "Reactions of Chlorosilanes with Silica Surfaces" *Journal of Physical Chemistry* **1969**, *73*, 2372-2378.
72. Roumeliotis, P.; Unger, K. K. "Structure and Properties of n-Alkyldimethylsilyl Bonded Silica Reversed-phase Packings" *Journal of Chromatography A* **1978**, *149*, 211-224.
73. Trau, M.; Murray, B. S.; Grant, K.; Griezer, F. "An Ellipsometric Study of Thin Films on Silica Plates Formed by Alkylchlorosilylation Reagents" *Journal of Colloid and Interface Science* **1992**, *148*, 182-189.
74. Xiao, S. J. "Tailored Organic Thin Films on Gold and Titanium: Peptide-Grafting, Protein Resistance and Physical Characterization" *Thesis; M. Sc. Chemistry, Fudan University, Shanghai China* **1999**, 7.
75. <http://www.purdue.edu/REM/rs/sem.htm>
76. Pantano, C.; Gañán-Calvo, A. M.; Barrero, A. "Zeroth-order, Electrohydrostatic Solution for Electro spraying in Cone-jet Mode" *Journal of Aerosol Science* **1994**, *25*, 1065-1077.
77. Lee, K. H.; Kim, H. Y.; Bang, H. J.; Jung, Y. H.; Lee, S. G. "The Change of Bead Morphology Formed on Electrospun Polystyrene Fibers" *Polymer* **2003**, *44*, 4029-4034.



APPENDIX

สถาบันวิทยบริการ
จุฬาลงกรณ์มหาวิทยาลัย

Table A-1 Viscosity at 27°C of water and as-prepared PVA solutions with different concentration

Parameter	PVA solution concentration (%(w/v))						
	0 (water)	5	6	7	8	10	12
Viscosity (mPa.s)	1	15.4	22.7	44.4	60.5	189.5	302.6
Speed (rpm)	250	250	250	250	250	250	164
Shear Rate (s ⁻¹)	233	233	233	233	233	233	153
Torque (%)	0.5	7.7	11.3	22.2	30.2	94.8	99.8

Table A-2 Some properties of as-prepared PVA solutions.

PVA concentration (%(w/v))	Viscosity (mPa.s)	Fiber diameter (nm)	Water contact angle (θ_A)
5	15.4	74.53 ± 1.63	59.34 ± 2.08
6	22.7	90.42 ± 9.04	56.36 ± 1.44
7	44.4	114.51 ± 27.26	54.24 ± 2.07
8	60.5	175.85 ± 17.19	53.90 ± 2.32
10	189.5	297.05 ± 33.59	52.31 ± 1.22
12	302.6	328.60 ± 36.25	49.41 ± 2.51

Table A-3 Water contact angle data (θ_A) of PVA fiber mats after reactions with acyl chlorides in vapor phase.

Time (h)	HFBC at RT	BC at 70°C	HC at 120°C	LC at 120°C
0.5	119.91 ± 5.60	114.48 ± 2.50	106.30 ± 5.70	113.79 ± 3.37
1	137.71 ± 3.96	115.67 ± 5.67	112.88 ± 6.36	112.79 ± 3.15
3	137.86 ± 3.33	115.09 ± 3.17	114.28 ± 4.44	115.55 ± 6.42

Table A-4 Water contact angle (θ_A) and Si/C ratio of PVA-silanol fiber mats

Sample	Water contact angle (θ_A)	Si/C	Fiber diameter (nm)
PVA fiber mats	52.31 ± 1.22	0	297.05 ± 33.59
-SiO ₂ 1 cycle	0	1.34	305.50 ± 31.71
-SiO ₂ 3 cycles	0	3.38	364.75 ± 33.05
-SiO ₂ 5 cycles	0	6.05	440.20 ± 36.03

Table A-5 Water contact angle data (θ_A) of PVA-silanol fiber mats after silanization with monochlorosilanes in vapor phase

Time (h)	CDPS at 70°C	CDODS at 120°C	DOCS at 120°C
0.5	106.71 ± 2.10	132.00 ± 2.42	67.40 ± 4.71
1	126.17 ± 3.20	141.83 ± 4.04	135.43 ± 2.37
3	131.05 ± 1.54	140.14 ± 4.98	144.06 ± 5.22

Table A-6 Water contact angle data (θ_A) of PVA-silanol fiber mats after silanization with di- and trichlorosilanes in vapor phase

Time (h)	DDS at 70°C	TMS at 70°C	TOS at 120°C	TFOS at 120°C
0.5	143.20 ± 2.06	137.66 ± 2.61	140.74 ± 3.89	142.46 ± 3.15
1	151.09 ± 2.96	139.89 ± 7.66	147.10 ± 2.83	147.56 ± 3.43
3	145.76 ± 3.27	136.21 ± 2.84	150.38 ± 3.21	158.38 ± 2.70
5	N/A	N/A	160.28 ± 1.71	162.10 ± 4.18
8	N/A	N/A	150.65 ± 7.10	167.64 ± 3.83

Table A-7 Water contact angle data (θ_A) of PVA-silanol fiber mats after silanization with alkylchlorosilanes in solution

Time (h)	CDPS	CDODS	DOCS	DDS	TMS
0.5	50.46±3.54	57.34±1.01	53.24±2.96	141.20±1.01	137.50±3.78
1	111.31±3.61	75.90±8.41	112.60±3.33	133.31±0.07	134.64±0.06
3	131.02±0.50	105.47±2.84	116.84±0.97	135.60±1.75	134.05±4.10
5	130.67±3.44	125.96±2.57	124.71±3.33	132.50±1.72	136.60±1.23
18	129.92±1.17	120.76±2.14	130.71±2.35	136.04±4.30	140.57±2.56
24	130.07±8.02	122.03±0.77	131.64±1.40	136.48±1.29	138.58±1.69

Table A-8 Water contact angle data (θ_A) of PVA-silanol beaded fiber mats after silanization with alkylchlorosilanes in vapor phase

Time (h)	CDPS at 70°C	CDODS at 120°C	DOCS at 120°C	DDS at 70°C	TMS at 70°C
0.5	126.93±2.56	120.58±2.88	123.24±3.41	131.63±3.14	136.16±1.49
1	130.41±3.22	127.86±3.14	131.21±2.70	142.09±1.83	152.51±1.99
3	134.25±3.21	131.69±2.10	132.12±1.52	140.25±2.31	142.12±6.39
5	132.54±0.32	129.41±1.36	130.52±1.69	137.89±2.41	138.69±0.97
18	133.05±2.11	129.68±2.69	130.87±2.66	138.52±2.68	140.12±2.79

Table A-9 Water contact angle data (θ_A) of PVA-silanol beaded fiber mats after silanization with alkylchlorosilanes in solution

Time (h)	CDPS	CDODS	DOCS	DDS	TMS
0.5 h	89.33±8.24	87.65±2.07	86.28±2.55	125.71±2.54	144.41±2.24
1 h	129.68±6.97	121.96±3.69	125.22±2.74	140.71±2.54	151.30±2.77
3 h	132.86±2.81	130.23±1.51	133.65±3.44	135.20±1.11	139.35±5.24
5 h	131.98±3.14	130.01±3.33	131.65±2.71	136.85±2.39	141.63±1.28
18 h	132.11±1.65	127.22±0.58	132.64±3.66	135.23±5.69	143.88±2.69

VITAE

Miss Navarun Chaim-ngoen was born on April 4, 1983 in Bangkok, Thailand. She received the Degree of Bachelor of Engineering (Petrochemicals and Polymeric Materials), Faculty of Engineering and Industrial Technology, Silpakorn University, Sanamchan, Nakornprathom, Thailand in 2004. In the same year, she was admitted to a Master's Degree in Program of Petrochemistry and Polymer Science, Faculty of Science, Chulalongkorn University and completed the program in 2007. Her address is 206/133 Siriradsattha road, Tambon Paknam, Aumpher Muang, Samutprakarn 10270.



สถาบันวิทยบริการ
จุฬาลงกรณ์มหาวิทยาลัย